DEVELOPMENT AND ASSESSMENT OF NEW ELECTRICAL STEELS FOR HIGH FREQUENCY APPLICATIONS

By

ELMAZEG ELGAMLI

Thesis submitted in fulfilment of the requirement for the degree of Doctor of Philosophy

School of Engineering

Cardiff University

September 2023

ABSTRACT

This research work aims to decrease the power loss of electrical steel by enhancing its surface resistivity. The proposed approach involves introducing additional alloying elements through diffusion after the steel sheet reaches its final thickness. Various methods for increasing the resistivity of the strip have been proposed and tested. The technique involves creating a paste by mixing the diffusant element in powder form with specific solutions, which are then applied to the steel surface. Upon firing the sample, successful transfer of some elements to the steel is observed. The quantity and distribution of these elements can be controlled by adjusting the paste's composition, the firing conditions, and the subsequent annealing processes. This thesis investigates the effects of adding manganese oxide (IV) and cobalt oxide (II, III) to electrical steel to reduce power loss and magnetostriction. The tested samples consist of non-oriented electrical steels with a composition of 2.4wt% Si-Fe and dimensions of 0.305 mm x 300 mm x 30 mm. Power loss and permeability are measured before and after treatment using a single strip tester in a magnetic field range of 0.5 T to 1.7 Tesla. The measurements are conducted using an AC magnetic properties measurement system under controlled sinusoidal conditions at different frequencies.

The results demonstrate that the depth of manganese oxide (IV) diffusion decreases with varying temperatures. The optimal diffusion of manganese into the strips occurs at 525 °C, compared to 700 °C and 800 °C. Therefore, it was concluded that the power losses (W/kg) in the coating samples were improved by 7 % as compared with uncoated samples.

For cobalt oxide (II, III), successful diffusion into steel is observed when added to sodium silicate solution to form a paste. This paste significantly reduces power loss in non-oriented material. The reduction achieved with cobalt paste (14% at 400 Hz, 23% at 1 kHz) surpasses that achieved with manganese paste (6% at 400 Hz and 3% at 1 kHz) on similar steel. This improvement is attributed to the absence of a porous layer containing a high percentage of the diffusing element, as seen in the manganese experiments. The relative amounts of manganese and cobalt entering the steel are difficult to compare due to the formation of the porous layer in the former case.

The formation of porosity in the cobalt addition is found to be more sensitive to firing temperature at the melting point. The diffusion of both materials is examined using scanning electron microscopy coupled with energy dispersive X-ray spectroscopy. The results indicate improved power losses in the coated samples compared to the uncoated samples. Consequently, this study concludes that the properties of non-oriented electrical steels can be improved through a less hazardous process than those employed by previous researchers.

DEDICATION

To my blessed parents

The priceless people whose is lighting my life.

To my beloved Wife and Children*,*

The beauty, happiness, and shiny part of my life

To my brothers, Sisters, and family

The great and blessed persons who accompanying my success.

To my beloved Country ...'Libya'

To all others who love me

ACKNOWLEDGEMENTS

The greatest praise goes to Allah (God), who has given me the wisdom, health, and patience to accomplish this task. I am deeply thankful to God for the amazing graces, without his blessing and help this endeavour would not have been possible.

With the deepest gratitude, I would like to extend my best wishes to my supervisor, Dr Fatih Anayi, for the outstanding guidance, intellectual support, and encouragement he provided during the period of my doctoral study. Throughout my time studying under Dr. Fatih Anayi, I have learned a great deal academically and personally. The comments and advice you provided regarding my research, as well as my life and career, his vision and understanding of the key research challenges in this area have been invaluable for guiding my work.

I am eternally grateful to the Ministry of Higher Education and Scientific Research in Libya for their unwavering financial support throughout my entire PhD study.

I would also like to extend my heartfelt thanks to all my colleagues at the Wolfson Centre for Magnetics for their continuous support, encouragement, and fruitful discussions during meetings and seminars.

I thank the members of Wolfson Centre, Dr Philip Anderson and Dr Christopher Harrison for their advice and comments at all levels of my research. I would also like to acknowledge Mrs Aderyn Reid and Ms Jeanette C Whyte, in research office. I am extremely appreciative to Mr Steve Mead, Mr Malcolm Seaborne, Mr Andrew Rankmore, Mr Justin Merridew and Dr Franck Lacan in the mechanical workshop for taking time out of their busy schedule to help and support my project during my study in Cardiff University.

I am also grateful to civil workshop staff for aiding me in preparing the samples and test them as early as possible. I am thankful to my colleagues in Wolfson centre, for the help and motivation that they provided during my research.

LIST OF CONTENTS

LIST OF FIGURES

LIST OF TABLES

LIST OF ABBERVIATION

∇	Divergence
AC	Alternating current
CGO	Conventional grain oriented electrical steel
Co Fe	Cobalt–Iron
DC	Direct current
G	Gauss
GO	Grain oriented electrical steel
H	Magnetic field strength
I	Current
I_{sc}	Short circuit current
k	Material constant
l	Distance
L	Half Spacing between domain walls
M	Magnetisation
m	Magnetic moment
N	Number of turns
Ni Fe	Nickel–Iron
NO	Non-oriented electrical steel
O_e	Oersted
R_{ct}	Contact resistance of the laminations
RD	Rolling direction

R_{eq}	Equivalent resistance
R_{lam}	Lamination path resistance
S	Power flux
Si Fe	Silicon Iron
SST	Single Strip Tester
T	Tesla
TD	Transverse direction
w	Angular frequency
A	Surface area
P	Dipole strength
Bz	instantaneous flux density in Z direction
D	Material density 7650
E	Electric field
J	Eddy Current density
K_h	Hysteresis loss coefficient
K_e	Eddy current loss coefficient
K_{ex}	Excess loss coefficient
R	Reluctance
d	Sheet thickness
lm	Magnetic path length
n	Component normal the surface
$\boldsymbol{F}$	Magneto motive force
B	Magnetic flux density

LIST OF Symbols

Symbol	Description
P_{cu}	Copper losses
P_{me}	Mechanical losses
P_e	Eddy current losses
P_h	Hysteresis losses
P_a	Anomalous loss
$\boldsymbol{\Phi}$	Magnetic flux
μ_0	Permeability of free space
μ_r	Relative permeability of the material
$\nabla\times$	Curl
ρ_v	Volume charge density
ε_0	Permittivity of free space
ρ	Resistivity
δ	Skin depth
σ	Electrical conductivity of the material
B_{pk}	Peak value of the magnetic flux density
I_{pk}	Peak magnetising current
$\mu_Z{}'$	Absolute static permeability
γ	Propagation constant
λ	Flux linkage
ß	Phase angle
η	Anomaly factor
χ	Susceptibility

Chapter 1: Introduction

1.1 Background

Electrical steel sheets are used as magnetic flux conductors in a wide range of electromagnetic applications, such as inductors, transformers, and rotating electrical machines. Electrical steel plays a vital role in electromagnetic energy transfer. During the energy transfer process, core losses resulting from hysteresis and eddy currents occur as heat dissipates from electrical steel. The core losses reduce the overall efficiency of electromagnetic devices. In addition, either a heat sink or cooling system is needed to evacuate the heat generated from the electromagnetic system. Thus, the electrical steel's magnetic characteristic is essential from the electromagnetic design and performance perspective. Furthermore, accurately representing electrical steel's magnetic characteristics is indispensable in designing efficient, compact, and robust electromagnetic devices. Thus, analysing core losses in electromagnetic devices has been given special attention in industrial and academic research.

The electrical steels are categorised as soft magnetic materials, due to the low value of the coercive field strength and high saturation flux density. In contrast, permanent magnets are categorised as hard magnetic materials because of their high coercive field strength. A further classification of silicon steel is based on the manufacturing details considering the orientation of the grains. Silicon steel can be either grain-oriented (GO) or non-oriented (NO), based on the grain orientation. The GO steels are primarily used in the applications in which the magnetic flux is confined to a specific direction, such as in the limbs of a large power transformer or the stator core of a high megawatt synchronous generator. In contrast, NO steels are preferred in applications in which the magnetic flux points to different directions, such as in the stator yoke of a medium-sized induction or synchronous machine. Several factors affect the magnetic characteristics of NO and GO silicon steels, such as composition (percentage of silicon and

aluminium), thickness (rolling process), and heat treatment (annealing). The grain size, which the heat treatment can control, affects the overall magnetic characteristics. Other factors, such as residual stress due to cutting, punching, drilling, and so on, may be induced during the production of electromagnetic devices. Research of electrical steel production can be divided into metallurgy dealing with electrical steel (raw electrical steel sheet) production and its use (processed steel) in electrical machines. Electromagnetic design engineers and academic researchers are interested in the characterisation of processed silicon steel. However, characterising and modelling magnetic behaviours of processed silicon steel can be challenging. Ideally, a magnetic material model should be capable of predicting magnetic behaviours under thermal and stress loadings, such as tension, compression, torsion, and so on. Besides thermal and stress loadings, the microstructure and texture almost always lead to magnetic anisotropy, whose effects are often neglected in NO silicon steels and can have a significant impact on the magnetic characteristics.

The current research is focused on understanding the technique of diffusing silicon or aluminium into non-oriented silicon-iron to offer a controllable and effective way of improving its magnetic properties. The most important effect is that after treatment the stress sensitivity of both power loss and magnetostriction are reduced. The treatment has not yet been optimised, so it is feasible that further improvements may be possible by changing the diffusion conditions and the composition of the paste. This technique has been used successfully to diffuse both silicon and aluminium into no-oriented silicon-iron. Although the process has not yet been optimised, aluminium seems far more promising than silicon at present.

1.2 Motivation

Escalating fuel costs and diminishing resources have combined to produce a greater awareness of the need for energy conservation, and this in turn has led to strenuous efforts being made to improve the efficiency of electrical machines and power transformers. Although efficiency of a large power transformer may be as high as 98–99%, even a small improvement in efficiency, such as just one percent, can yield substantial benefits in the face of rising fuel costs and dwindling resources. The best material that is available for the construction of cores for many applications is non-oriented electrical steel 2.4% Si-Fe. This thesis aims to investigate a method of further improving this material. The attraction of this research is that eddy currents that are present in a sheet subjected to alternating current AC magnetisation at high frequency occur to a greater extent near to the surface of the sheet due to skin effect. If an element such as manganese or cobalt that increases the resistivity of the steel can be added in these regions, then these eddy currents will be reduced. This is important because eddy currents not only constitute a power loss but also produce fields which oppose magnetisation. Because both manganese and cobalt reduce the saturation magnetisation of iron, it is important to minimise their concentration and ensure that they are distributed as efficiently as possible. Only few methods of diffusing aluminium and silicon into silicon-iron have been described in the literature, which have mostly aimed at producing uniform concentration distributions and have in general yielded promising results. The original aim of this project was to investigate one of these methods further. However, the author did not consider the process to be commercially viable, and it was therefore decided to attempt to devise an alternative. Consequently, both manganese and cobalt were diffused into non-oriented silicon-iron from a paste and the effects of this on the properties of the material, such as power loss and magnetostriction, were measured. The effects of varying certain parameters (e.g., the composition of the paste, the

time and temperature of firing, and the atmosphere under which it was carried out) were evaluated and attempts were made to discern the reasons for the changes observed. Some of the samples were examined using a scanning electron microscope (SEM)to discern the concentration gradients within them and to observe any physical changes that might have occurred due to the processing.

1.3 Aim and objectives

This research reduces eddy current losses by increasing the resistivity of electrical steel. Introducing manganese oxide (IV) and employing it as a diffusion material implementation of cobalt oxide (II, III) as a diffusion material constitutes a unique contribution. As a result, this research covers the following objectives:

1. Measure the magnetic properties of the tested strips before and after treatment to determine the impact of the introduced impurities.

2. Examine the effectiveness of the diffusion of the materials through the use of electronic microscopy to observe the distribution of the impurities and their impact on the resistivity of the steel.

3. Investigate the impact of different treatment temperatures on the depth of diffusion and magnetic characteristic changes to determine the optimal temperature to achieve the desired resistivity increase.

4. Study the impact of thickness, relative permeability, and flux concentration due to the skin effect on eddy current in a soft material.

5. Calculate the power loss and separate it into three components to understand the mechanisms responsible for the loss and their impact on resistivity.

6. Observe the distribution of the material using available techniques to understand how the impurities are distributed on the surface of the steel strips and their impact on resistivity.

1.4 Scientific contribution

The research presented in this study encompasses three significant scientific contributions, as described in the following subsections.

1.4.1 Novel material: manganese oxide (IV)

The introduction of manganese oxide (IV) using this material as coating is a novel work. This research demonstrates that this material possesses excellent high-frequency properties at 1 kHz. By incorporating manganese oxide (IV) into Si-Fe, the resistivity of the composite material increases. This increase in resistivity is particularly advantageous because it helps to reduce power losses. The utilisation of manganese oxide (IV) in Si-Fe represents a promising avenue to improve the efficiency of power systems.

1.4.2 Novel material: cobalt oxide (II, III)

The discovery and characterization of cobalt oxide (II, III) when used as a coating represent novel contributions. This research underscores that cobalt oxide (II, III) exhibits an increase in resistivity due to the inclusion of high-resistivity material, which proves particularly advantageous as it aids in reducing power losses, especially at 1 kHz. These properties render it an attractive material for a range of applications, notably in high-frequency circuits and systems.

To enhance the scientific contribution of cobalt oxide inductance, future research could focus on exploring its unique properties in detail, investigating the underlying factors that contribute to its favourable pulse response and high inductance, and optimising its synthesis methods for better performance.

1.4.3 Technique: diffusion of manganese and cobalt

An important scientific contribution of this study is the utilization and enhancement of a previously established technique for diffusing manganese and cobalt into non-oriented electrical steel sheets. This technique has been recognized as a controllable and effective means of improving the magnetic properties of steel, as demonstrated in prior research. To further advance this scientific contribution, future research endeavours may focus on optimizing the diffusion process to achieve even more enhanced magnetic properties, exploring the impact of varying diffusion parameters on resultant properties, and investigating potential applications of diffused silicon in magnetic devices and systems.

1.5 Outline of this thesis

To provide a clear and concise presentation of the research, this thesis is structured into six chapters.

Chapter 1 introduces the aim and scope of the research and highlights the scientific contributions of the study.

Chapter 2 reviews the literature, which presents the existing knowledge on the effect of alloying elements in electrical steel. This chapter provides the theoretical background that is necessary to understand the context of this research.

Chapter 3 details the preparation of samples and the techniques that were used to analyse them. This chapter presents information on the synthesis of the materials used in this research, along with the tools and procedures that were used to investigate their magnetic properties. Hence, different simulations were used in this study, including power loss and the relative permeability of the material.

Chapter 4 this chapter is based on the electrical and magnetic properties of the core material and analytical method to calculate the power loess components. Hence, used LabVIEW was used in this study, including power loss and the relative permeability of the material. It also presents the results and discussions of the impact of manganese diffusion into non-oriented electrical steel on power loss and permeability at different temperatures. Additionally, this chapter analyses the results obtained from the techniques described in Chapter 3.

Chapter 5 describes the methods used to control the quantity and distribution of cobalt entering the sheet. This chapter explains the techniques that were used to apply cobalt to the surface of non-oriented electrical steel strips and examines their impact on resistivity.

Chapter 6 provides the concluding remarks, summarises the key findings and contributions of the study, and makes a number of recommendations for future directions of research.

1.6 Publications

1.6.1 Journal papers

1. **Elgamli, E**. and Anayi, F. (2023) 'Advancements in Electrical Steels: A Comprehensive Review of Microstructure, Loss Analysis, Magnetic Properties, Alloying Elements, and the Influence of Coatings', Applied Sciences, 13(18), p. 10283. Available at: https://doi.org/10.3390/app131810283. **(Chapter 2).**
2. **Elgamli, E.,** Anayi, F. and Shouran, M. (2023) 'Impact of manganese diffusion into non-oriented electrical steel on power loss and permeability at different temperatures', Frontiers in Materials, 9(January), pp. 1–13. Available at: https://doi.org/10.3389/fmats.2022.1108308 .**(Chapter 4)**.
3. **Elgamli, E.** and Anayi, F. (2023) 'Diffusion of Alloying Cobalt Oxide (II, III) into Electrical Steel', Materials, 16(18), p. 6315. Available at: https://doi.org/10.3390/ma16186315. **(Chapter 5).**

Chapter 2: Literature review

2.1 Introduction

Electrical steel, which is a soft magnetic steel, encompasses specific steel grades that are renowned for their exceptional soft magnetic properties. These properties include magnetisation behaviour, permeability, coercive field, and specific magnetic losses. Electrical motors and transformers typically employ these steels as their primary construction materials [1]. The main types of electrical steels are iron-silicon Fe-Si and iron-silicon-aluminium Fe-Si-Al alloys. These alloys are primarily available in plate form, with a thickness of less than 1mm. The typical range for these plates is between 0.35 mm and 0.5 mm [1].

Electrical steels are used in the core of transformers, generators, and motors. These steels are of two types: grain-oriented electrical steel (GOES) and non-oriented electrical steel (NOES). (GOES) is a special type of cold-rolled electrical steel that is made up of 3% silicon in iron and is used in the core of transformers [2]. In GOES, the grains are oriented in the direction of rolling, resulting in superior magnetic properties in that direction[3]. Non-oriented electrical steel is mostly used in motors and generators, which have a cubic texture with (001) and (110) planes parallel to the plane of the sheet and a uniformly distributed [100] direction [4][5].

When electrical steel is subjected to AC magnetisation, it generates heat and sound, which contribute to power loss in terms of anomalous, eddy currents, and hysteresis loss[6] . Domestic power is supplied at low voltages of approximately 220–240V but is transmitted at 400 kV from electric power stations. This high voltage cannot be directly delivered to residential and industrial areas, necessitating the use of transformers to step up or step down the voltage. This system minimises, power losses during low-voltage transmission. However,

cyclic magnetisation and demagnetisation caused by magnetostriction (i.e., change in the length of material in the presence of a magnetic field) can lead to transformer hum noise, which may be bothersome to residents [7]. While noise-isolating enclosures can be constructed to attenuate the noise, they can significantly increase costs. The optimal solution is to control magnetostriction by modifying the material properties. Coatings can help reduce magnetostriction by eliminating surface closure domains [6].

There is a growing trend in the production of electrical steel to increase the concentration of silicon (Si) and/or aluminium (Al) beyond the traditional 3% weight composition. This stems from the fact that these alloy compositions exhibit lower values of magnetic friction and magnetic contrast (K), while demonstrating higher electrical resistance. These characteristics contribute to reduced losses from eddy currents, which drives significant interest in the production of steel with higher Si and/or Al concentrations [8].

These properties include a low hysteresis loss, low core loss, and high permeability. Typically, electrical steel is manufactured in the form of cold-rolled strips with a thickness of less than 2 mm [9]. These strips are then cut and stacked together to form laminated cores for transformers, as well as the stator and rotor components of electric motors. Furthermore, these strips can be shaped into the final form through techniques such as punch and die cutting, laser cutting, or Electrical discharge machining (EDM) wire cutting.

In recent years, significant efforts have been directed towards developing improved steel grades that minimise iron loss and enhance energy efficiency [6]. An effective coating applied to GOES provides both insulation and introduce tensional stress in the material, effectively reducing power loss and magnetostriction. Furthermore, the coating's magnetic activity and thickness help to improve the stacking factor, which denotes the amount of magnetic material present in the core. Conventional coating systems, such as forsterite and

aluminium orthophosphate, typically have thicknesses ranging from 4 to 8 microns. However, these non-magnetic coatings reduce permeability and saturation, which results in a stacking factor of around 96% [9].

Iron loss in electrical steel is conventionally classified into three components: hysteresis loss, eddy current loss, and anomalous or excess eddy current loss. Hysteresis loss is influenced by factors such as the volume, size, and distribution of impurities, crystallographic orientation, and the stress levels within the material. Eddy current losses can be described using the following equation:

$$P_e = \frac{\pi^2}{6\rho} d^2 f^2 {B_{pk}}^2 \tag{2.1}$$

Where:

P_e eddy current loss

B_{pk} peak flux density

f frequency

t lamination thickness

ρ resistivity

Electrical steel is an iron alloy that can contains varying amounts of silicon (Si), ranging from zero to 6.5% (Si:5Fe). Commercial alloys typically have a silicon content up to 3.2%, because higher concentrations can lead to brittleness during the cold rolling process. Manganese and aluminium can also be added in quantities up to 0.5% [10].

The addition of silicon significantly increases the electrical resistance of the steel. This change reduces the magnitude of induced eddy currents and narrows the hysteresis loop of the

material, resulting in reduced core losses [5]. However, the grain structure of the alloy becomes harder and weaker, which can adversely affect its workability, especially during recycling processes [11] . During alloying, it is important to maintain low levels of carbon, sulphur, oxygen, and nitrogen because they can form compounds such as carbides, sulphides, oxides, and nitrides. Even small amounts of these compounds, with a diameter of one micrometre, can increase hysteresis loss and reduce magnetic permeability. Carbon has a more detrimental effect than sulphur or oxygen and can lead to magnetic ageing, where it slowly precipitates as carbides, causing an increase in energy loss over time. To mitigate these effects, the carbon level is typically maintained at 0.005% or lower. The carbon content can be reduced through annealing the alloy in a decarburising atmosphere, such as hydrogen.

Approximately 97% of the soft magnetic materials that are produced today are electrical steels [12]. More than 12 million tons of these steels are produced every year, of which about 80% are unguided grades (NO) and the rest are 3% silicon steels grains (GO). Growing global demand for efficient power generation and distribution equipment has led to the development of low magnetic loss and high permeability steels. Magnetic losses in steel cores represent between 5–10% of the total electric power produced in developed countries [12], despite continuous improvements over many decades (as shown in Figure 2.1). It is interesting to note that occasional improvements in these numbers are due to the introduction of new processes in the production and processing of steel, unlike the major improvements made to permanent magnets, that resulted from the discovery of completely new material families [12].

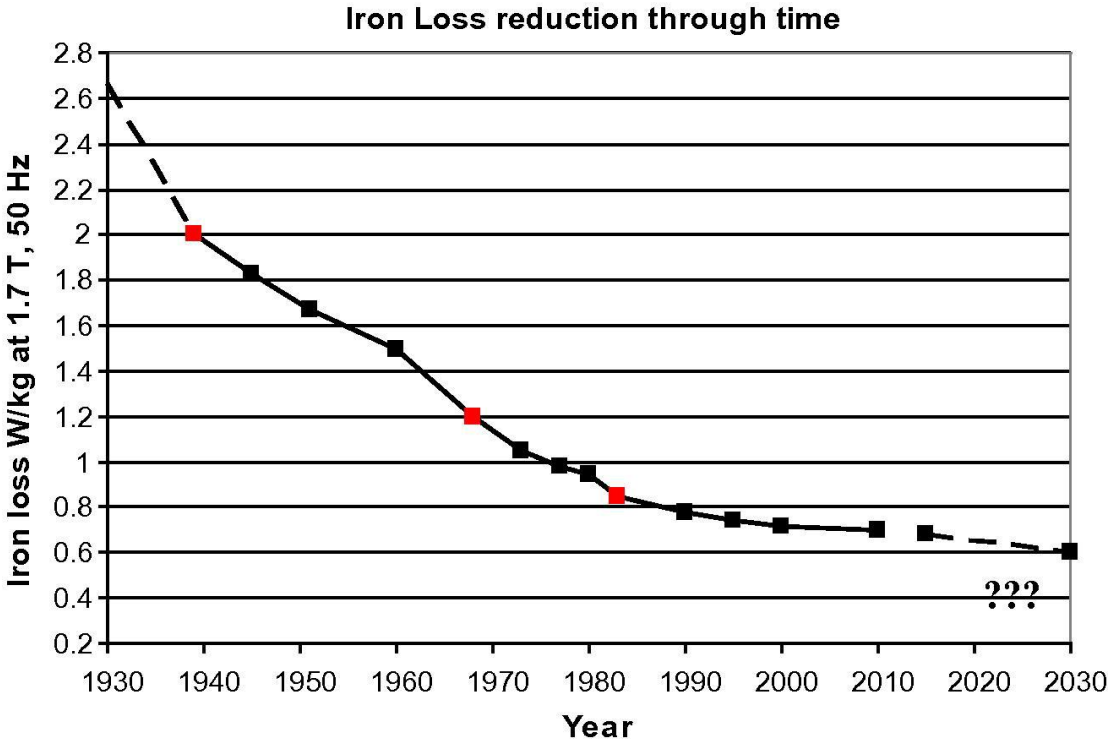

Figure 2-1 Losses (at 1.7 T, 50 Hz) in highest available grades of commercial electrical steels produced since 1930, showing occasion rapid improvement due to the introduction of new technology [12].

2.2 Microstructure of electrical steel

The magnetic properties of soft magnetic materials (e.g., electrical steel grades) are related to the microscopic structure and texture of the steel material [13].The microstructural parameters that have a strong influence on magnetic properties (e.g., magnetisation curves, permeability, force field, and specific magnetic loss) are mainly the grain size, inclusions, and internal pressures, with respect to the value of magnetic friction and surface defects. These microstructural parameters define the subculture of the field wall (i.e., the coercive force of the material), as well as the motion of the field wall, which is responsible for magnetic behaviour at low and medium values of the field. The crystalline structure is important because the behaviour of grid magnetism varies in different crystalline directions: [100] directions are magnetised much more easily than the directional [110] or [111], or body cantered cubic (bcc) (as shown in Figure 2.2). The magnetic fabric in polycrystalline material determines residual

magnetic induction and field rotation at high values of the applied outer magnetic field. Therefore, the optimal texture of the electrical steel used in rotary machines is the cubic fibre fabric where most grains have a normal [100] orientation of the leaf level [14]. An even distribution of crystalline orientations along these fibres provides maximum permeability and magnetic properties at the sheet level. This type of electric steel is called non-oriented electrical steel [15]. In applications of static electrical machines, such as transformers, it may be desirable to use a clear Goss texture (110) and [001] because the magnetic field can be aligned with the direction [001] [16]. These steels have electrically oriented grains. However, assessing the effect of tissue on the magnetic properties remains a challenge because it is extremely difficult to separate its effect from the effect of grain size or second phase impurities [17].

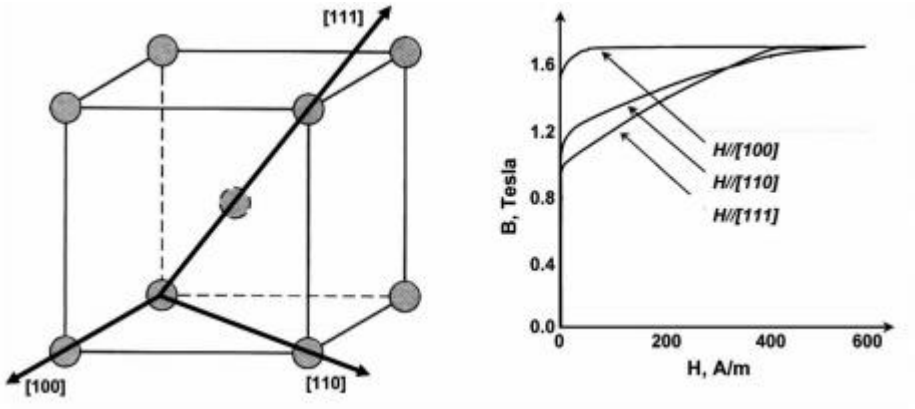

Figure 2-2 Magnetisation curves for a single crystal of bcc iron as a function of the crystallographic direction [18].

2.3 Analysis of losses in electrical steels

To accurately model to predict losses or estimate the effect of controlling the mineral and other physical properties, it is necessary to consider the possible inaccuracies in loss measurements, which are generally ignored in the commercial classification of electrical steels. Because steel is mainly used in AC magnetospheres, its magnetic properties are evaluated by testing under time-varying flow density and sinuses, with maximum values of 1.5 or 1.7 T at 50 or 60 Hz in IEC Epstein square or with a Single Sheet Tester (SST) [19], which are well-established methods of commercial classification of electrical steels. However, the use of the Epstein square as a research tool to study loss mechanisms is limited and, in some cases, misleading because it does not give an accurate signal or an absolute value of the loss under the ideal optimal magnetic conditions.

The most important reason for the standard is due to the need to use a constant value for the length of the magnetic path of the Epstein square, although it has long been known that it varies with the composition of materials and magnetic conditions [20]. Recent reports show that considering this to be consistent leads to significant errors when comparing losses of similar steel grades [21]. In the worst scenario, although highly reproducible, the loss indicated by the Epstein square may be 5–10% different from the absolute value.

In the cores of electrical machines, factors such as mechanical pressures, flux harmonics, and rotational magnetisation increase the rolling losses to varying degrees in different grades of steel. Therefore, it is important to ensure that it will not compensate for the improvements in the fundamental physical characteristics referred to by the Epstein test. The effects of these harmful factors can be minimised by carefully designing and building a magnetic core, although they increase the basic losses by 10–30% overall [22].

Losses and other magnetic properties of the structure can be very sensitive to mechanical pressures [23]. Because it is very difficult to eliminate many sources of stress in the core of electrical machines, it is necessary to consider the stress sensitivity curves such (e.g., those shown in Figure 2.3) and to ensure that the stress characteristics of the proposed new steel are at least as equally as good as those in the original material [24]. However, it is difficult to apply these properties directly to predict core loss because stress in a large nucleus is randomly distributed in size and direction to the extreme where local pressure may be useful [23].

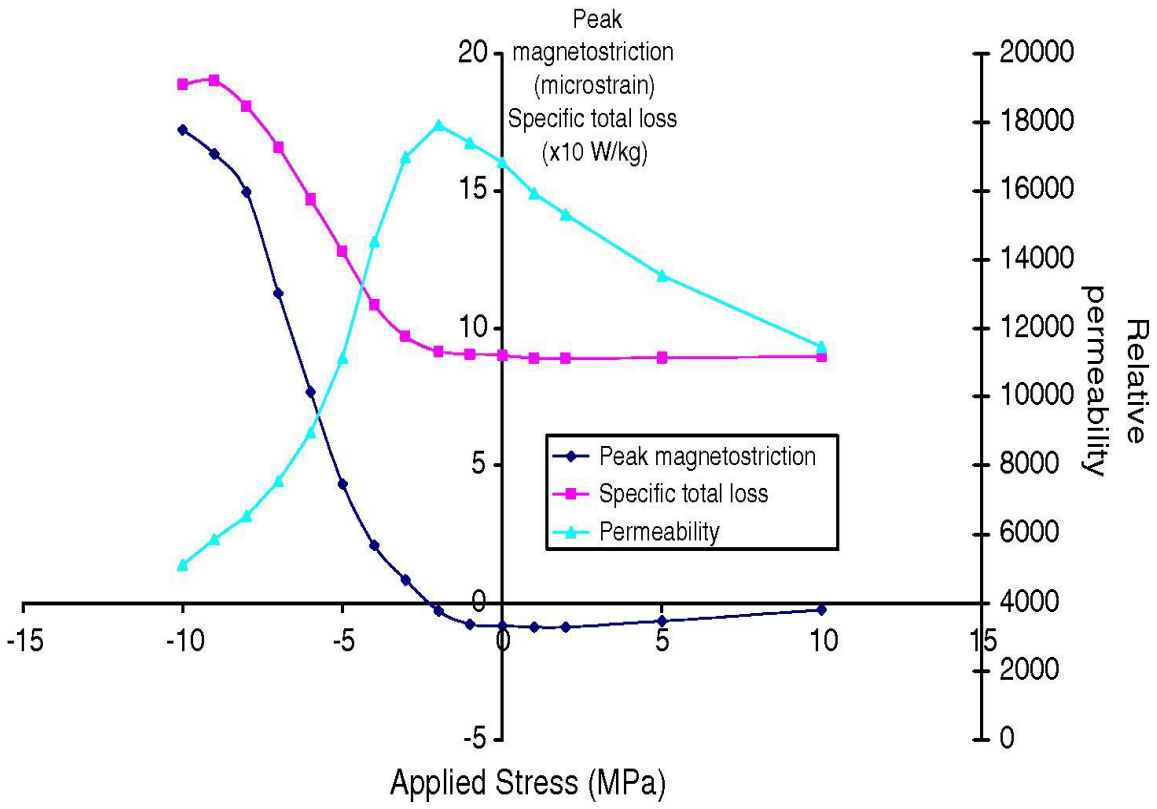

Figure 2-3 Variation of loss, permeability and magnetostriction of an Epstein strip of typical GO steel magnetised (1.5 T, 50 Hz) along its longitudinal direction (RD) while external stress is applied simultaneously along the same direction [23].

2.4 Conventional method for studying losses in electrical steels

The processing of electrical steels has a significant impact on the total losses. Plastic deformation increases the loss of hysteresis and reduces excess losses, while annealing promotes an increase in grain size, that decreases the first and increases the second (as shown in Figure 2.4). The total losses of non-oriented electrical steels, at 1.5T and 60 Hz, range from 10 W/kg to 3 W/kg in annealed condition, as stated by steel makers catalogues [25].

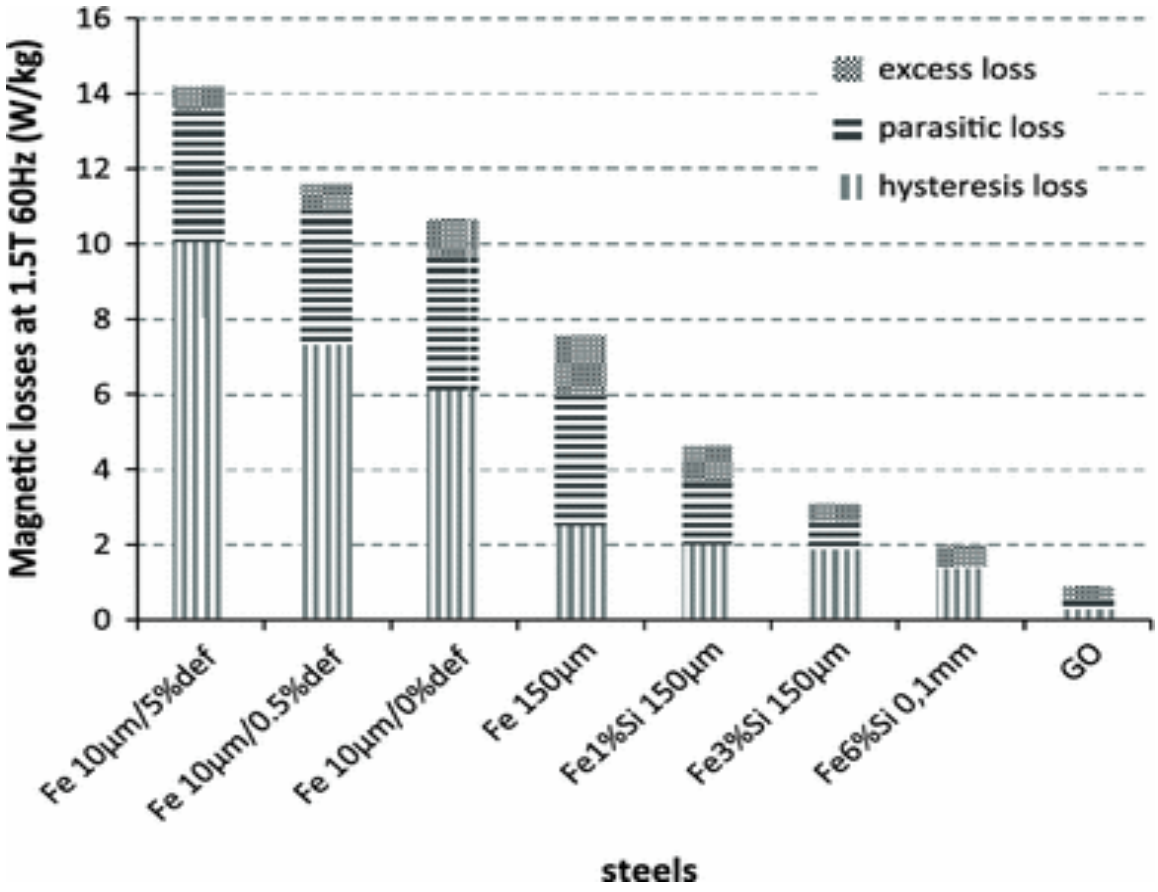

Figure 2-4 Total loss and its components for steels with different silicon content and processing conditions, keeping constant maximum induction (1.5T), frequency (60 Hz), and thickness (0.5 mm), except for the GO material (0.35 mm) [25].

Motors, generators, and transformers play major roles in power systems. Therefore, these machines should be designed efficiently to provide consistent power delivery with reduced power loss. Most recent studies regarding these machines focus on power loss

optimisation. Power loss plays a significant part in machine design and the material from which the core is made is normally characterised by its magnetic properties under specific frequencies. There is increased competition between the material designers to provide the most efficient material with the lowest power loss. Power loss is generally divided into three categories: copper loss P_{cu} ,which occurs in machine winding; mechanical loss P_{me}, which is due to rotating parts in electrical machines or the friction loss of a machine, including bearing friction; and magnetic core loss, which occurs in core laminations due to the alternating magnetic field. Meanwhile, magnetic core loss originates from three main sources: eddy current power loss P_e, hysteresis loss P_h and anomalous loss P_a [26][27]. The cores of electrical machines and other magnetic devices serve a significant role as magnetic field concentrators, which are required to contain as much magnetic flux as possible because the magnetic flux changes over time [28]. Therefore, an electromotive force is generated in the core lamination, which will induce eddy currents, and energy will be lost in the form of heat along the eddy current path [29]. Eddy current power loss P_e is found to be the highest when compared to other loss components, and in some cases has led to complete machine failure [30]. Consequently, procedures have been put into place to minimise the impact of this loss. These include building the cores from a thin stack of laminations, typically 0.23–0.65 mm, based on the type of material and its application. The lamination of the material forces the eddy currents to flow in long and narrow paths, thus greatly reducing their values and the accompanying heating within the material. Moreover, the laminations are coated on both sides with insulating layers to prevent direct contact between the sheets [31]. This reduces the eddy current circulating in the core. It also provides a reduction of both hysteresis [32] and anomalous loss as a result of beneficial tensile stress [33]. Tensile stress applied to the material helps to minimise losses by reducing the size of the domains that are perpendicular to the magnetisation direction. Moreover, tensile stress causes a narrowing of the domain wall spacing, which decreases the

anomalous loss due to the reduction in the average domain wall velocity. Finally, 3% high silicon content is added to the material to increase its resistivity, and hence reduced the eddy current [28], which may improve the efficiency of modern electrical devices. Table 2-1 illustrates the effect of silicon content on power loss components at 50 Hz and 100 Hz.

Dividing losses into hysteresis and eddy current components can help us to understand the influence of controlling factors and is also a tool for predicting losses in electrical machine cores. The loss per cycle P_c at magnetising frequency f and peak flux density B_m, is commonly expressed as the sum of the static (DC) hysteresis loss P_h, the classical eddy current loss P_e and the excess loss P_{exc}, and is written in forms such as:

$$P_c = P_h + \frac{d^2\pi^2 {B_m}^2}{k.\rho}.f + C_3.{B_m}^{1.5}.f^{0.5} \tag{2.2}$$

where d is the sheet thickness, ρ is the electrical resistivity, k is a magnetisation waveform-dependent constant, and C_3 is a material-dependent fitting parameter.

P_h is proportional to the area enclosed by the B–H loop when the magnetic field H is varied very slowly and is found by experiment. Figure 2.5 shows the relationship between the loss per cycle and frequency, which can be extrapolated to zero to obtain P_h. During slow, cyclic magnetisation, domain walls move in well-quantified ways [34]. In addition, it is assumed that hysteresis loss occurs due to micro eddy currents, which occur on a microscopic scale when the walls are randomly released from material pinning sites [35].

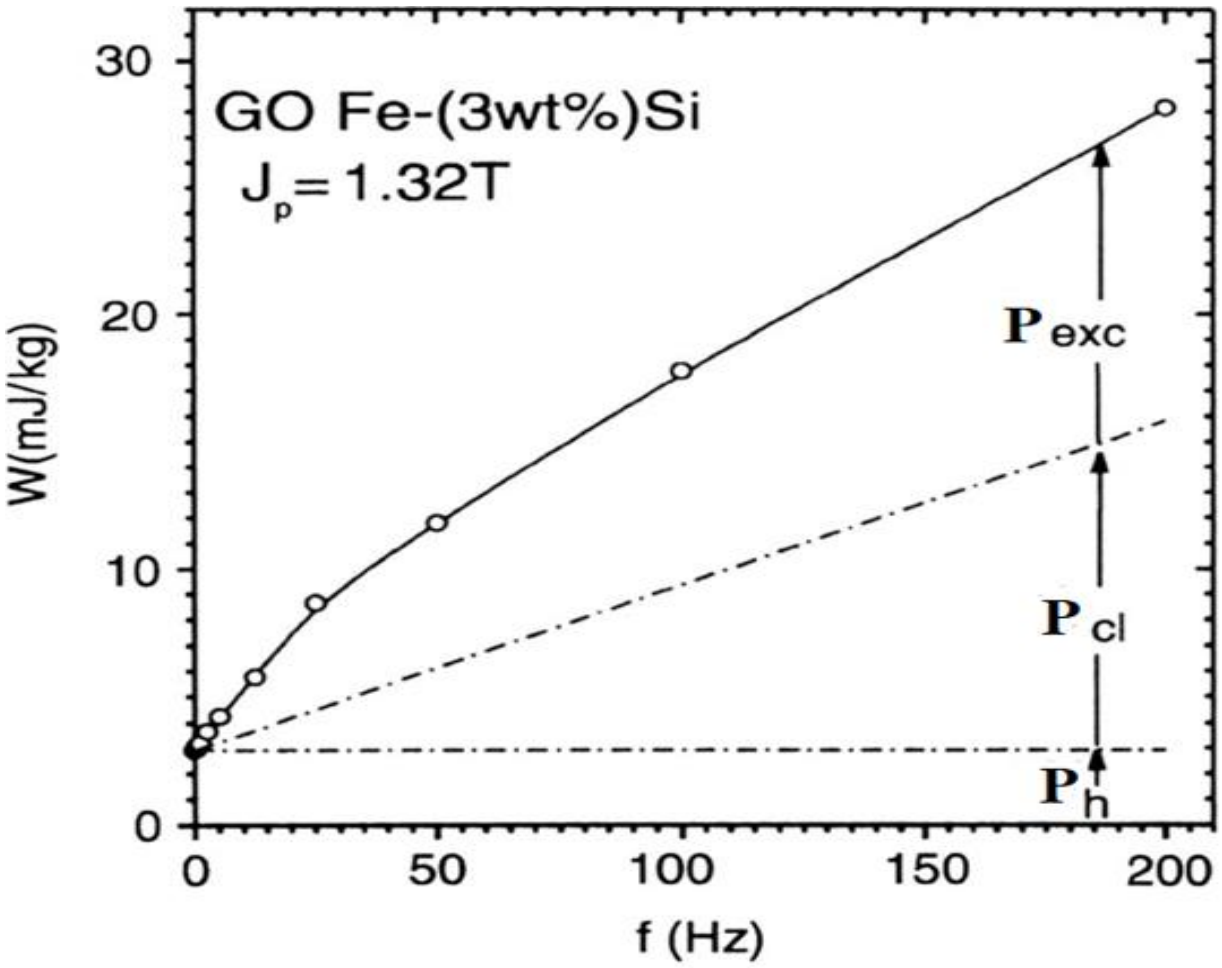

Figure 2-5 Example of the variation of traditional hysteresis, eddy current, and excess loss components with magnetising frequency in typical commercial GO 3% silicon steel measured at 1.32 T, 50 Hz [34].

P_e is calculated from classical Maxwell equations assuming a thin, infinite sheet with constant permeability and a time varying, unidirectional alternating flux and magnetic field in its plane. Eq. (2.2) is often written with $k = 6$, which is only true if the flux varies sinusoidally with time everywhere within the sheet. However, the justification for each assumption is dubious because in practice the permeability is not constant, the flux density is not sinusoidal, and the localised flux density is not unidirectional.

There is still debate about the origin of this phenomenon, P_{exc}, and numerous attempts have been made to design and numerically adapt it to the difference between the total measured loss and the total of P_h and P_e at the density and frequency of the given flow. Table 2-1 shows

the typical distribution of loss components in a range of NO electrical steels where, in general, P_h predominates at power frequency and drops with reducing thickness. Meanwhile, the excess loss is illustrated by the example shown in Figure 2.5, which happens because of differences in the magnetisation processes due to its much larger and regularly distributed domain. Because P_{exc} is usually the smallest component of NO steel, it is important to have a reliable estimate of the total, and of P_h and P_e. Table 2-2 presents the factors that influence the loss components. If a large grained thick steel has little residual stress and few pinning sites caused by impurities, then P_h is relatively low. Conversely, if a thin material has a small grain and high electrical resistance, then P_e is relatively low. Obviously, there are conflicting requirements for minimising P_h, P_e and P_{exc}. Although in practice a perfect combination of grain thickness and grain size can be found, it depends on the frequency and flux density of the grain. The effects of many of the parameters in Table 2 are not independent of each other. Therefore, according to our current understanding, it is not possible to produce analytical equations that can quantitatively predict them [36] .The increased proportion of Ph and decreased Pe with decreasing thickness is clearly seen reproduced from [2-2].

Table 2-1 Range of variation of percentage of power loss components (per cycle) with silicon content and thickness in NO steels at 50 Hz and 100 Hz.

Frequency (Hz)	Material specification	Hysteresis loss (P_h)	Eddy current loss (Pe)	Excess loss (P_{exe})
50	Low silicon	30-50	40-60	0-20
	High silicon	55-75	20-30	10-20
	Thin high Si	80-90	1-2	5-15
100	Low silicon	20-30	50-70	10-20
	High silicon	25-35	40-60	15-25
	Thin high Si	80-90	1-2	5-15

Table 2-2 Qualitative effect of some of the important parameters on traditional loss component (per cycle) in electrical steels, reproduced from [2-1].

P_h	Pe	P_{exc}
High for increased defects, impurities, internal stress, high texture, poor surface topology	**High** for low resistivity and increased thickness	**High** for increased defects impurities, internal stress
Low for thick material or large grains	**Low** for thin material or small grains	**Low** for narrow domain width and small grains
Decreases with increasing texture	**Probably not** texture dependent	I**ncreases** with increasing texture
Obtained from proportionality. of measured static B-H loop or extrapolation of loss/cycle vs f curve to f=0	**Calculated** from Maxwell equations for thin sheet assuming linear B-H loop and no skin effect and flux harmonics	**Calculated** with empirical models or from difference between measured loss and (Ph+Pe)
Independent of frequency	**Proportional** to frequency	**Proportional** to (frequency)$^{0.5}$

It is becoming more widely accepted that this approach can lead to misleading conclusions for low loss or for a thin sheet, or for predictions under the non-standard magnetisation conditions that are demanded today, simply because it does not take account of the effect of magnetic domain activity or microstructure on losses.

2.5 Types of electrical steel

Electrical steels can be split into two main categories: oriented and non-oriented (NGO) steels. Oriented steels can be further divided in g (GO) and high- permeability (HiB) steels [37].

2.5.1 Grain-oriented electrical steels

Grain-oriented electrical steels have significant variation in magnetic properties. They also have superior magnetic properties in the direction of rolling. These steels were developed to provide low core loss and high permeability, which is achieved by combining a well-defined chemical composition with heat treatment. Consequently, grain-oriented electrical steels are typically used in the magnetic cores of transformers, where the magnetic flux follows mainly one direction. However, grain-oriented steels are expensive when compared to non-oriented steels.

The observation of domain structures has contributed to the development of ferromagnetic materials through metallurgical studies, production process studies, and magnetic application studies, among others. At the present time, several industrial techniques for dynamic domain wall behaviour control have been developed [38].

2.5.2 Non-oriented steels

The addition of silicon to iron to provide useful electromagnetic properties was first discovered in 1900 by Hadfield et al. [39]. These steels have been one of the most important magnetic materials for industrial use since 1905 and they have been used for the manufacture of magnetic cores in transformers and slewing machines [40]. These alloys are called electrical steels or silicon steels and are soft magnetic materials. They are easily magnetisable and demagnetise. Upon the discovery of the magnetic iron contrast in 1926 by Honda and Caia [41], it was recognised that the addition of silicon reduces magnetic contrast and provides other advantages when added to the iron used in rotating machines. Non-oriented electrical steels (NOES) are a class of electric steels in which individual crystals in the material are randomly oriented [42][43]. Their magnetic properties are useful in applications requiring a magnetic flux passing through steel [44]. This makes them excellent candidates for use in rotating

machines, such as electric motors, where the magnetic flux constantly changes direction. The primary focus on material efficiency in electromechanical applications was discussed in the introduction. In particular Oda et al. [45] reported that 60% of Japan's electricity consumption was used by electric motors in 2009 and that a 1% increase in the efficiency of these electric motors would equal the output of a 500MW nuclear power plant. Binesti and Ducreux [46] indicated that 70% of French industrial electricity consumption in 1996 was attributed to electric motors and, according to previous procedures, 75% of the losses in electric motors used were due to electricity loss and magnetism. Given the CO_2 losses, 4.5% of the total energy produced by the United States in 1992 was calculated as energy losses from electric steel. These central losses correspond to 4 × 10 million tons of carbon dioxide in the energy production process [46]. Although electrical steel manufacturers compete to produce electrical steels with fewer losses, the many variables in defining the final properties of electric steel are a frequent obstacle [47]. These include the chemical composition, the different stages of treatment, and finally the environmental process, which all affect the microstructure and physical properties. In summary [48]:

(1) Electrical resistance increases, which reduces induced eddy currents and energy loss.

(2) The magnetic anisotropy decreases, which lowers magnetic hysteresis losses and ensures that the magnetic properties of the material are more isotropic.

(3) The magnetostriction decreases, which leads to smaller dimensional changes with magnetisation and demagnetisation, and to a lower magnetic hysteresis loss.

(4) The saturation induction decreases as the density of the magnetically polarised atoms of the materials atoms decreases, which lowers the magnetic induction and maximising magnetic permeability.

(5) When the silicon content is higher than 3 wt-%, the brittleness of the steel is increased and the cold deformability is significantly impaired, which makes the material extremely difficult and costly to process.

The following sections will detail the effects of silicon addition on the microstructure and the consequences of its processing, electrical and its magnetic properties [49].

2.6 Magnetic properties

The magnetic properties of electrical steel depend on the heat treatment because increasing the average crystal size decreases the hysteresis loss. Hysteresis loss is determined by a standard Epstein tester and, for common grades of electrical steel, may range from about 2 to 10 watts per kilogram (1 to 5 watts per pound) at 60 Hz and 1.5 tesla magnetic field density. Electrical steel can be delivered in a semi-processed state. Consequently, after punching the final shape, a final heat treatment can be applied to form the normally required 150-micrometre grain size. Fully processed electrical steel is usually delivered with an insulating coating, full heat treatment, and defined magnetic properties, and is used for applications where punching does not significantly degrade the electrical steel properties. However, excessive bending, incorrect heat treatment, or even rough handling can adversely affect the electrical steel's magnetic properties and may also increase noise due to magnetostriction [50]. The magnetic properties of electrical steel are tested using the internationally standard Epstein frame method.

There are many properties that affect the final product of the electrical steel. A description of the most important properties follows:

2.6.1 Magnetic permeability

The permeability μ is the degree of magnetisation of a material that responds linearly to an applied magnetic field. which is a constant of proportionality that exists between magnetic induction *B* and magnetic field intensity *H*. It is determined as follows:

$$\mu = B/H \tag{2.3}$$

2.6.2 Magnetostriction

Magnetostriction is a property of magnetic materials that causes them to change their dimensions in the presence of a magnetic field. Magnetic materials have a structure that is divided into fields, each of which has a uniform magnetic polarisation zone. When a magnetic field is applied to the material, the boundaries between the fields change and the fields rotate.

Both of these effects lead to a change in the dimensions of the material [51]. High-friction magnetic materials can be used for different sensor applications, which causes them to change their shape or dimensions during the process of magnetisation. Although the magnetic friction of Fe-Si alloys is low (less than 10 ppm), it is responsible for acoustic noise in transformers.

2.6.3 Power loss

Figure 2. 6 illustrates the timeline for the improvement in the core loss of electrical steel over the past 100 years. Loss has been reduced very close to the theoretical value of 0.4 W/kg from the initial 15 W/kg at 1.5 T under 50 Hz AC magnetisation [52]. The four milestones during this history are the addition of Si in 1900, Goss texture in 1934, HGO steel in 1970, and amorphous material in 1980.

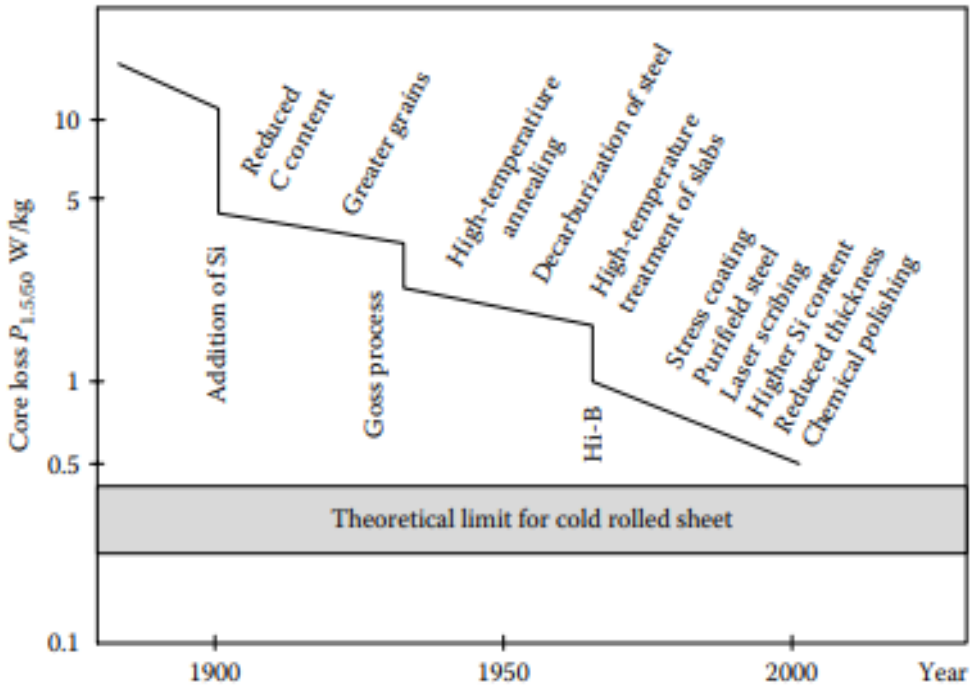

Figure 2-6 The timeline for the improvement in core loss of electrical steel [52].

In transformers or inductors, some of the power that would ideally be transferred through the device is lost in the core, resulting in heat. Electrical steels undergo cycles of magnetisation and demagnetisation, which dissipate energy. The difference between the input and output power is termed the power loss. The advance in production methods after 1934, when (GOES) was discovered, has reduced losses. However, around 5% [16] of the input power still lost in the transformer, which is due to the core loss and copper loss. Core loss is due to the hysteresis, eddy, and anomalous loss in the transformer, whereas the copper loss is due to the resistance in the transformer windings. The losses can also be categorised into load and no-load losses: the losses in the windings of the transformer are called load losses, whereas the losses in the coil of the transformer are called no-load losses. The core loss is subdivided into the following three categories.

2.6.3.1 Hysteresis loss

The greater the loop area, the greater the loss of each cycle. Hysteresis loss is the heating loss that is caused by the magnetic properties of iron. When the motor's core is in a magnetic field, the magnetic particles in the heart tend to conform to the magnetic field [53]. When the electrical machine core rotates, its magnetic field continues to change direction. The constant motion of magnetic particles when trying to conform to the magnetic field produces molecular friction.

The area of the B-H curve is equal to the hysteresis loss if measured at 0 Hz frequency for transformer steels. In cyclic magnetisation, the domain walls move constantly backwards and forwards, although these walls may be pinned by defects such as dislocations, grain boundary, impurity, or imperfection. Hysteresis loss occurs when these walls are annihilated, moved, or created. Although hysteresis loss is independent of frequency, practically it depends upon frequency. The frequency determines the number of domain walls in motion, which determines the hysteresis loss [16].

In Figure 2.7, when the magnetic field is initially increased, the magnetisation is reversible until a certain point, after which a further increase would result in an irreversible magnetisation. Point **a** in the loop denotes saturation induction, which means that a further increase in the magnetic field will not affect the magnetic flux density to a large extent. When the magnetisation is reduced to zero from **a**, the magnetic flux density does not become zero, but some magnetism is retained in the material, which is called as remanence. If the magnetic field is applied in the negative direction it, then goes to point **Hc** called the coercivity which denotes the amount of magnetic field required to reduce the magnetisation to zero. Point d is known as the saturation flux density in the negative direction. Hence, a cyclic loop is formed, which is known as the hysteresis loop.

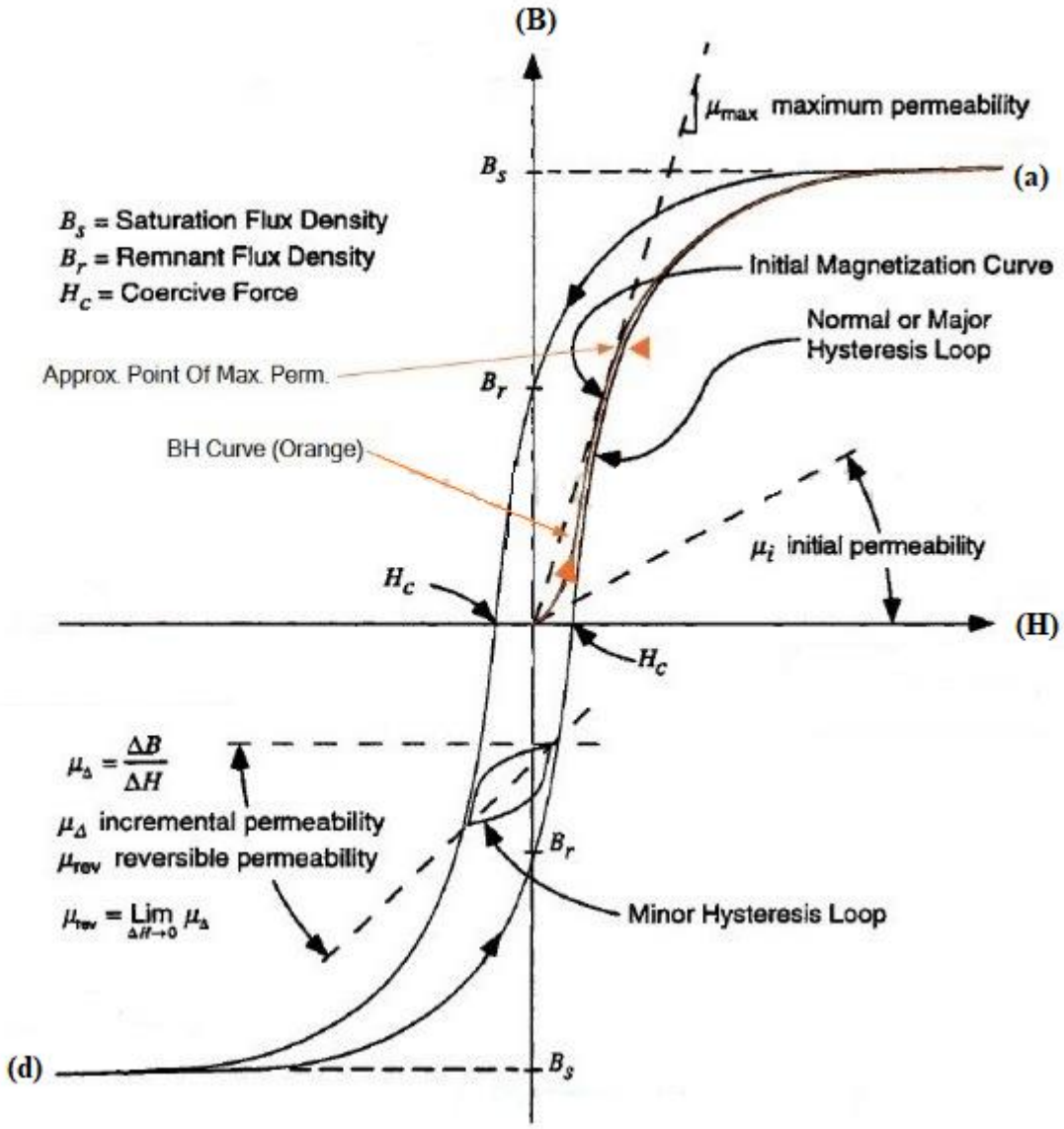

Figure 2-7 Hysteresis curve for a magnetic material.

2.6.3.2 Eddy current loss

The induction of eddy currents within the core causes a resistive loss. The higher the resistance of the core material, the lower the loss will be. Lamination of the core material can reduce the eddy current loss. A change in the magnetic field produces an opposing induced voltage, as per Faraday's law. This induced emf will produce currents that do not contribute to the output power and are lost as heat. Which is called eddy current loss and forms a significant

share of the total loss. A thinner laminated sheet, higher silicon content, and small grain size will decrease the eddy currents. As the thickness of the sheets is reduced, the electrons are restricted within the laminations, and hence wider current loops are avoided, overall reducing the eddy currents (as shown in Figure 2.8). The reduction of thickness sounds promising, but it also has many disadvantages: first, secondary-recrystallisation behaviour becomes unstable as the product becomes thinner; and second, hysteresis loss increases as the sheet thickness is reduced because the surface roughness contributes a major share of loss at reduced thickness [19].

Therefore, a balance has to be obtained for optimum thickness. The resistivity of steel can be enhanced by increasing the silicon content, which helps to reduce the eddy currents. Chun [20] increased the silicon content from 0.21 to 2 % in an electrical steel and increased the resistivity from 15 to 38 μΩ.cm. The eddy currents assuming uniform magnetic field, uniform material and no skin effect are calculated by equation (2.4). The classical eddy current loss for a constant permeability can be calculated from:

$$P_e = \frac{\pi^2}{6\rho} d^2 f^2 {B_{pk}}^2 \tag{2.4}$$

where ρ is steel lamination resistivity and d is the thickness of the lamination. P_e can be reduced by building the core from a stack of thin laminations with high resistivity to restrict the flow of the eddy current [54].

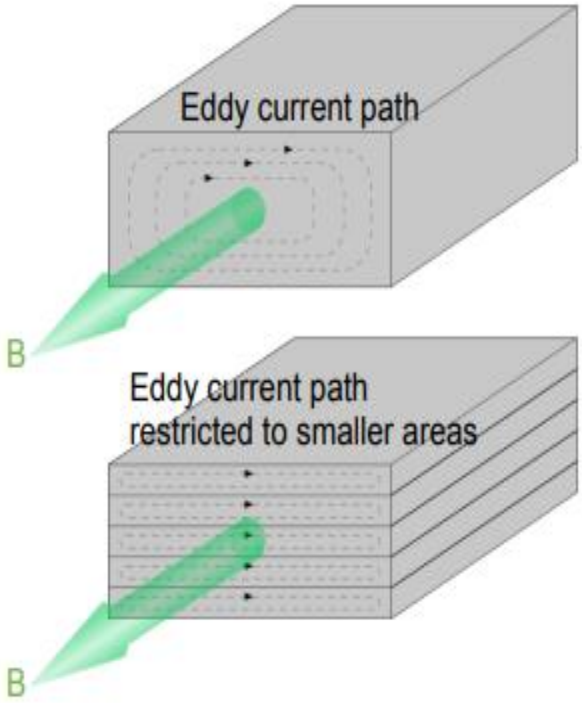

Figure 2-8 Schematic diagram of the eddy current path in a solid core and a laminated core [55].

2.6.3.3 Anomalous loss

Initially the difference between the practical loss and the theoretical loss was related to the flux harmonics, which occur due to the nonlinear B-H relationship. However, Brailsford et al. [56] proved that the extra loss could not be entirely due to the flux harmonics by modelling thin ferromagnetic laminations. To explain the anomalous loss, Agarwal et al.[57] introduced the factor of domain wall bowing. According to this effect, the centre of the wall moved more slowly than the surface, and hence the difference between practical and theoretical loss was termed an anomalous loss. The anomalous loss could be 50% of the total loss at frequencies of 50 and 60 Hz [58]. Anomalous losses depend upon the grain size a smaller grain size reduces the domain width. The domain width depends upon two energies: magnetostatic and domain wall energy. Minimising the sum of both energies determines the domain width, which is proportional to the square root of the grain size [59]. Because the domain width is smaller, the

domain wall travels less distance in the given time, which reduces the velocity of walls and minimises the anomalous loss.

2.7 Factors that affect the loss of electrical steel.

The effects of these factors will be explained in terms of total loss P_c, hysteresis loss P_h, and eddy current loss P_e, which are imported in terms of grain size, silicon content, and domain control.

2.7.1 Grain size

Grain size is a critical factor in magnetic materials and varies with the amount of cold rolling done, and upon subsequent annealing temperature and time. A large grain tends to have beneficial effect on magnetic permeability because it will have uniformly oriented domains throughout and a small field is required to align them; however, it will also have wide domain wall spacing, which increases loss. The wide domain spacing requires the walls to move rapidly at higher frequencies to revert to the initial state. Energy is dissipated in the creation of new walls or when there is bowing in the walls due to a large distance between the walls. Meanwhile, a small grain size will limit the anomalous losses because the domain wall velocity will be small but will have a large proportion of grain boundaries, which will limit the domain wall motion by pinning [40]. Although a balance has to be reached on the size of grain that is optimum for loss minimisation, the domains can be refined (narrowed) to reduce losses.

2.7.2 Impurity content

Impurities are present as precipitates of metal sulphides, carbides, or nitrides and their size varies from 10 – 400 nm. Aluminium nitride (AlN) and manganese sulphide (MnS) precipitates are useful inhibitors that allow preferential grain growth in the easy magnetisation direction.

However, too much precipitation hinders domain wall movement by pinning the walls. The amount of silicon content determines the magnetic permeability and the eddy currents that are observed. The addition of silicon raises the A3 (upper critical temperature 910 °C for 0% alloy addition) and lowers the A4 (1395°C for 0% alloy addition) temperatures as shown in Figure2.9, forming a gamma loop at 2.5% silicon and 1170˚C. As the silicon content is increased further, no change in phase occurs while cooling from high temperature. In this process, all forms of grain refinement are restricted, and the desired large grains are obtained. More silicon largely reduces the eddy currents. Furthermore, silicon increases permeability in low magnetic fields but decreases it at high magnetic fields. However, the brittleness of the material increases as the amount of silicon increases, so rolling becomes a problem once silicon exceeds 3%. Rolling transforms harmful carbides to graphite which is beneficial. Carbon is useful in getting a sharp crystallographic orientation simultaneously with large cold reduction. However, it is harmful in the form of pearlite because it mixes with iron to form undesired products and affects the magnetic properties. In addition, if carbon is present in the solid solution, it precipitates with the passage of time. This process is known as magnetic machinal and affects the domain wall motion, and hence increases the losses [60].

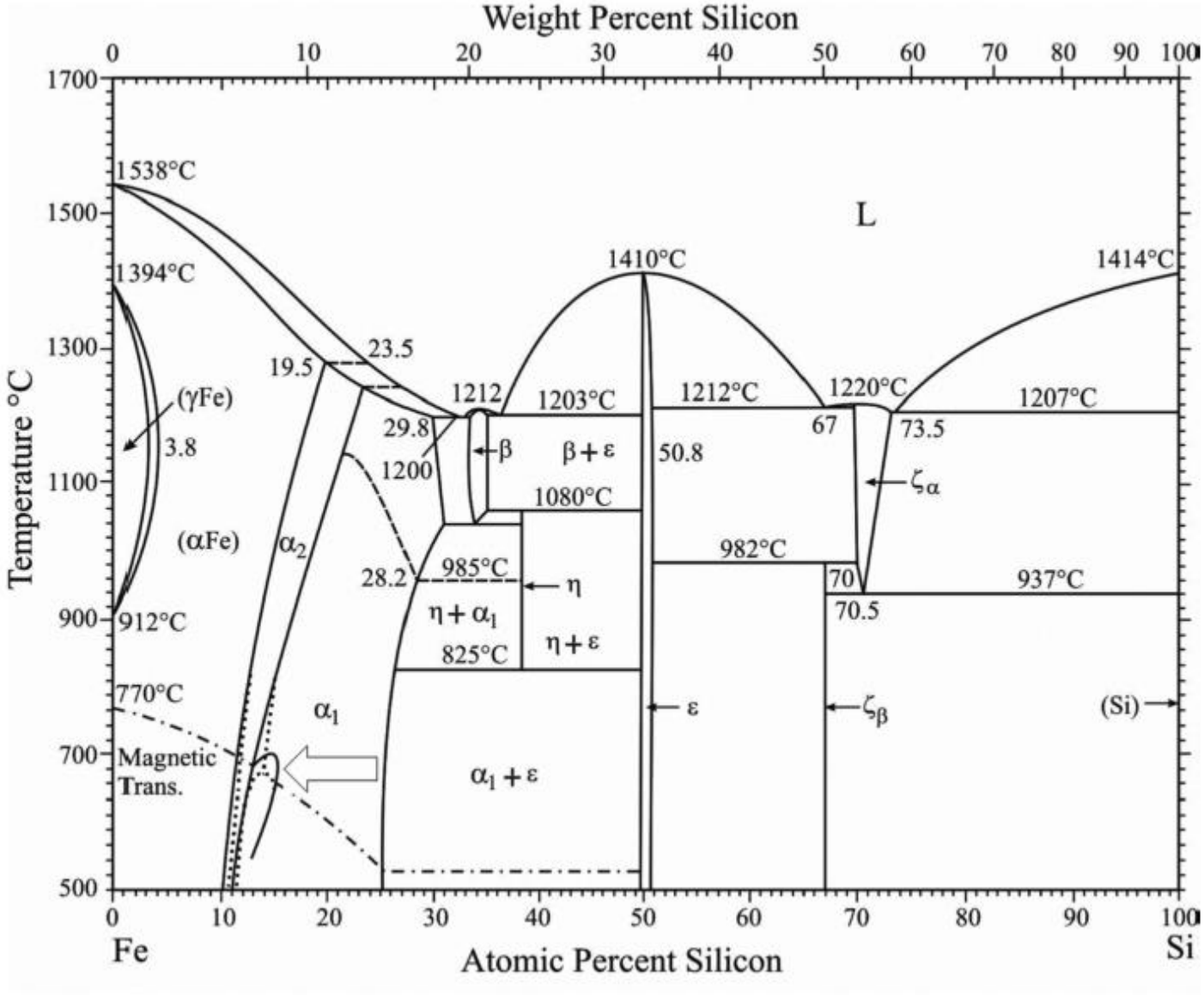

Figure 2-9 Iron-Silicon equilibrium diagram [60].

2.7.3 Soft magnetic materials

These materials are easily magnetised, and therefore a low coercive field is a prime requirement. The main application of these materials is in the cores of rotating electrical machines and transformers. The parameter that is often used as a figure of merit for soft magnetic materials is the relative permeability μ_r, which is a measure of how readily the material responds to the applied magnetic field. The other main parameters of interest are the

coercivity and saturation magnetisation, which are characterised by the hysteresis loop. The loop should exhibit a small area, which is proportional to the losses.

2.7.4 Hard magnetic materials

These materials are stable, are a permanent source of magnetic field, and are insensitive to external actions. They are characterised by a broad hysteresis loop. Hysteresis loops may take many different shapes. There are two important quantities, which are the remanent magnetisation: remanence *Mr*, and coercive field *Hc*.

2.7.4.1 Remanence

This is natural quantity expressing the fact that the ferromagnetic material can be spontaneously magnetised, even in the absence of external actions.

2.7.4.2 Coercive field

This is the field needed to bring magnetisation from the remanent value to zero. It measures the order of magnitude of the fields that must be applied to a material in order to inverse its magnetisation. Materials can be classified according to the values taken by these parameters. It is common to subdivide materials into soft and hard magnetic materials [61].

2.8 The effect of alloying elements on an electrical steel

An alloying element can alter the mechanical and chemical properties of steel. Alloys are regularly used to adjust the attributes of steel to make it more viable. A mixture of carbon and iron, steel has many advantages, such as corrosion resistance and added strength when alloyed with other elements. Which will be described in the following subsections.

2.8.1 Effect of aluminium

The addition of aluminium (and silicon) to steel increases electrical resistance and thus reduces energy loss in electrical appliances. It also has a favourable effect on magnetostriction. However, these additives make the steel extremely brittle and difficult to process in a conventional thermal-mechanical manner. Calvillo et al. [62] developed an innovative processing process that avoids the need to roll a fragile steel sheet. Their method consists hot dipping of solid steel in a pure aluminium bath, followed by diffusion treatment of the steel [62]. To study the interaction of aluminium with substrates and the diffusion process during the subsequent annealing process, two substrates (ultra-low carbon steel (ULC) and a Fe +3.4 % Si steel) were used for immersion in a pure aluminium bath. Dipping times and temperatures ranged between 700–750 °C and for between 5–1000 seconds. The different surface layers formed during dipping and after annealing were characterised with an Elcometer, by SEM and by Energy Dispersive Spectroscopy (EDS). The results show that the chemical composition of the obtained layers is highly dependent on the initial composition of the substrate. Diffusion gradients of Al and Si appear in the steel after hot dipping and diffusion annealing. Samples were produced showing the Si and Al concentration gradients. The energy loss of the substrate is only slightly reduced by 3.4%, and the ULC substrate offers an increase in energy loss after processing. However, this treatment still needs to be improved [63]. Aluminium has been added by a cladding method to 31% silicon-iron [64].

The study conducted by [65] has shown that using silicon as a diffusant may minimise the power loss of non-oriented silicon iron. Layer thickness is reduced when aluminium is placed unevenly across surface areas, including in terms of both content and thickness penetration. On both sides of the samples, there was evidence of a thin coating of porosity. When this method of diffusion is used, the composition changes the anisotropy constants very slightly, which possibly creates the right amount of internal stress [66]. However, a significant

drawback of this method is that a permeable material is created on the side of the steel. The amount of diffusant that permeates the steel sheet from the paste can be regulated by means of restricting several diffusants, either by means of the structure of the paste and depth or by creating an appropriate paste to guarantee that an excess of diffusant is always accessible. Prior to completely removing the remaining coating, the quantity of soft material can be modified by adjusting duration and heat. In addition, by establishing a controlled resistivity gradient along the thickness of the sheet, it might be possible to increase the steels effectiveness in distorted magnetisation conditions. To ascertain what happens to the magnetic properties of an electrical steel sheet when a distorted flux waveform is present, materials with different resistivities all the way through their thickness were made by diffusing tiny amounts of aluminium into silicon steel [67].

Aluminium is often added to electrical steels because this element improves the magnetic properties. However, the addition of aluminium is generally limited to 0.30% by weight. The semi-finished electrical-steel types that are produced with this technique have reached full growth of tubercle grains after decarburisation treatment. In terms of electrical resistance, the increase in Al content has led to a steady increase in this property. With regard to crystalline tissue, the increase in aluminium content caused a strong attenuation of gamma fibres, alpha fibres, cubed fibres, and Rolling Direction (RD) fibres. Regarding magnetic properties, an increase in the addition of aluminium has been shown to lead to a decrease in the loss of the magnetic core and did not significantly modify the magnetic permeability. The difference in magnetic core loss can be justified by the effect of aluminium on electrical resistance. In terms of magnetic permeability, the randomness of the texture and the more intense presence of the second phase molecules resulting from an increase in the content of aluminium had no strong negative effect. Therefore, alloys with concentrations higher than about 1% Al, showed the best magnetic properties along the RD; that is, a core loss of about

3.5 W / kg (1.5 Tesla and 60 Hz) and permeability close to 4000 g / Oe (1.5 tesla and 60 Hz) [68].

The effects of Al content ($0.53 \leq Al \leq 9.65$ wt%) on microstructure, texture, magnetic flux density, permeability, core loss and magnetic domain structure of Fe-Al based electrical steel were measured or observed. Average grain size decreased as Al content increased but the Al content had no severe effects on texture. Magnetic flux density and permeability tend to decrease as the Al content is increased [69]. The addition of aluminium to Goss-oriented silicon-iron has also been described [70][71]. This method takes samples of the sheet from which the glassy coating had been removed and a layer of aluminium is vacuum deposited onto it. The steel is then heated to a temperature of between 900° and 1100°C to allow the aluminium should diffuse into it and eventually become homogeneously distributed.

2.8.2 Effect of silicon-iron (Si Fe)

The most common materials that are used in electrical machines are iron alloys with a certain amount of silicon. These materials are available in a GO state (i.e., anisotropic material with different permeability in different directions) or in a non-oriented state (i.e., isotropic magnetic properties in all directions) [72]. Silicon makes the mechanical processing of iron more difficult and increases electrical resistance. The disadvantage is that there is a slight decrease in the magnetisation of saturation and reduced permeability [73]. Aluminium has a similar effect on electrical resistance but also reduces the permeability of the material. High manganese content results in large grains and thus increased permeability, but also increases losses [74]. Current trends in Si Fe steels mainly focus on reducing iron loss, witan emphasis on higher base frequencies due to increased machine speed and increased harmonics. It is claimed that an increase in the silicon content of a sheet may also be achieved by the selective removal of the iron by acidic attack [75]. In addition, oriented silicon-iron has been produced

by adding a secondary alloying non-element, such as nickel, manganese, or aluminium, to the melt in addition to, or partly as a substitute, for silicon [76][77].

2.8.2.1 High silicon-content non-oriented Si Fe

Silicon-containing layers were developed to increase the electrical resistance of the material and thus lose the eddy current. At present, the silicon content of these laths reaches 6.5%. However, in addition to reducing the maximum flux density and permeability of the high SiFe material, the silicon content makes alloys brittle and harder. This makes manufacturing processes more expensive and requires more complex and expensive tools [78]. Work had been done on the siliconising of steel for the purpose of increasing the hardness and corrosion resistance of components, and a method based on such processes has been used on Goss-oriented steel [79]. The original method placed the component in contact with silicon carbide. It was then heated to 1000°C and chlorine was passed over it [80]. One patent describes a process where ferrosilicon is mixed with alumina, an activating agent (e.g., ammonium iodide), and a polyalcohol binder diluted with water [81]. Another method to enrich non-oriented material consists of coating the sheet with tridecyl alcohol on to which powdered silicon is adhered [82].

2.8.3 Effect of cobalt–iron (Co Fe)

Co Fe is generally a more expensive alloy due to its high cobalt content. If mixed with iron, cobalt achieves the highest magnetisation of all materials at room temperature (2.43 tesla) for co-alloys of 35% and 65% iron[83]. In general, the Co content ranges between 15 and 49%, and generally includes about 2% Vanadium.

The mechanical strength of the material in terms of reducing iron loss and increasing magnetic permeability can be controlled by changing the ratio of the cobalt and iron content in the material [83], which leads to further integration of the material with Niobium or by

changing the temperature cycle during the annealing process that ranges from 750–950 C° [84] [85]. Low temperatures of the steel are favourable for improving the mechanical properties of the material, while high temperatures lead to larger grain sizes and hence magnetic properties improvement [86].

2.8.4 Effect of nickel–iron (Ni Fe)

Typical Ni Fe mills for electrical machines have a nickel content of 40–50%. Where the value is higher, the nickel content generally leads to increased permeability. However, the electrical conductivity and consequently the loss of eddy current also increase with the nickel content [87]. To develop fully advanced magnetic properties, NiFe alloys require a very high-temperature annealing process (usually> 1100 ° C), accompanied by the introduction of the surface oxide layer to develop their optimum magnetic properties.

About 45–50% of NiFe alloys are used in electrical machines where the focus is on low loss, such as dental and surgical instruments that operate in highly regulated thermal environments. Aerospace applications use low-loss and non-driving devices such as analysers [88], [89]. Figure 2-10 compares the initial BH magnetisation curve of typical lamination alloys of 0.35 mm thickness to 50% NiFe and 50% CoFe.

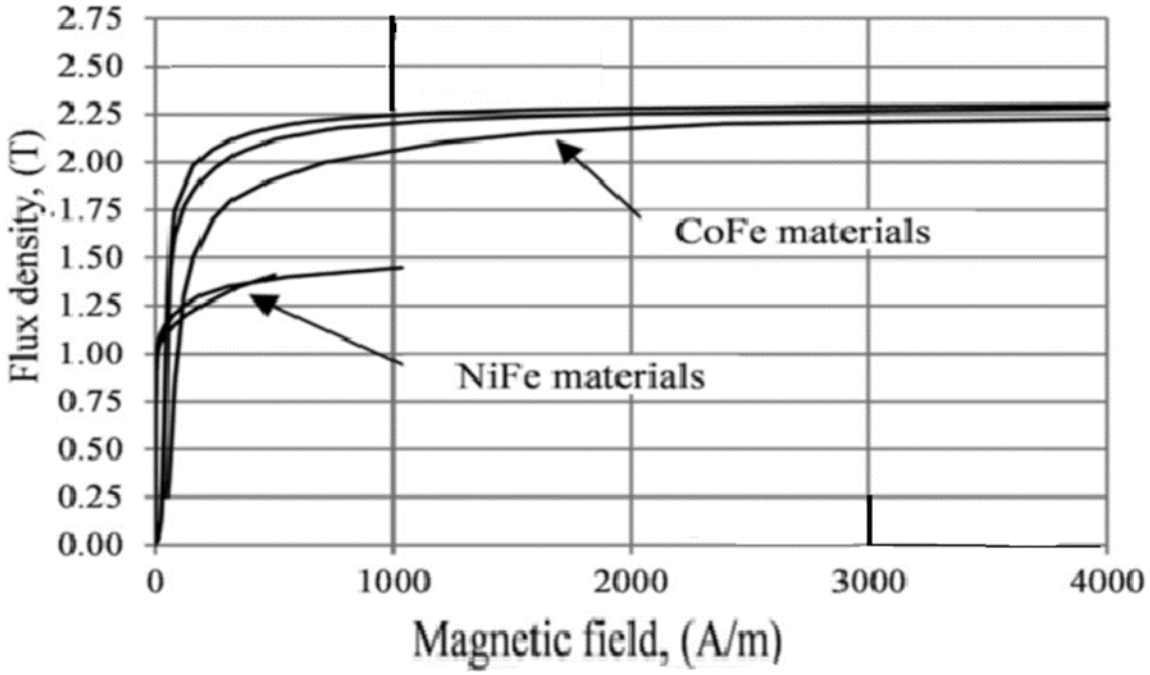

Figure 2-10 Initial magnetisation curves of 0.35 mm thick CoFe and NiFe [90].

The advantage of the high permeability and large resistivity of Ni Fe is further shown in Figure 2-11, where the iron losses are presented for the same materials at 400 Hz frequency.

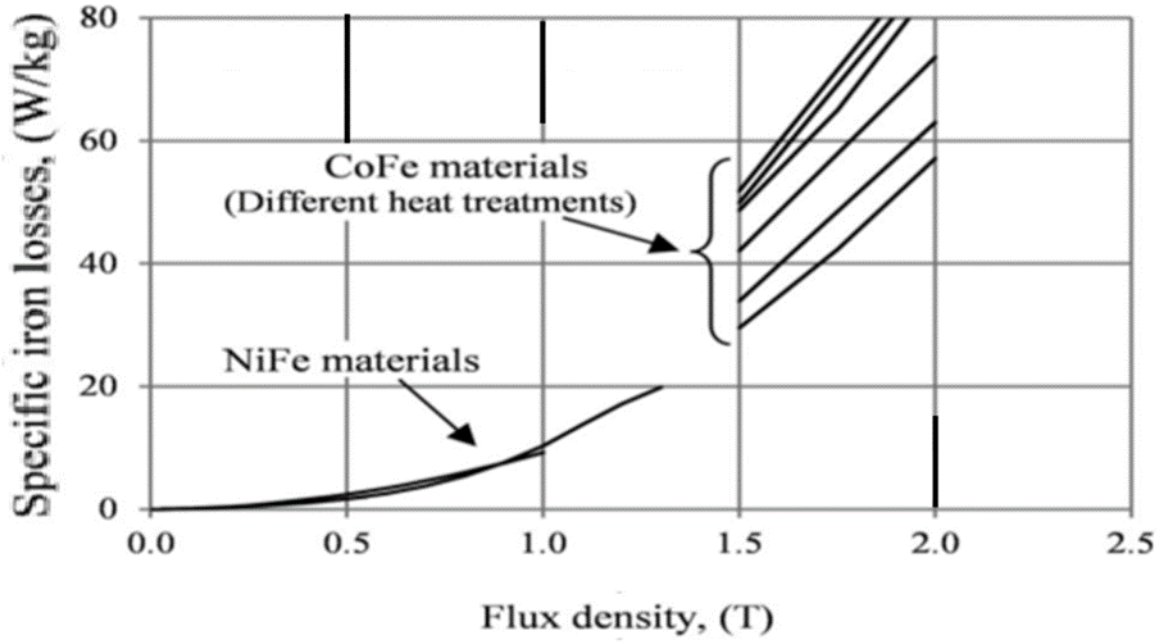

Figure 2-11 Typical iron losses of 0.35 mm thick CoFe and NiFe alloys at 400 Hz [35].

2.8.5 Effect of manganese

Manganese (Mn) is an ideal element in the case of an alloy because it has the ability to increase electrical resistance and thus reduce losses. If the sulphur content is low, then unwanted precipitation of MnS can be avoided and Mn stays in a solid solution [91]. Mn additives range from 0.25–0.64% by weight in an S free steel material, which linearly reduces losses (2.40 W/wt% Mn), and increases permeability and grain growth. Liao [92] found improved magnetic properties for electrical steels with 0.3–1.25 wt% Mn in Si free steels while higher Mn content causes smaller grains, which deteriorates the magnetic losses. In Yashiki and Kaneko [93], there was a decrease in grain size after final annealing and an increase in{222} tissue components due to precipitation of $MnSiN_2$ in in ultra-low S grades with 0.5 wt% Si, the amount of precipitation MnS remains constant when the content of Mn up to 0.94 wt%. In [74], an improvement in texture by 0.5 wt% of manganese was reported in alloy steels with a high Si content. The same is shown by alloying 1.3 wt% Mn in high purity 0.5 wt% Si steel, While Mn content increases, core loss decreases significantly and magnetic induction increases slightly at the same time [82] . Kubota [94] found a decrease in magnetic induction and an increase in core loss up to 2.0 wt% manganese in 3.0 wt% Si steels. Yield strength increases by solid solution strengthening of around 33 MPa/1 wt% Mn but no mention was made of the exact chemical composition of the material. Increased S content leads to deterioration of the material properties at each manganese level [95]. Very low S and O contents are essential for Mn alloyed electrical steels to keep Mn in solid solution and to avoid Mn precipitations such as oxides and sulphides[96] [97]. The results obtained so far are very contradictory and the net effect of Mn in alloy steels with a high silicon content has not been satisfactorily studied in steels that currently have very low levels of damping elements. Therefore, manganese increases the electrical resistance of 0.062 μΩm / 1 wt%Mn, which leads

to a decrease of losses at f> 100 Hz due to a decrease in the dynamic part of the iron losses, which makes manganese alloy suitable for high-alloy steel sheets [98].

Several efforts have been made to investigate the influence of manganese on high silicon alloyed electric steels with varying Mn contents (0.20, 0.69, and 1.38 wt%). The effect of Mn on mechanical, microstructural, and magnetic properties has been thoroughly investigated in [98]. The addition of Mn reduced grain size while also improving electrical resistance, results in decreased core losses at higher frequencies. The authors found that revealed that Mn (0.3–1.5 wt%) in electrical steel improves its magnetic characteristics. However, if the Mn concentration exceeds the range 1.5 wt%, the grains become smaller and the magnetic losses increase[99]. It has also been found that when Mn concentrations are high, core loss drops significantly and magnetic flux density rises modestly [92].

2.8.6 Effect of phosphorus

Tanaka and Yashiki [100] studied the effect of phosphorus on the magnetic properties and texture of crystallisation. Magnetic induction increases with the addition of phosphorus and the magnetic induction of high-phosphorus steel decreases slightly with an increasing deficiency in cold rolling. In recrystallisation materials, the strength of high- phosphorus steel {111} <112> is lower than that of low phosphorus steel. These textures correspond to the change of magnetic induction with the addition of phosphorus. High-phosphorus steel recrystallisation without separation treatment is close to that of low phosphorus steel. Therefore, the separation of phosphorus within the limits of primary grains is responsible for controlling the crystallisation texture [100].

2.8.7 Effect of chromium

The effects of chromium additives on the microstructure desired phase and magnetic properties of Fe-6.5% Si alloys manufactured by hot-rolling and warm-rolling have been

studied. The results show that the chromium additives effectively reduced the size of the alloy bead and that the extraction density decreased with increasing chromium content. The amount of phase required in the alloys with chromium content was reduced by 1.0 wt%. In addition, the magnetic properties of the alloy with chromium did not deteriorate [101].

Komatsubara et al. [102] studied a new magnetic material has been developed for high-frequency appliances, and its properties have been investigated and compared with conventional electrical steel and 6.5% Si steel. The new material has extremely low iron loss at high frequencies over 5 kHz as well as 6.5% Si steel, which was obtained by increasing electric resistivity, or by reducing its eddy current loss. Generally, increasing resistivity makes steels brittle and deteriorates their workability. However, this material showed a good workability with the effect of Cr addition. This material also has a good property of pulse response and showed an excellent performance for power electronic devices using an active filter operated at 15 kHz.

2.8.8 Effect of tin

The effects of Sn addition on core loss and texture of NOES have been investigated. The reasons for reducing core loss and the intensity of unfavourable texture were analysed [103]. Iron loss of indirect electrical steel includes loss of hysteresis and loss of eddy current, while the loss of hysteresis is a large part of power loss. A study was made to improve the crystalline texture in view of reduced hysteresis loss and increased magnetic flux density and permeability [104]. As result, it was found that Sn can also significantly improve the crystalline texture. According to [105], the grain size is associated with the separation of Sn, which hinders the growth of the grain. The improvement in magnetic properties is induced by the addition of Sn. By adding Sn, both reduced core loss and increased magnetic flux density are attained. However, by adding more than 0.1wt% Sn, core loss begins to increase, which is the contrary effect obtained when less than 0.1 wt% Sn is added. These improvements in magnetic

properties that are induced by the addition of Sn correspond to the improvement in crystalline texture provided by the addition of Sn [106].

2.9 The production and advancement of electrical steels

Electrical steels (Fe-3wt. %Si) are mostly used in the core of transformers, generators, and motors. Figure 2-12 shows the evolution of electrical steel in the twentieth century. The development of electrical steel started with Hadfield's production of 3% silicon steel in 1903, which had a significant effect on loss reduction [47]. Advances in material processing reduced the impurity content in steel, which enhanced the magnetic properties. The development of the cold rolling process further reduced the thickness and improved the magnetic properties.

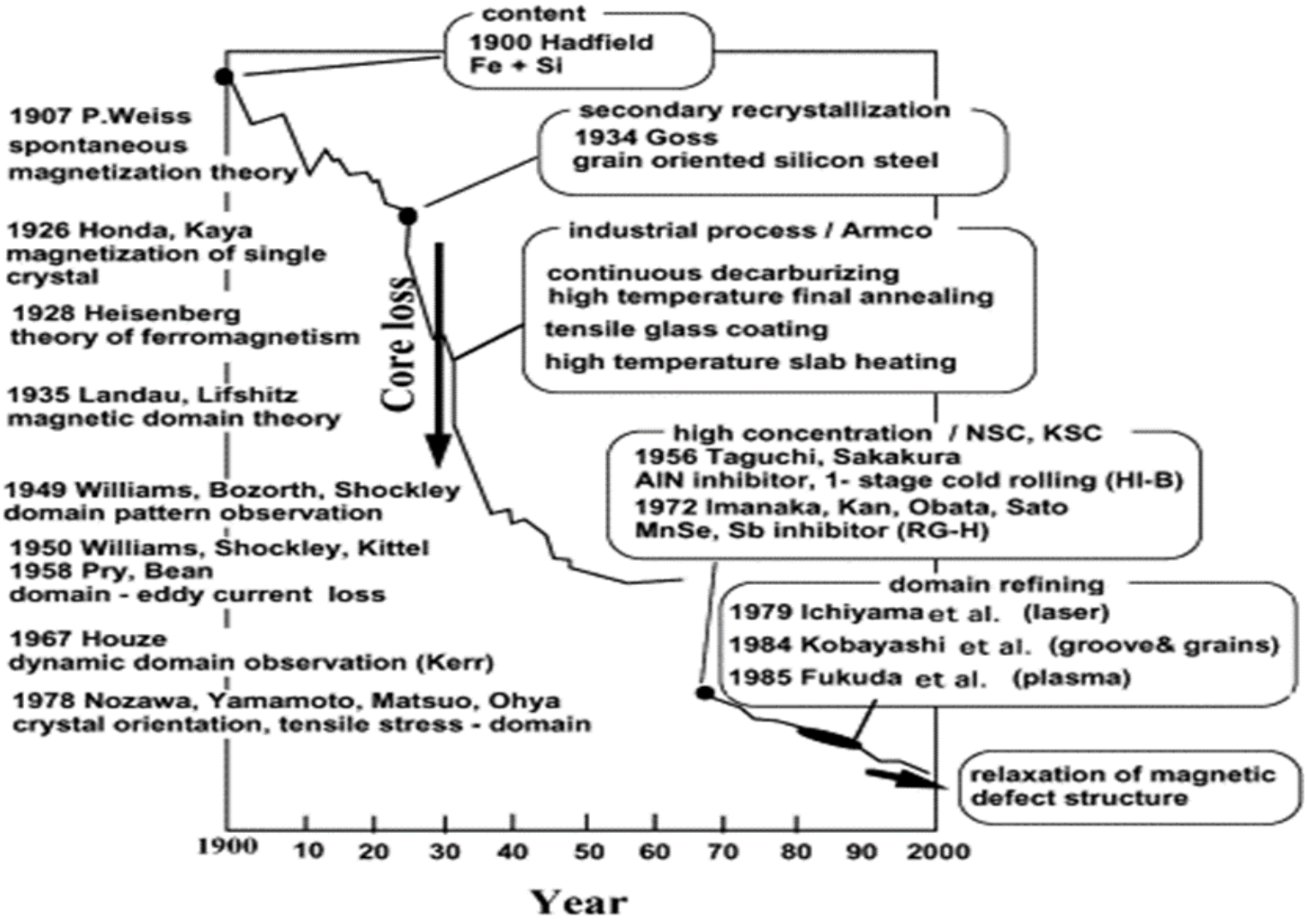

Figure 2-12 Historical development of core loss reduction in GO silicon steel and progress of relevant science and technology [42].

In 1934, Goss developed the idea from the works of Beck [48] and Ruder [49] that iron has high magnetic permeability in certain crystallographic directions and planes. In this type of steel, the grains are oriented such that the (100) direction is parallel to the direction of rolling and the (110) planes are parallel to the surface of sheet. This production process involved two stages cold reduction and intermediate annealing, followed by decarburisation, batch annealing, and flattening. Modern day production of electrical steel still relies on this texture, which is commonly known as Goss texture and the steel is popularly called GO steel.

Nippon Steel in 1994 produced a new type of high permeability steel, known as HiB [50]. This manufacturing process was different from that fore Goss steel because only one cold rolling reduction was applied, and AlN was used as the primary inhibitor while MnS was used as the secondary. The angle of orientation with the RD was decreased from 7˚ to 3˚ but the grain size increased from 0.3mm to 1 cm [51].

The ever-increasing demand to increase efficiency led to new domain refining techniques, and Nippon Steel developed laser scribing [28], where losses were found to be 0.85 W/kg at 1.7T for a thickness of 0.23mm. These losses were 5 – 8% less than the unscratched HiB steel [51]. A recoat on the damaged surface was necessary as the coating vaporised. Other methods have also been employed to achieve the same where grooves were made on steel on which a ceramic coating was deposited [54]. The grooves were able to refine domains and the ceramic coating was able to apply tension on the GOES substrate.

2.10 Influence of coating on electrical steel

Efforts are being made to produce high performance electrical steels through several methods including better secondary-recrystallisation methods [74], grain orientation control [78], increasing the electrical resistivity, gauge reduction [83], and understanding the magnetic domain structure [40][84][85]. Perhaps the greatest gains can be made by employing effective stress coatings, which can play a dominant role in minimising losses and magnetostriction [19][86].While manufacturing a transformer, the steel sheets are free from any stress. However compressive stress develops in the process, which increases magnetostriction. If we can induce tensile stress in the sheet, then the compressive stress that is developed will be counter balanced. This is the reason for the application of coatings which can apply tensile stress on steel.

Power losses can be minimised by exploiting the surface of GOES [87]. The surface roughness can be manipulated, or surface stress could be varied to bring down the overall power loss by using coatings. Wada et al. [88] have shown that power losses could be reduced by 30–40 % on improving the surface roughness. Tensile stress is beneficial to reduce power losses. Conventionally, coatings which have low coefficient of thermal expansion when cooled from high temperature are used because they contract less than the substrate. This difference in cooling applies a tensile stress on the substrate.

Coating the steel helps to reduce both the losses and the magnetostriction. Coating minimises the eddy current loss by providing insulation resistance and reduces the hysteresis and anomalous loss by improving the surface roughness and beneficial tensile stress to the substrate [40][88]. A higher surface roughness increases the number of free poles. These free poles pin the domain wall motion. The number of mobile domains is reduced, and this leads to inhomogeneous domain wall motion. Freeing up these domains leads to a significant amount of energy loss. Improvement in surface roughness would lead to an increase in the number of mobile domains and reduce the energy consumption which reduces the total loss. Tensile stress imparted from the coating on the steel sheet eliminates the surface closure domains whereas losses are reduced as tensile stress helps in narrowing the domain wall spacing which decreases the anomalous loss. The reverse happens when compressive stress is applied on GOES. According to Kuppers et al. [89], the coercivity of the magnetic material can be reduced by eliminating the supplementary structures, and hence the hysteresis loss can be improved. The refinement in hysteresis loss is due to the reduction in the surface closure domains.

There are a number of alternative methods that can be used to apply a coating on the surface of steel sheet, such as sol gel [99], CVD [92], PVD [93], plasma spraying, wet coating, printing, and electroless and electro chemical plating [107]. The desirable properties in a coating are insulation resistance, heat resistance, chemical resistance, punchability,

weldability, corrosion resistance, burn out characteristics, resistance to compression, coating thickness, surface roughness, and scratch resistance [108]. A previous study aimed to produce siliconised steel by reacting the steel with silicon tetrachloride by plasma spraying either silicon or iron onto the surface of the steel followed by diffusing anneals [109] .

Yamaguchi et al. [92] deposited a titanium carbide (TiC) coating of 1 μm thickness on 0.23 mm thick GOES and found that the coating was effective in reducing losses up to 0.586 W/kg. The coating was deposited by chemical vapour deposition. The authors found that the eddy current loss was reduced by the coating, whereas no effect on hysteresis loss was noticed.

Nishiike et al. [94] combined the effect of surface roughness and tensile stress and measured a loss of 0.6 W/kg. The GOES was chemically polished to surface roughness R_a of 0.05 μm and stressed to tensile stress of 45 MPa. It was shown that the reduction of power loss was due to the increase in the number of mobile domain walls by polishing and the application of tensile stress, which reduced the eddy current loss. The application of tensile stress was divided into two parts. Below 10 MPa tensile stresses, the mechanism of loss reduction was due to reduction in domain size. Above 10 MPa, the rotation of magnetisation in the direction of rolling improved the performance of electrical steel. It was also shown that above 10 MPa the power loss was saturated and parallel to the horizontal axis of tension [110]. Electrodeposition has been used to coat unalloyed iron with a layer of silicon-iron [111].

2.11 Summary

The chapter provides a comprehensive review of research on power losses in electrical steel dating back to the nineteenth century. It highlights numerous studies focusing on methods to reduce power losses, such as enhancing resistivity through material additives. This review forms the basis for upcoming chapters, which will investigate the effects of various materials on electrical-steel cores. The objectives of the research are formulated based on identified

knowledge gaps, aiming to deepen understanding and contribute new insights to the field. Through this approach, the study aims to advance the development of more efficient electrical steel materials.

Chapter 3: Experimental works

3.1 Introduction

This chapter will present the details of the preparation of the samples and the techniques used in analysing them. The experimental details for the preparation of both uncoated and coated samples are provided. A description of the basic background theory of the analytical techniques used throughout this study will follow.

3.2 The method of diffusing an element into steel sheet

An idea was formed to incorporate the elemental materials in the form of a powder into a paste that could be applied to the metal surface. It was hoped that upon drying this paste and heating it to a suitable temperature that a proportion of the materials would diffuse into the steel, and hence further anneals could be used to obtain the desired concentration profiles. The crucial part of this scheme was to select a suitable liquid medium to act as the binder for the paste. Because the magnetic properties of steels are adversely affected by the pick-up of very small amounts of carbon, it seemed desirable to avoid the use of any organic materials that might decompose to yield elemental carbon at the elevated temperatures necessary to effect diffusion. In addition, it was clearly necessary for the paste to wet the steel surface and remain adhered to it after drying and further heating. Clearly the binder must remain (i.e., neither evaporate nor decompose) until at least a planned temperature is reached where the materials start to diffuse. The materials that appeared to fit these conditions were sodium silicate solution and silicon oil. Upon drying, this liquid becomes an amorphous glassy solid that could be expected to adhere the material's particles to the steel surface at elevated temperatures. To test this idea, an apparatus was required to fulfil the following functions:

1. Mixing the paste and applying it to the steel surface.

2. Heating the coated sample in a controlled atmosphere to such a temperature to affect the diffusion of the materials into the steel.

3. Testing the sample to measure changes in its electromagnetic properties.

4. Testing the sample to measure changes in its chemical composition.

3.3 Experiments to assess the viability of the paste process

The first priority was to establish whether or not materials could be diffused into steel from a paste made from that element in powder form, and sodium silicate solution and silicon oil. Therefore, a paste was mixed with sufficient silicone oil solution added to the manganese (IV) oxide (MnO2) powder to achieve a thick creamy consistency. The density of the solution was 0.5 gm/ml. The paste was subsequently subjected to a drying process at 50°C for 1 hour to confirm complete acetone evaporation and adequate adhesion of the manganese and was left to air dry overnight. This paste was then brushed onto both sides of a coated 0.35 mm thick same-size sample (non-oriented 2.4% silicon steel). The firing was carried out in the annealing box furnace that was described in Section 3.2.3.1 at a temperature of 525°C for 1.5 hours under an atmosphere of hydrogen. The rate of heating of the furnace was 200°C per hour. They were left in the furnace to cool down to room temperature. Upon removal from the furnace, the coating had become cracked and crumbly in some places, while remaining coherent and firmly adhered in others. Before testing the sample, the coating residue was removed by a combination of abrasion by emery paper and scraping with a blade edge.

3.4 Parameters of the process

This section has four sub sections, as follows: materials selection, preparation of samples, annealing and heat treatment, and magnetic property measurements selection. The experiments conducted for this study had two distinct stages. In the first step, the permeability and power loss for NO electrical steel samples prior of both materials, manganese (IV) oxide paste, and cobalt oxide (II, III) paste coating, were measured. In the second step, the permeability and power loss of the samples coated with manganese (IV) oxide paste and cobalt oxide paste were measured and compared to the uncoated samples. The term "coating" subsequently refers to applying paste of both materials to the coated Si-Fe strips.

3.4.1Material selection

3.4 .1.1 Powder compaction (MnO2)

The material proposed in this chapter is manganese (IV) oxide (MnO_2) powder activated, ~85%, (Merck Life Science UK Limited), with particle size <10 μm (as analysed by the supplier). In addition, this study made use of silicone oil supplied by Merck Life Science UK Limited, which was utilised as the adhesive and diluted by using acetone as a pure solution. The adhesive's physical characteristics are listed in Table 3.1.

Table 3-1 Characteristics of the adhesive.

Adhesive type	Density	Melting point	Boiling point
Silicone oil	0.967 g/mL at 20 °C	55 °C	140 °C

3.4.1.2 Mixing silicone oil into MnO2 powder

Powdered manganese (IV) oxide (MnO_2) and silicone oil solution were combined to make a paste. Silicone oil comprised 0.5 wt% of the paste composition per gram of manganese (IV) oxide. The paste was then dried at 50°C for 1 hour to verify that the acetone had fully evaporated, and the powdered manganese had adhered sufficiently.

3.4.1.3 Powder compaction (Co_3O_4)

The preparation of cobalt (II, III) oxide (Co_3O_4) was powder activated, ~99%, (Merck Life Science UK Limited), with particle size <10 μm (as analysed by the supplier). Similarly, this study made use of sodium silicate solution that was provided by Scientific Laboratory Supplies, which was utilised as the adhesive.

3.4.1.4 Mixing sodium silicate solution into Co_3O_4 powder

Powdered cobalt (II, III) oxide (Co_3O_4) and sodium silicate solution were combined to make a paste. Silicate solution was provided by "Scientific Laboratory Supplies" and was used as a lubricant between the particles, as well as to reduce die wall friction, and hence to avoid non-homogeneous density distribution. Sodium silicate solution comprised 0.5 wt% of the paste composition per gramme of cobalt oxide. The paste was then dried at 50°C for 1 hour and the powdered cobalt adhered sufficiently.

3.4.2 Sample preparation

3.4.2.1 Preparation of samples without coating

NOES, 2.4wt %Si-Fe, 30 mm × 0.305mm × 300 mm (width × thickness × length) M330-35A was employed in this study. Table 3-2 details the variation in the chemical properties of the grade, which further contains minimal quantities of other components that are

consistent between the grades. The steel was supplied by Tata Steel/Cogent Power Limited and punched using new tooling by Wingard & Co, Baltimore, USA. The manufacturer's material data for the M330-35A samples are given in Table 3-3 [112], [113].Figure3-1 shows the samples before annealing.

Table 3-2 Chemical composition of M330-35A samples.

Grade	C%	Si%	Fe%	Al%
M330	0.0035	2.4	Balance	0.3

Table 3-3 Manufacturer-provided material data for M330-35A samples.

Grade	Thickness (mm)	Resistivity (μΩcm)	Elastic Modulus, Rolling Direction (N/mm^2)	Elastic Modulus, Transverse Direction (N/mm^2)	Yield strength (N/mm^2)
M330	0.35	2.4000	200 000	210 000	315

Prior to coating the samples, the power loss and permeability of the NOES were tested using a Single Strip Tester (SST) at inductions of 0.5–1.7T and magnetising frequencies of 50, 100, 200, 400, 500, and 700 Hz, up to 1 kHz. In typical applications, frequencies are commonly at 50 Hz, 400 Hz, and 1 kHz, to maximize the operational amplifier capabilities according to its specifications.

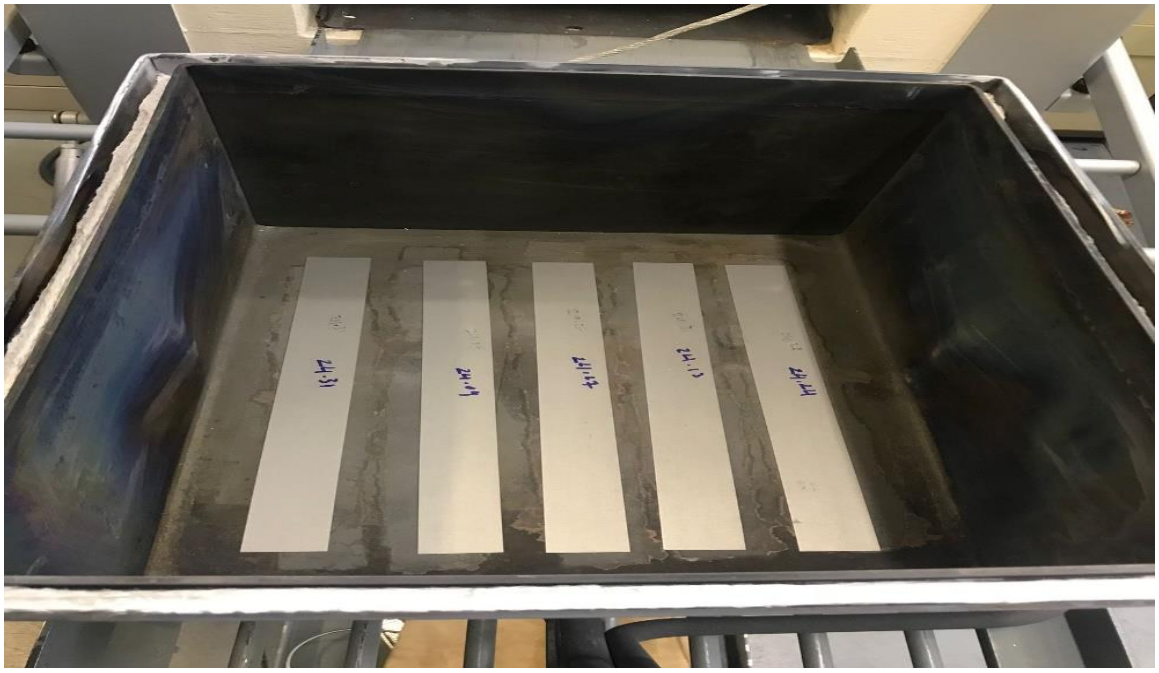

Figure 3-1 The samples before annealing.

3.4.2.2 Preparation of samples with coating

The laboratory was equipped with tools for mixing and applying pastes. A glass beaker and spatula were employed for paste blending. Powders were weighed using a balance, while liquids (silicone oil solution and sodium silicate solution) were utilized in appropriate quantities. The measurement of sodium silicate and silicone oil was carried out using a graduated syringe. Application of the paste onto the steel sheet was achieved using a brush with fine hairs.

3.4.2.2.1 Samples coated with MnO_2.

Manganese (IV) oxide (MnO_2) powder was mixed with a silicone oil solution to form a paste. The MnO_2 paste was applied onto the sample surface, which was then coated on both

sides of the NOES strips, as shown in Figure 3-2.

Figure 3-2 The coated samples.

In the next stage, the annealed samples were reheated after coating (see Figure 3-3). The samples were then annealed at three distinct temperatures (i.e., 535, 700, and 800°C) and at three different times (i.e.,180, 60, and 45 minutes). Subsequently, they were left in the furnace to cool down to room temperature.

Figure 3-3 The samples after annealing.

3.4.2.2.2 Samples Coated with Co_3O_4

The Co_3O_4 powder was mixed with a sodium silicate solution to form a paste. The resulting paste was then used to coat the strips, as depicted in Figure 3-4.

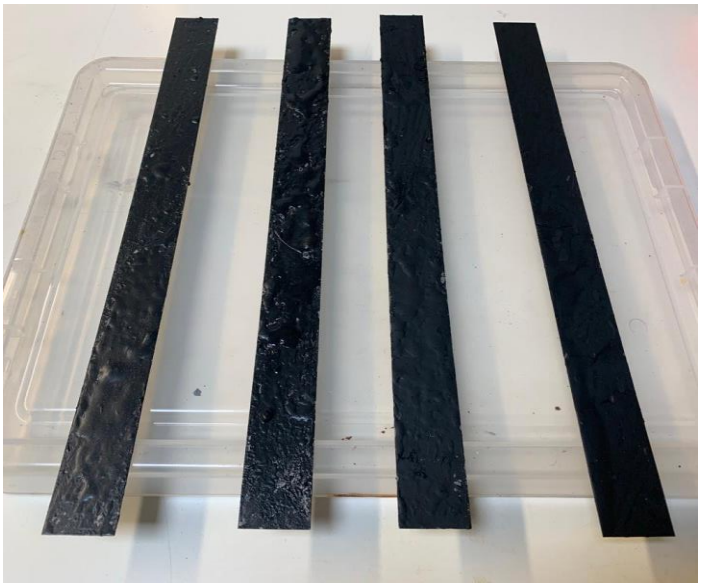

Figure 3-4 the coated samples.

3.4.3 Annealing

Figure 3-5 illustrates the specially designed firing and annealing apparatus used in this study. The system included chamber furnaces (N 7/H - N 87/H) with a maximum temperature capability of 1280 °C and was controlled by a B400 controller offering 5 programs, each with 4 segments. The temperature uniformity within the system was maintained at approximately +/− 10 °C, complying with DIN 17052-1 standards, and was provided by Nabertherm.

Figure 3-5 Firing and annealing the samples.

The heating chamber comprises various components for heat treatment in a protective gas environment, which include protective gas boxes, annealing furnaces, forced convection furnaces, and pit-type furnaces. These furnaces can be upgraded to accommodate heat treatment processes involving non-flammable protective and reactive gases. Figure 3-6 illustrates the use of a charging cart in conjunction with protective gas boxes to create a protective gas atmosphere. Figure 3-7 depicts the annealing box used for placing the samples during the charging process.

Figure 3-6 Box for a protective gas atmosphere using a charging cart.

Figure 3-7 The samples in the annealing box.

The heating elements are mounted on support tubes to ensure efficient heat radiation and extended lifespan. The movement of the door is cushioned by gas damper struts. Figure 3-8 shows the table-top model of the chamber furnace, specifically the N 7/H model, equipped with a B400 controller that is capable of handling five programmes with four segments each.

Figure 3-8 The table-top model chamber furnace N 7/H.

The Nabertherm compact hardening systems has several components, a hardening furnace, a tempering furnace, a quenching bath, and a cleaning bath. The system is versatile and can be utilised for various heat treatment processes within a workshop setting. Figure 3-9 shows a deep furnace chamber with three-sided heating, employing heat from both side walls and the bottom.

Figure 3-9 A deep furnace chamber with three-side heating (i.e., from both side walls and the bottom).

3.4.3.1 Heat treatment

The furnace is heated by eight cruciate rods that are mounted symmetrically around the tube at such a distance from it as to obtain uniform heating around its circumference. Control of the furnace temperature is by a platinum/platinum-rhodium thermocouple that is inserted into a sheath that is mounted onto one of the endcaps, whose output is fed into a cam-operated controller that regulates the heating element current. The cams were cut to produce the required rise and fall rates, together with the soak temperature. The length of the heated zone was 30 cm, and the temperature was found to be constant to within +/− 3° cover the middle section of 15 cm at a nominal temperature of 800°C. The samples were annealed in an argon gas atmosphere in a fired furnace at a temperature rate increase of 200 °C/h to reach 800 °C after 4 hrs, which was then held for up to 2 hours. For stress relief, annealing at 800 °C was carried out downstream of the main annealing process. The temperature curve of the stress-relief annealing in relation to the recording of the furnace cycle is shown in Figure 3-10.

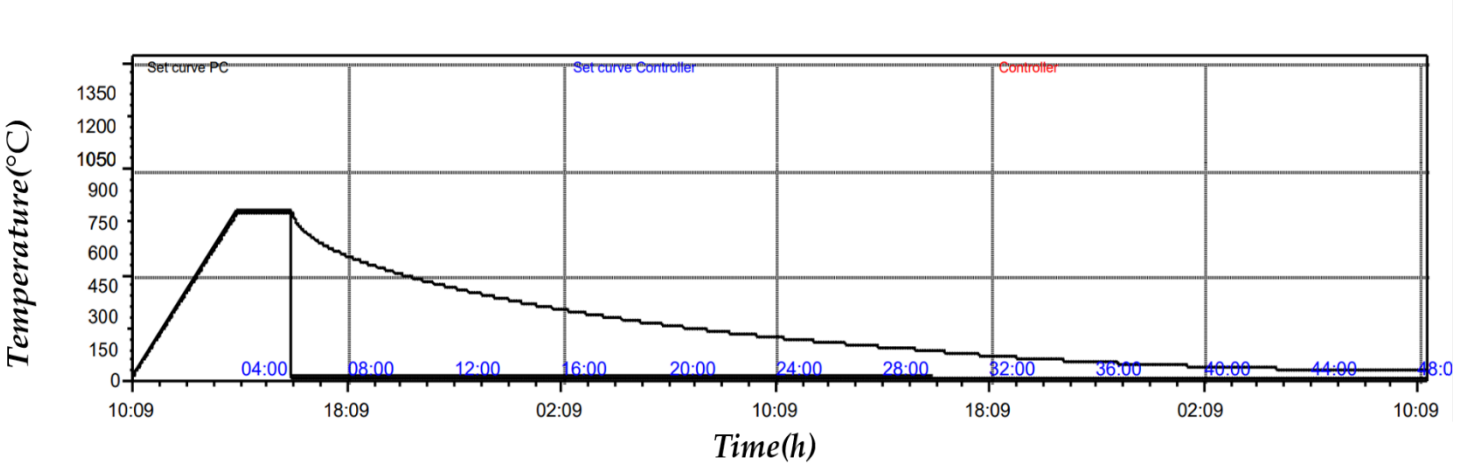

Figure 3-10 Temperature and times for the diffusion annealing process.

During the sintering process, argon gas was utilised as a protective environment (as shown Figure 3-11). Prior to the annealing cycle, the furnace was cleansed for 30 minutes with an argon gas flow of 5 l/min to remove any traces of the ambient air. The flow rate of the argon gas was set at 4 l/min throughout the duration of the heat treatment. Because there was nothing to prevent argon from escaping through the slot or air from entering while the sample was in the furnace, a high through put of the gas had to be maintained to prevent oxidation. It was found that special care had to be taken to ensure that the paste was dry before inserting the samples into the furnace because if this was not the case, then serious bubbling occurred due to the rapid rise in temperature.

Figure 3-11 The flow rate of argon gas during the annealing process.

3.4.4 Magnetic property measurements by SST

Measurements of power loss and magnetostriction were carried out under sinusoidal flux conditions with frequencies of magnetisation ranging from 50–1000 Hz. SSTs, as shown in Figure 3-12, or Epstein frames are regularly used to determine the characteristics of electrical steel, as recommended by IEC-Standards (IEC 404-2) [114] and (IEC 404-3)[115]. The significance of this type of measurement system is specific to the permeability and power loss (W/kg) at various magnetising frequencies. The Magnetics and Materials Research Group at Cardiff University developed the SST system, which delivers highly accurate and automatic measurements. With the exception of the frame itself, the Epstein frame system is comparable to the SST [116]. The system is shown in Figure 3-13 and comprises a PC with LabVIEW version 2019 already installed (as shown in figure 3-14), a DAQ (data acquisition Card) from NI PCI-6120, a power of amplifier, a 1 ohm shunt resistor (Rshunt), and an air flux adjusted SST [117], [118]. According to IEC 404-3, twin vertical yokes of GO silicon steel or nickel-iron alloy are employed. The main winding has 865 turns (N_1) and is wrapped around the

secondary winding, while a secondary winding of 250 turns (N_2) is wrapped around a plastic frame. Between the yokes is a typical Epstein strip sheet that is 305 mm long and 30 mm wide. This setup provides a low reluctance path. Alternating current (AC) tests were performed under comparable settings, with frequencies ranging from 50–1000 Hz.

Figure 3-12 Single strip tester for magnetic characteristics.

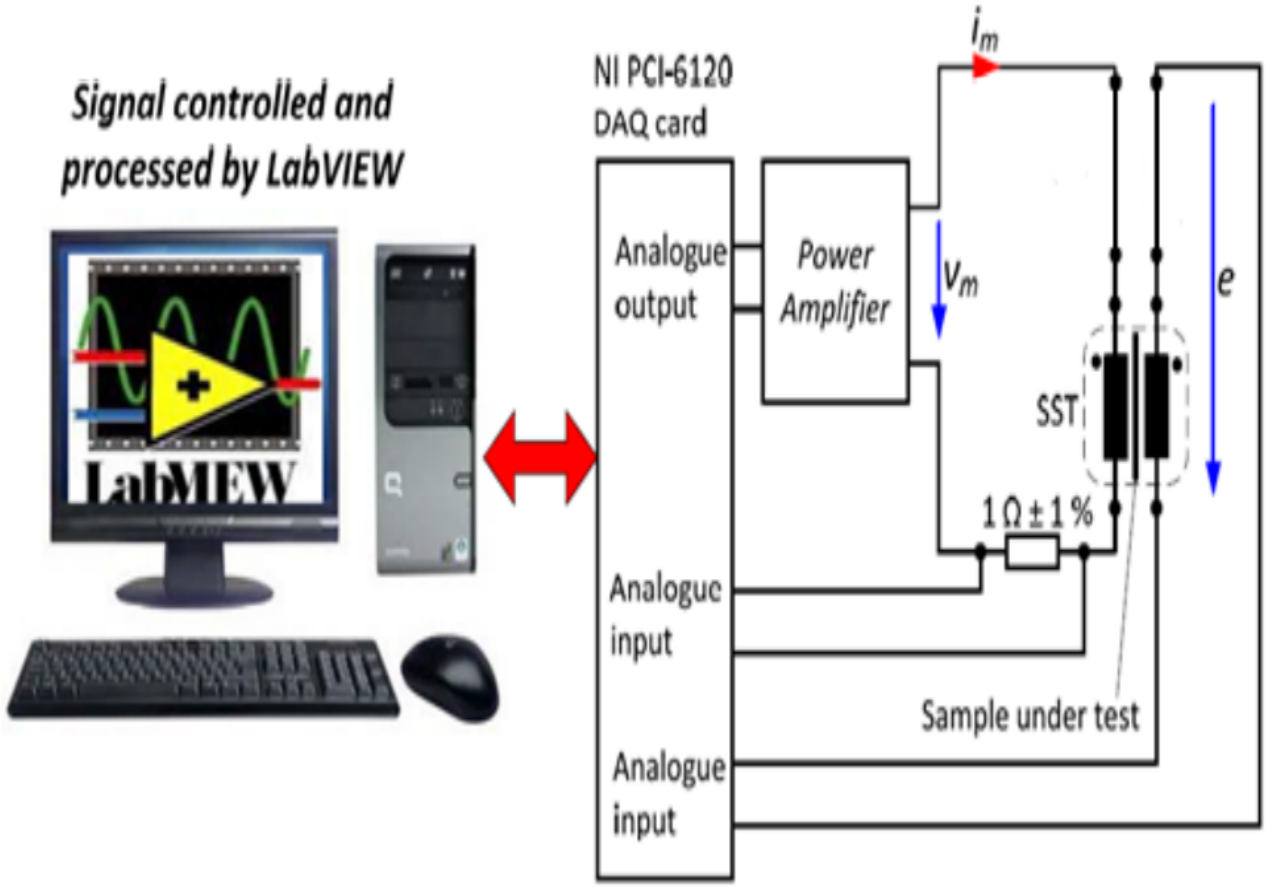

Figure 3-13 Magnetic property measurement system.

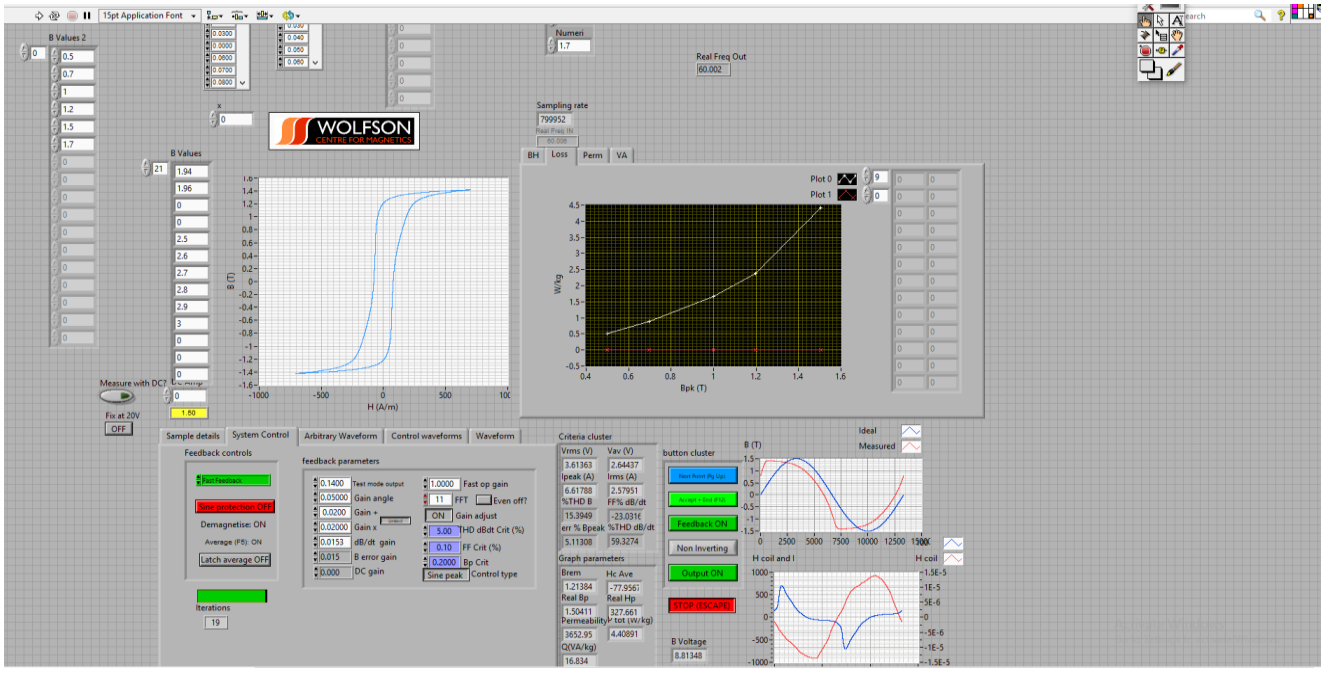

Figure 3-14 LabView interface for the magnetising system

3.5 Characterisation of the microstructure

The samples were sliced and prepared (roughly 15–20 mm square) for examination under a scanning electron microscope to determine the diffusion effects (as illustrated in Figure 3-15) so that their cross-sections could be examined. Polishing was then carried out using emery paper and diamond-pasted wheels. The scanning electron microscope may be used either to give a high-magnification picture of the sample or as an analytical tool to give the concentration of a particular element at a given spot. The minimum area over which chemical analysis was resolvable was a spot of 200 Å diameter. Both modes of operation were used, with concentration profiles being superimposed onto photographs of relevant parts of the sample.

The final distribution relating to the effectiveness of the diffusion of the materials to both surfaces was investigated for strips of NOES and were tested as follows:

1. Concentration profiles were measured by EDS by using SEM.
2. SEM was used to characterise the sample's composite-coated steel. Inclusions were observed by SEM and EDS for elemental analysis.
3. Electron micrographs were carried out on the samples, and these clearly showed the diffusion of materials into the steel (which will be discussed in the next chapter).

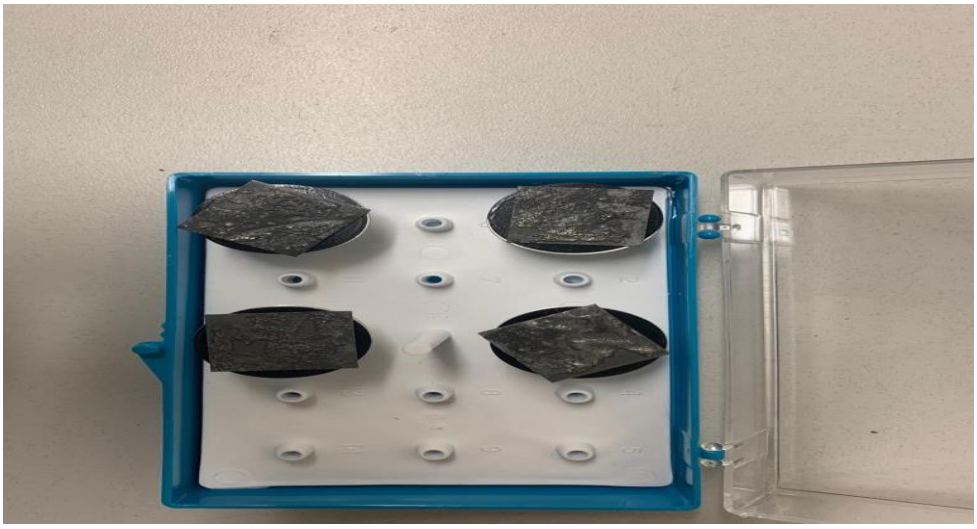

Figure 3-15 The sliced and prepared samples (roughly 15–20 mm square).

3.6 Summary

The preliminary experiments clearly demonstrated that it is possible to diffuse materials into steel from a paste made from a mixture of manganese oxide powder and silicone oil solution. They also showed that the process, if carried out under the correct conditions, could result in the reduction of the power losses in non-oriented silicon iron. Before the effect of the variation of concentration gradients through the thickness of the material could be evaluated, it was clearly necessary to obtain homogeneous diffusion over the surface areas, both along and across the width of the samples and on the two surfaces. The length of the sample over which uniform diffusion might be obtained was limited by the constant temperature region of the furnace, but it was hoped to eliminate other variations. The number of variables present in the process for any given starting material was large, and therefore it was necessary to fix some of these in order that sensible comparisons could be made. To choose the appropriate variables to investigate, it is necessary to consider in greater depth the nature of the process.

Chapter 4: Experiments using manganese paste

4.1 Introduction

Although it has been demonstrated that the use of silicon paste [65] has a certain potential, because of the difficulties involved it was decided to investigate the possibility of using manganese made into a similar paste. It was that some of the problems associated with the use of silicon paste would be absent when the manganese paste was substituted. After comparing the relative merits of the two elements, it was to investigate whichever proved to be the more promising in greater detail. One of the possibly significant differences between the two elements is that whereas the melting point of silicon is 1410°C that of manganese is only 525°C. This could mean that a lower temperature would be necessary for the initial firing, which might eliminate some of the problems found in the use of silicon at this stage. However, the diffusion characteristics for the two elements in iron are similar, and therefore the annealing treatments would need to be of similar temperature and duration if the same penetration depths were to be achieved. One possible problem with the use of manganese is its tendency to oxidise in a suitable environment, such as an alkaline liquid might provide. Against this, the thin oxide layers initially formed on manganese are extremely tenacious and can form an effective barrier against further oxidation. However, this oxide layer might provide a considerable hindrance to the diffusion of the manganese through the paste.

4.2 Diffusion experiment

An experiment was carried out with the aim of studying the diffusion characteristics of materials in both the paste and the steel. A sample of pure iron of 0.3 mm thickness was coated

with a paste to the same thickness by pouring the paste into a using a flask that had been glued onto the metal surface of electrical steel.

4.3 Preliminary work

As was the case in the silicon paste investigation [65], it was decided to conduct preliminary experiments on non-oriented materials to determine whether or not manganese could be successfully diffused into steel using the paste method. This was done because the non-oriented steel was available conveniently in the non-insulated state. It was first necessary to establish a suitable paste composition that would give the required adhesive and homogeneous qualities, and it was decided to start with similar compositions to those which had appeared to be the most suitable in the silicon and aluminium experiments [67].

The manganese powder that was used had granular shape and was 10 μ m. The purity of the powder was 85%, with the main impurity being iron. The same composition of silicon oil solution that was used for the silicon experiments was again employed [119]. It was found that similar paste compositions as had been used in the silicon and aluminium experiments yielded suitable brushing on consistencies and good adhesion to the steel [65]. The paste compositions that were used were 1.25 ml silicon oil per gram of manganese and 0.5 ml silicon oil per gram of manganese. Instead of being made up freshly for each batch of samples that was coated, a bulk quantity of paste of the second composition was produced. This was a feasible proposition because it was observed that the manganese paste was not as unstable as its silicon counterpart [119]. A certain amount of reaction between the silicon oil and the powder was observable, but this took the form of slight bubble formation in the liquid and did not result in the solidification of the paste, as had been the case with silicon. In addition, the reaction was observable only over days rather than hours, as had formerly been seen. The

temperature of the firings and anneals was less than the range 700–800°C, while an argon protective atmosphere was again employed in each case. All the other processing was carried out in the manner described for the aluminium experiments [67], although a post-firing anneal was generally added to attain sufficient penetration depth. This was most necessary when firing was carried out at the lower end of the temperature range.

4.4 Core loss separation method

Increasing the resistivity at the surface of the lamination is important to reduce the eddy currents calculated on the surface at high frequencies due to the skin effect, as the skin depth $\delta = \sqrt{\frac{\rho}{\Pi f \mu}}$ will be reduced. This work aims to mitigate eddy current losses, and separation is a crucial aspect. The overall loss contains both hysteresis and eddy current loss components. The per-cycle hysteresis loss is presently determined using a different method. This approach measures core loss at various frequencies. When the magnetisation frequency curves at different flux densities are extrapolated to zero frequency, the hysteresis loss per cycle, which is the hysteresis energy loss per cycle, can be determined [120].

$$\frac{P_c}{f} = C_h B_{pk}^n + C_e f {B_{pk}}^2 \quad (4.1)$$

The linear equation is the reason for the magnetising frequency using the maximum flux density B. Subsequently, the core loss data are applied with the aim of plotting the curves of *Pc /f* versus *f*. The curves are straight lines.

$$\frac{P_c}{f} = A + Bf \quad (4.2)$$

Where A = $K_h\ B_{pk}^n$ denotes hysteresis loss per cycle and B=$K_e\ {B_{pk}}^2$. More information for determining these coefficients is available in[27],[30],[121].

To obtain the overall hysteresis loss, the static hysteresis power is multiplied by the magnetising frequency. The hysteresis power loss per cycle is frequency independent. Having this knowledge is essential when applying the extrapolation method. Nevertheless, only at low frequencies is this supposition valid. This would result in a non-uniform magnetic field throughout the lamination at higher frequencies, which would complicate the calculation. Consequently, at every point within the lamination, each cycle's hysteresis loop and hysteresis power losses are distinct. Therefore, it is better to use the extrapolation method to determine the core loss separation at a low frequency, otherwise, the skin effect should be considered [122].

4.4.1 Core loss separation.

The three-term formula follows the same approaches employed to separate losses into their eddy current and hysteresis components. However, in this instance, a third term reflecting the excess loss is provided.

$$P_C = P_h + P_e + P_a \quad (\mathrm{W/kg}) \tag{4.3}$$

By dividing Equation (4.3) by the magnetising frequency, we obtain Equation (4.4), which represents the total power losses.

$$\frac{P_c}{f} = C_h f B_{pk}^n + C_e (f B_{pk})^2 + C_a (B_{pk} f)^{1.5} \tag{4.4}$$

In this approach, which is similar to the two-term separation technique, the first right hand (P_h) represents the hysteresis loss component, the second (P_e) represents the eddy current loss component, whereas the third (P_a) represents the excess or anomalous loss component. Because the latter is influenced by microstructural interaction, magnetic anisotropy, and the non-homogeneous domestically driven eddy current [123], the constant coefficients are as follows:

$$\frac{P_c}{f} = A + Bf + C\sqrt{f} \tag{4.5}$$

There is an alternative viable method for finding the coefficients. The core loss per cycle is shown against the square root of frequency √ f rather than the frequency f for different levels of flux density B ranging from the smallest to the highest frequency [124]. Consequently, (4.6) may be adjusted by:

$$\frac{P_c}{f} = A + B(\sqrt{f})^2 + C\sqrt{f} \tag{4.6}$$

Where $Pc\ /f$ is shown on the y-axis and √f is plotted on the x-axis; and A, B, and C may be determined using nominal curve fitting. A comparison of (4.4) and (4.6) gives.

$$A=C_h B_{pk}^n \tag{4.7}$$

$$B= C_e f {B_{pk}}^2 \tag{4.8}$$

$$C= C_a (f B_{pk})^{1.5} \tag{4.9}$$

Thus, when using this approach with certain flux densities, the loss coefficients C_h, C_e and C_a can be obtained.

In conclusion, equations (4-1) and (4-6) emphasise that the extrapolation technique is employed to determine that eddy currents cause a linear relationship between the frequency and the amount of power lost per cycle. Additionally, it is believed that hysteresis loss per cycle is frequency independent.

4.5 Results and discussion

4.5.1 Microstructure, grain size, and texture

Observations conducted with the SEM demonstrated the successful diffusion of manganese into the steel from the paste. Figure 4-1 provides a comprehensive explanation of the SEM and EDS analysis of typical inclusions found in the annealed samples. Prior to analysis, the samples underwent coating and polishing using acetone. The SEM and EDS analyses were then performed to examine the manganese inclusions. The EDS analysis revealed a significant presence of manganese in the analysed samples. The majority of the observed inclusions containing manganese were smaller in size, with diameters below 250 µm. Figures 4-1, 4-2, and 4-3 depict inclusions with varying temperatures, and the results of the EDS analysis are presented in the accompanying tables for each figure. The table associated with Figure 4-3 highlights that the inclusions containing small amounts of manganese are highly complex, with a higher zirconium content than manganese. The presence of manganese oxides is indicated by the elevated levels of oxygen and carbon in these inclusions. Following the coating of the electrical steel with MnO_2, deep element analysis was performed using EDS. Multiple areas of interest were examined during the EDS measurement. Figure 4-1 showcases a distinct peak, with MnO_2 clearly identifiable in the synthesised nanostructures within the EDS spectrum. The primary elements detected in spectrum 55 were manganese, oxygen, and carbon, with weight percentages of 59.2%, 25.79%, and 10.18%, respectively. Additionally, a small amount of impurity, along with reduced titanium, was observed after the heat treatment,

as observed in spectrum 24, with measured weight percentages of 20.2% for manganese, 28.95% for oxygen, and 2.68% for carbon. Furthermore, it was observed that the carbon content increased after the mixing of the manganese compound with Si oil particles, followed by heat treatment at 525 ℃ and 700 ℃. The presence of iron (Fe) in the EDS graphs confirms the successful coating of the manganese surface with Si oil. EDS analysis was used to determine the elemental composition of the material, providing insights into the nature of the composite and confirming the successful functionalisation. Details of the three EDS spectra, including the concentration values of manganese measured in atomic and weight percentages, are presented (in Figure 4-1, 4-2, and 4-3).

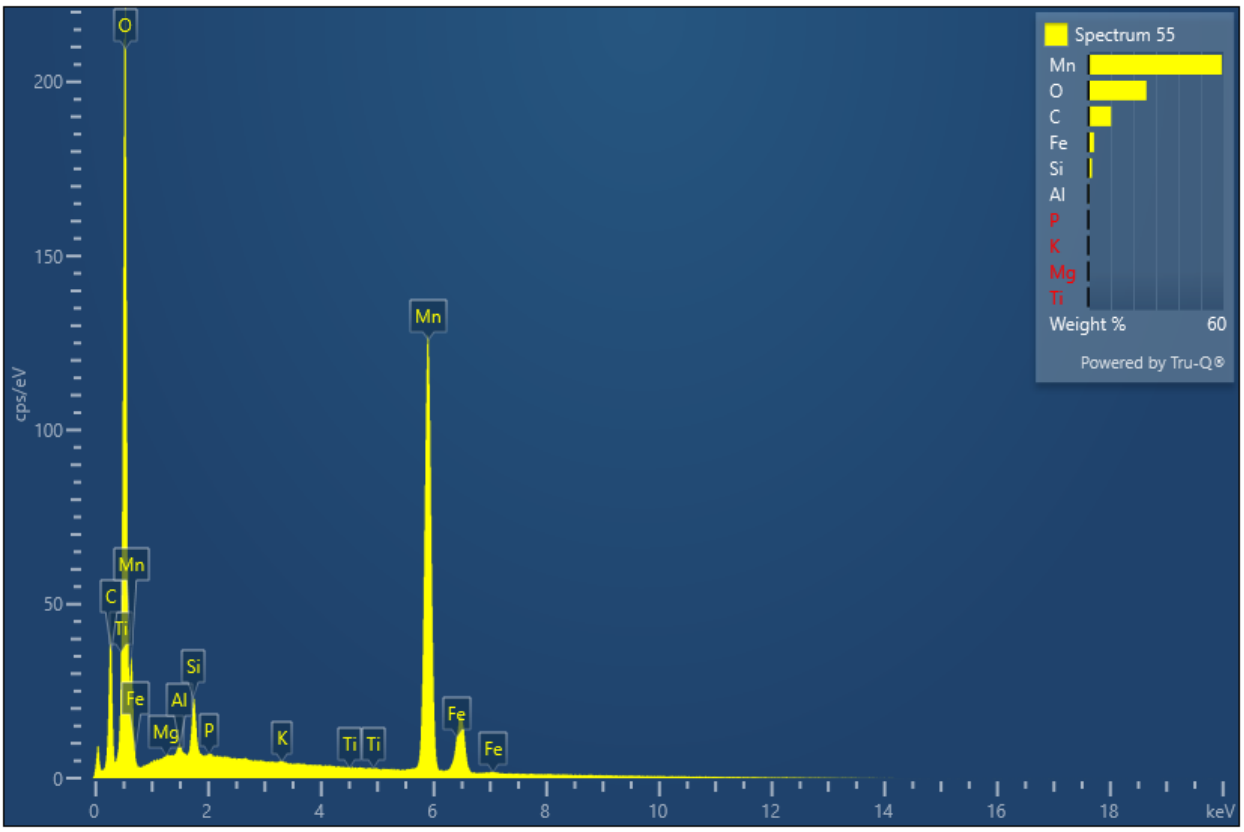

(a)

Element	Weight%	Atomic%	Oxide%	Formula
C	10.18	23.14	29.1	CO_2
O_2	25.79	44.02		
Fe	2.56	1.25	2.78	
Mg	0.07	0.08	0.09	
Al	0.34	0.34	0.52	Al_{2O3}
Ti	0.01	0.01	0.01	
Si	1.64	1.59	2.87	SiO_2
K	0.08	0.08	0.06	
P	0.08	0.07	0.16	P_2O_5
Mn	59.26	29.45	64.4	MnO
Totals	100.00			

(b)

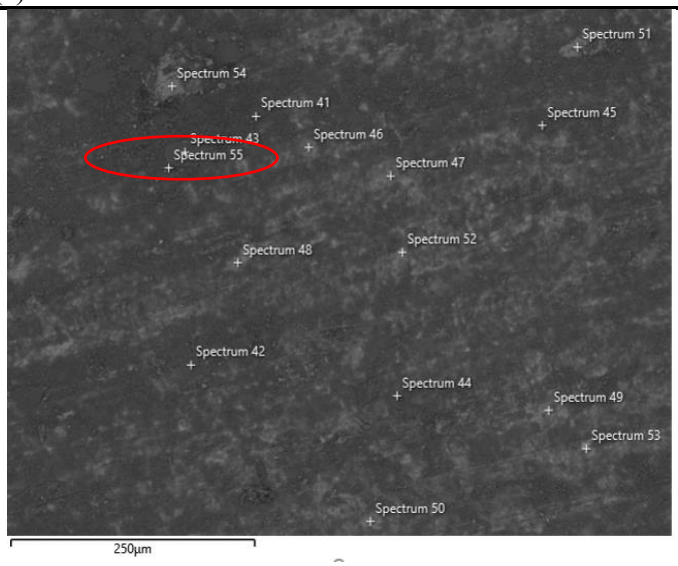

(c)

Figure 4-1 Distribution of elements after heat treatment at 525°C with Energy Dispersive System Analysis of X-rays using SEM. (a). Energy dispersive X-ray (EDX) spectra of sample, (b)Table EDS analysis of inclusions from Figure (c), (c) Complex inclusions in the sample of NOES sheet containing Mn59.26 wt %.

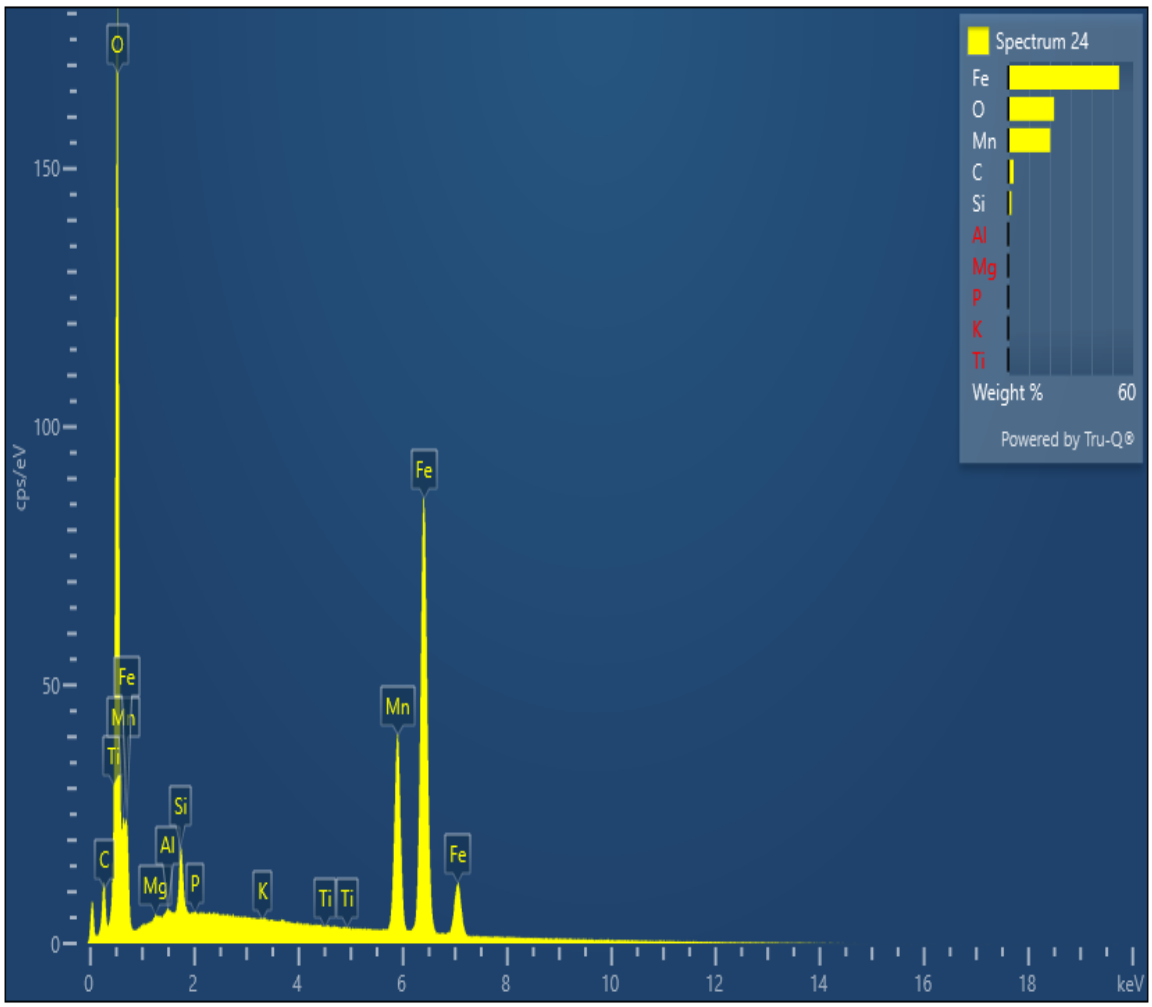

(a)

Element	Weight%	Atomic%	Oxide%	Formula
C	2.68	7.47	8.68	CO_2
Fe	53.21	31.89	63.55	
Mg	0.29	0.19	0.21	
Al	0.15	0.18	0.25	Al_{2O3}
O_2	28.95	46.07		
P	0.04	0.05	0.09	P_2O_5
Ti	0.00	0.00	0.00	
K	0.04	0.03	0.05	
Si	1.53	1.82	2.97	SiO_2
Mn	20.2	12.3	24.21	MnO
Totals	100.00			

(b)

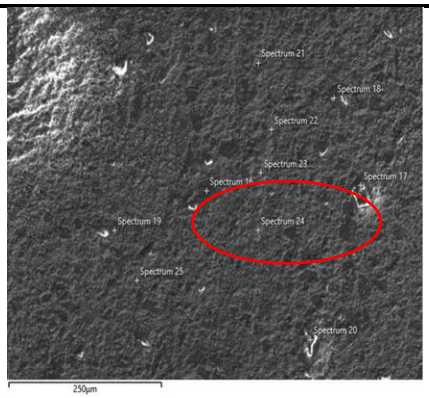

(c)

Figure 4-2 Distribution of elements after heat treatment at 700°C with Energy Dispersive System Analysis of X-rays using SEM. (a). EDX spectra of sample, (b)Table EDS analysis of inclusions from Figure (c), (c) Complex inclusions in the sample of NOES sheet containing Mn 20.2 wt %.

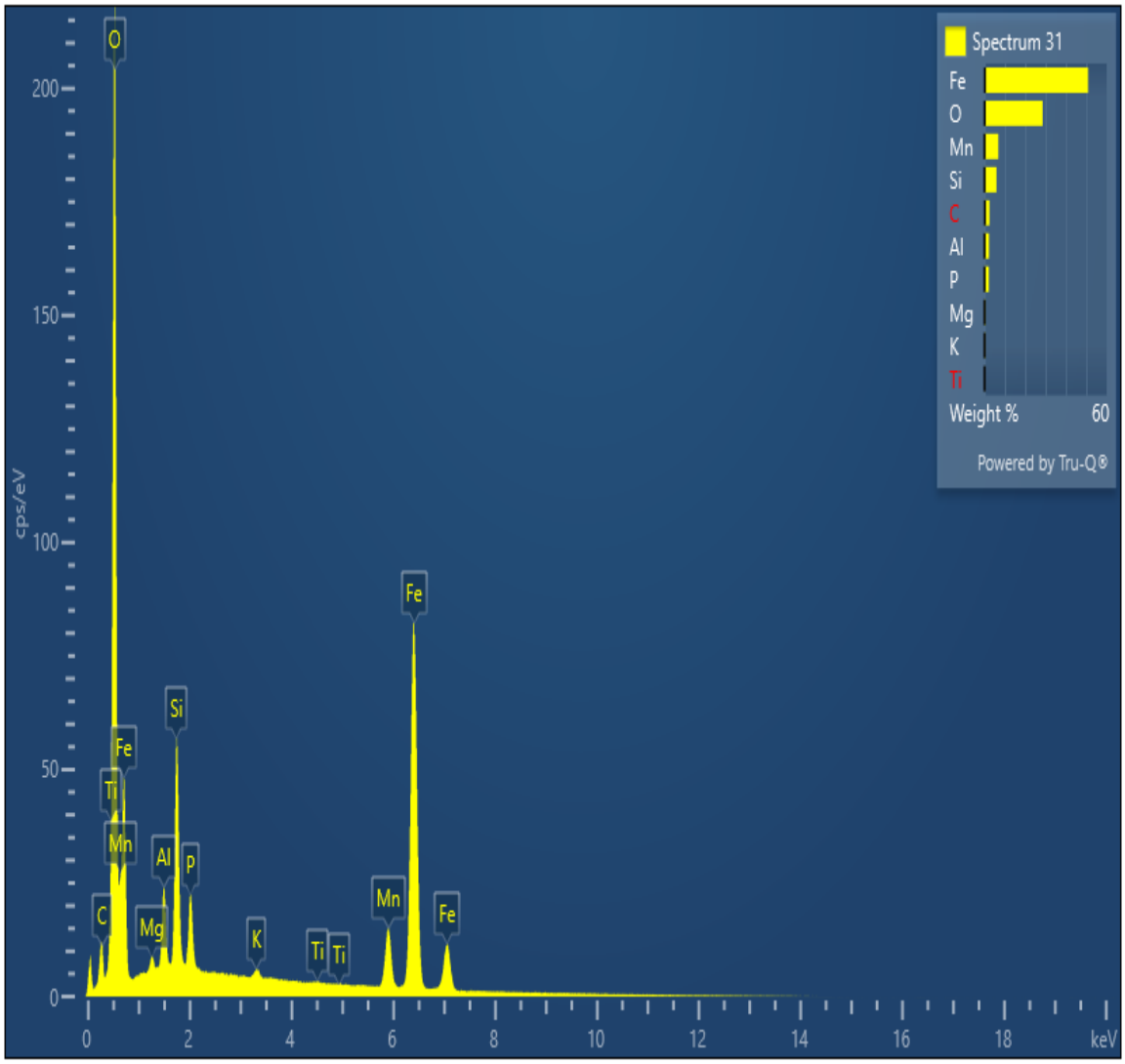

(a)

Element	Weight%	Atomic%	Oxide%	Formula
C	2.52	6.12	8.36	CO_2
O_2	28.58	52.17	63.55	
Fe	50.93	26.64	61.81	
Mg	0.48	0.58		
Al	2.26	2.44	3.97	Al_{2O3}
Si	5.88	6.12	11.74	SiO_2
K	0.33	0.25		
P	2.17	2.04	4.63	$P_2 O_5$
Ti	0.05	0.03		
Mn	6.81	3.62	8.29	MnO
Totals	100.00			

(b)

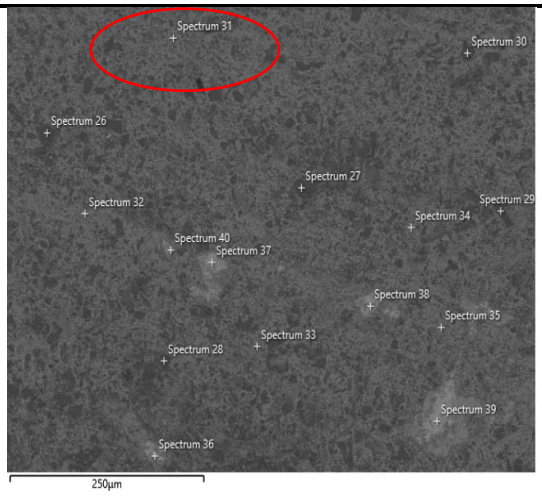

(c)

Figure 4-3 Distribution of elements after heat treatment at 800°C with DS analysis of X-rays using SEM. (a). EDX spectra of sample. (b) Table EDS analysis of inclusions from Figure (c). (c) Complex inclusions in the sample of NOES sheet containing Mn 6.81 wt %.

4.5.2 Effect of heat treatment temperature on power losses

Figure 4-4 focuses on the relationship between heat treatment temperature and power losses in a sample coated by manganese oxide. This study examines the effects of temperature on the sample's characteristics, specifically considering power losses at a frequency of 400 Hz and a magnetic field strength of 1.5 T. This figure illustrates that with an increase in the sample temperature, both coated and uncoated, there is a directly proportional increase in power losses. This implies that higher temperatures lead to greater power losses in the material. The previous observed this trend consistently across different temperature ranges.

Among the various temperature conditions investigated, the study identifies a significant increase in power loss at 52 W/kg when the temperature reaches 700 °C, with a firing time of 45 minutes. This suggests that the sample is particularly sensitive to temperature changes in this range, resulting in a substantial increase in power losses. Furthermore, the previous also analysed the behaviour of the sample near the melting point of manganese, which is approximately 525 °C. At this temperature, the uncoated sample exhibited power losses of 39 W/kg, while the coated sample showed slightly lower losses of 35 W/kg after a firing time of 60 minutes. These findings indicate that as the sample approaches its melting point, there is a noticeable increase in power losses. Figure 4-4 also illustrates that when the temperature is pushed to a maximum of 800 °C, there is a slight reduction in power losses to 49 W/kg compared to the losses observed at 700 °C.

Based on the experimental findings, annealing temperatures of 525°C, 700°C, and 800°C were selected for the study. Notably, the significance of operating near the melting point of manganese oxide at 525°C was highlighted. This approach was advocated as it was believed to enhance sample performance and reduce power losses.

Therefore, the figures and findings highlight the relationship between temperature and power losses in the manganese oxide sample, indicating the impact of annealing temperatures

on the material's characteristics. The results demonstrate the importance of considering temperature as a crucial factor in optimising the performance of the sample and minimising power losses.

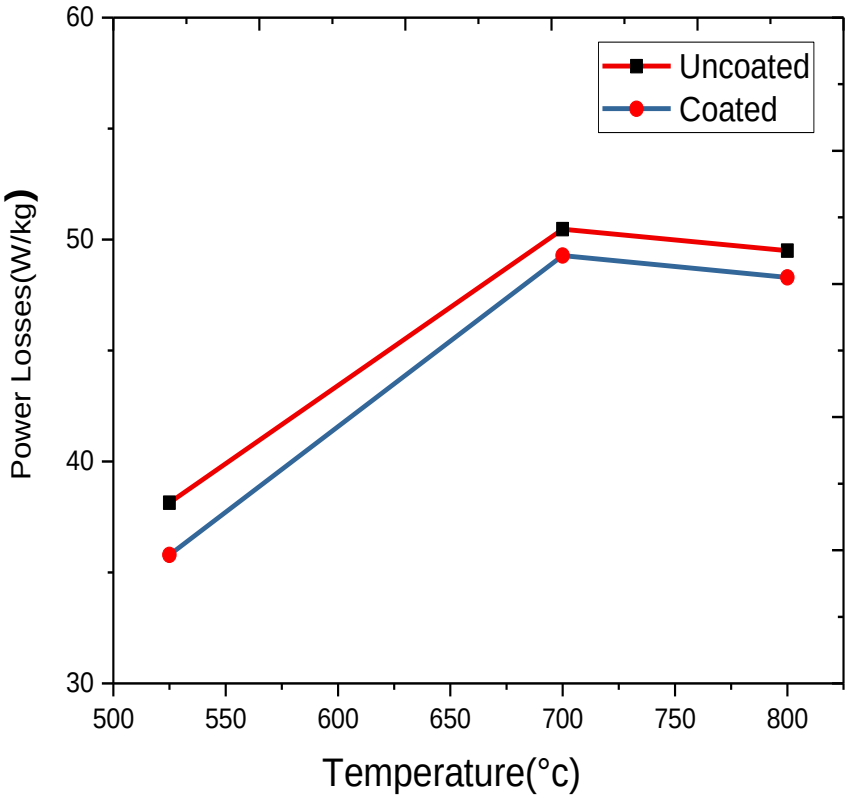

Figure 4-4 Power losses (400 Hz, 1.5 T) for coated and uncoated samples at different temperatures.

4.5.3 Effect of heat treatment temperature on permeability

Figure 4-5 presents the permeability data for both coated and uncoated samples containing manganese oxide at different temperatures and sintering times. The measurements were conducted at a frequency of 400 Hz and a magnetic field strength of 1.5 T. This figure reveals that, in general, the permeability of the samples increases as the annealing temperature rises. This indicates that higher temperatures contribute to enhancing the material's magnetic

permeability. However, it is important to note that there are some variations and specific conditions that affect the observed permeability trends.

At the temperature of 525 °C, a decrease in permeability is observed compared to other temperatures. This suggests that the magnetic properties of the samples are influenced by the specific conditions at this temperature. Interestingly, when the same temperature of 525 °C is applied without coating, the permeability remains high. This indicates that the presence of a coating has an impact on the magnetic properties of the material at this particular temperature range.

Moving on to the temperature of 700 °C, the coated samples exhibit lower permeability compared to the uncoated samples. This suggests that the coating has a significant effect on the magnetic properties of the material at this temperature. The reasons behind this discrepancy could be related to changes in the microstructure or the presence of certain materials in the coating that affect the magnetic response.

As the temperature increases further to 800 °C, a decrease in magnetic permeability is observed. This may be attributed to the conditions brought on by an excess of lubricant. The presence of excess lubricant during the annealing process can lead to changes in the material's microstructure, resulting in reduced permeability. This decrease in permeability indicates that the excess lubricant negatively affects the magnetic properties of the samples at this elevated temperature.

In addition to temperature, the duration of the sintering time also plays a role in determining the magnetic permeability. This suggests that a longer sintering time allows for more complete consolidation and reduction of flaws within the samples, which results in improved permeability.

Consequently, the results presented in Figure 4-5 demonstrate that the permeability of the composites increases as the annealing temperature increases. However, it is important to

consider other factors, such as the presence of coatings, the influence of lubricants, and the duration of the sintering time. These factors can lead to variations in the observed permeability trends and highlight the intricate relationship between temperature, coating, and permeability in the studied samples.

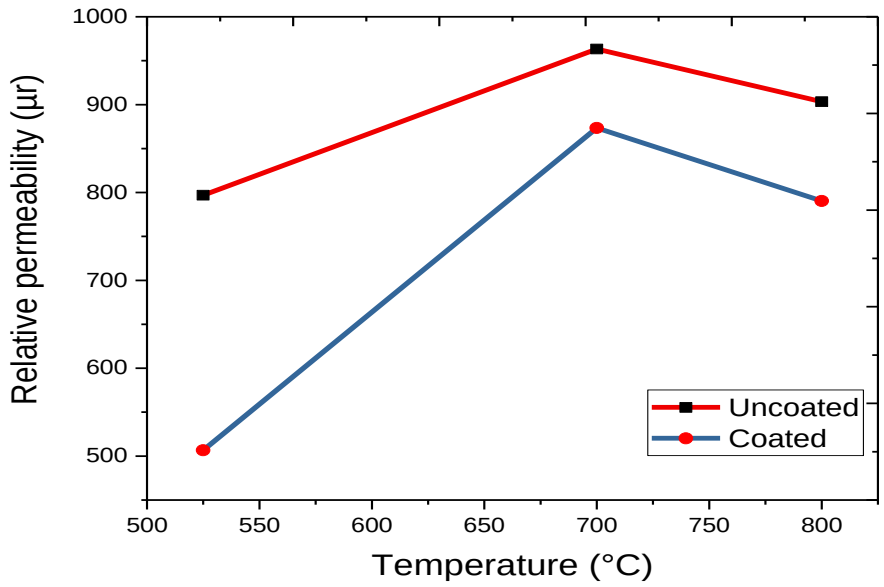

Figure 4-5 Permeability at 400 Hz, 1.5 T for coated and uncoated samples at different temperatures.

4.5.4 Power loss components

The power loss of NOES samples was measured using the SST system, as described in references [45] and [46]. The SST system allows for precise and accurate measurements of power loss in magnetic materials.

In this study, the power loss measurements were conducted under specific conditions. Table 4-1 presents the results obtained by applying the method to calculate power loss separation. The measurements were performed at a maximum flux density of 1.5 T and magnetizing frequencies ranging from 50 Hz to 1 kHz. The selected frequencies include 50, 100, 200, 400, 500, and 700 Hz. The power loss values presented in the table represent the power dissipated by the NOES samples under the given conditions. These measurements

provide insights into the power loss characteristics of the material at different frequencies. It is important to note that the power loss values depend on various factors, including the material properties, magnetic field strength, and frequency. The measurements conducted using the SST system offer valuable data for understanding the behaviour of NOES and assessing its performance in practical applications.

Table 4-1 Power loss of NO steel measured at various magnetising frequencies, with a total power loss per cycle uncoating at a peak flux density of 1.5 T.

Magnetising frequency (Hz)	**Measured power loss (W/kg)**	**Power loss per cycle (W/kg).sec**	**Square root of Frequency (√f)**
50	1.921	0.038	7.07
100	4.584	0.046	10
200	12.505	0.062	14.14
400	38.143	0.095	20
500	56.428	0.112	22.36
700	102.282	0.146	26.46
1000	198.126	0.198	31.62

It can be concluded that the power loss in the system is influenced by the magnetising frequency. Higher frequencies result in higher power losses, which indicates that more energy is dissipated during the magnetisation process. This indicates that higher frequencies result in greater power dissipation. Second, the power loss values increase nonlinearly with increasing frequency. For example, the power loss from 50 Hz to 100 Hz increases by 2.663 W/kg, whereas from 100 Hz to 200 Hz, it increases by 7.921 W/kg. This suggests that the relationship between power loss and frequency is not linear. Third, similar to the measured power loss, the

power loss per cycle also tends to increase as the magnetising frequency increases. Finally, the power loss per cycle values shows a linear relationship with frequency.

The relationship between the measured power loss per cycle and the square root of the frequency is shown in Figure 4-6. This approach is commonly used to investigate the power loss characteristics of materials and identify underlying trends. By fitting a polynomial curve to this data in software such as Microsoft Excel, it is possible to determine the coefficients of the power loss components as in Equation 4.6. The polynomial curve fitting technique allows us to approximate the relationship between power loss and the square root of the frequency using a mathematical equation. Excel's curve fitting capabilities provide a convenient method for determining the coefficients of the polynomial curve that best fits the measured data points.

By obtaining the coefficients of the power loss parts, we can gain valuable insights into the factors influencing power loss behaviour in the material. The coefficients reveal information about the material's intrinsic properties and the impact of frequency on power loss. However, it is important to note that the choice of polynomial degree for curve fitting may vary depending on the complexity of the data and the desired accuracy. Higher-degree polynomials can capture more intricate relationships between power loss and frequency, but they may also introduce greater complexity and potential overfitting of the data.

The coefficients obtained from the curve fitting process can be used to model and predict the power loss behaviour of the material within the frequency range under consideration. This information is crucial for designing and optimising electrical systems because it helps in determining the power loss and efficiency characteristics of components made from the studied material.

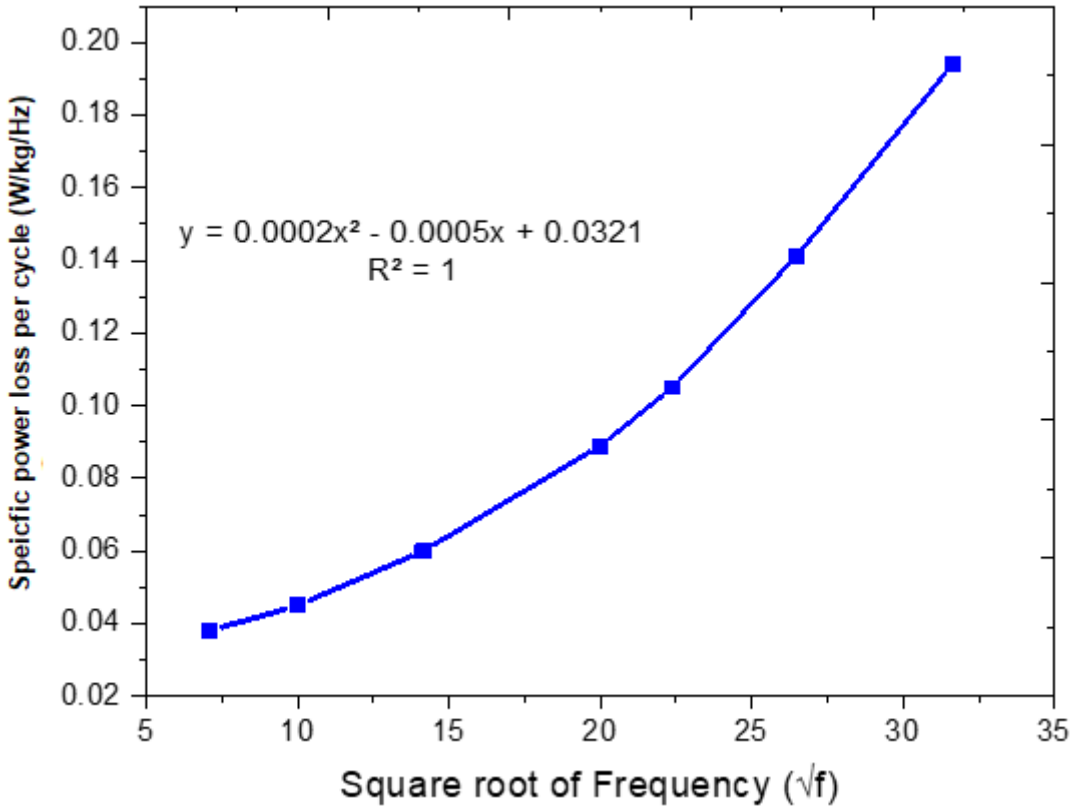

Figure 4-6 Total power loss per cycle of a magnetic sample made of non-oriented steel at a 1.5 T flux density against the square root of frequency.

When fitting a curve to the relationship between power loss per cycle and the square root of the frequency, the resulting fitting equation often produces residual values that are very close to unity ($R^2 = 1$). This indicates that the fitted equation provides an accurate approximation of the measured data.

The coefficient of determination, denoted as R^2, is a statistical measure that quantifies the goodness of fit between the fitted curve and the actual data points. An R^2 value of 1 indicates that the fitted equation explains all of the variation in the data, suggesting a highly accurate representation of the power loss behaviour as a function of frequency.

Table 4-2 displays the results obtained by applying the fitted equations derived from Figure 4-6 to determine the power loss components at various frequencies. These equations, which are derived through the process of curve fitting, enable the estimation of power loss

values based on the square root of the frequency. By using the derived equations, it becomes possible to determine the power loss components at frequencies that were not directly measured during the experiment. This expands our understanding of the material's power loss behaviour across a wider range of frequencies. The high accuracy of the fitted equations and the resulting power loss components is supported by the R^2 value close to 1. This indicates a strong correlation between the fitted curve and the measured data, which enhances the confidence in the validity and reliability of the obtained results.

The power loss components presented in Table 4-2 offer valuable insights into the individual contributions of different factors to the overall power loss at various frequencies. These findings facilitate a more comprehensive understanding of the material's power loss behaviour and enable predictions of power loss for similar frequency conditions. The close proximity of the residual values to unity ($R^2 = 1$) in the fitting equation suggests an accurate approximation of the measured data. In additionally, presents the power loss components determined by employing the fitted equations derived from Figure 4-6. These results provide detailed information about the material's power loss behaviour at various frequencies, which expands our understanding of the predictive capabilities of the power loss characteristics in the studied material.

A= $C_h B_{pk}^n$ =0.0321 (4.10)

B= $C_e f {B_{pk}}^2$=0.0002 (4.11)

C= $C_a (f B_{pk})^{1.5}$=0.0005 (4.12)

The power loss components, furthermore, are calculated by utilising the coefficients obtained from the curve fitting process. These coefficients are applied in Equation (4.6) to estimate the power loss components that are associated with hysteresis and eddy currents.

A comprehensive understanding of the power loss behaviour can be achieved by analysing the relationship between the magnetising frequency and the hysteresis and eddy current power loss components. This understanding is crucial for material selection, design optimisation of electrical components, and to ensure the efficient operation of electrical systems. The coefficients derived from the curve fitting process are applied in Equation (4.6) to calculate the power loss components presented in Table 4-2.

Table 4 -2 gives the data of the power loss at different frequencies, along with the calculated power loss components and error percentages, as follows:

1. Measured power loss (W/kg): The measured power loss values represent the actual energy dissipated per kilogram of material at each frequency. As the frequency increases, the measured power loss generally tends to also increase. This can be attributed to the intensified effects of eddy currents and hysteresis at higher frequencies, which leads to greater energy dissipation.
2. P_e (W/kg): The power loss component attributed to eddy currents demonstrates an increasing trend with frequency. This suggests that as the magnetising frequency rises, more energy is dissipated due to the induction of circulating currents within the material. Eddy currents tend to oppose the changes in the magnetic field, and this results in power loss through resistive heating.
3. P_h (W/kg): The power loss component that is associated with hysteresis also exhibits an increasing trend with frequency. This can be attributed to the fact that at higher

frequencies, the material undergoes more frequent magnetisation cycles, which leads to increased energy dissipation during each cycle. Hysteresis power loss is influenced by the material's magnetic properties and the shape of its hysteresis loop.

4. P_a (W/kg): The additional power loss component, represented by P_a, accounts for other minor contributions to power loss that are not solely attributed to eddy currents or hysteresis. The values in this column are relatively small when compared to the other components, which indicates that the majority of the power loss can be attributed to eddy currents and hysteresis.
5. $P_c = P_e + P_h + P_a$ (W/kg): The total power loss, calculated by summing the individual power loss components, demonstrates a clear increasing trend with frequency. This aligns with the observed trends in the individual components, which indicates that both the eddy currents and hysteresis contribute significantly to the overall power loss at higher frequencies.
6. **Error** = (P calculated – P measured) / P calculated × 100%: The error percentage provides insight into the accuracy of the calculated power loss components values compared to the measured values. The small error percentages indicate that the calculated values are in close agreement with the measured data. However, it is important to note that there is a slight underestimation (negative error percentages) in some cases and a slight overestimation (positive error percentages) in others. This suggests that the calculations capture the general trends but may have slight deviations from the actual measured values.

By comparing the power loss components at different frequencies, we can observe that both eddy currents and hysteresis play significant roles in power dissipation. At lower frequencies, eddy currents contribute less to the total power loss when compared to hysteresis.

However, as the frequency increases, the contribution of eddy currents becomes more pronounced, surpassing the hysteresis power loss component. The analysis of the power loss components and their trends with frequency provides valuable insights into the power dissipation mechanisms in the studied material. This information can help to optimise material selection, design efficient electrical components, and minimise energy losses in electrical systems.

Table 4-2 Power loss components of SST of NO steel at various magnetising frequencies and a peak flux density of 1.5 [T] with uncoated samples.

Frequency (Hz)	**Measured power loss (W/kg)**	**P_e (W/kg)**	**P_h (W/kg)**	**P_a (W/kg)**	**$P_c = P_e + P_h + P_a$ (W/kg)**	**Error= $\frac{P\ calculated - P\ measured}{Pcalculated} \times 100\%$ (%)**
50	1.921	0.6	1.141	0.18	1.921	0.00
100	4.584	1.71	2.65	0.36	4.72	0.03
200	12.505	6.4	4.42	1.41	12.23	-0.02
400	38.143	27.9	8.74	4	40.64	0.06
500	56.428	40	14.05	5.6	59.65	0.05
700	102.282	78	17.47	7.26	102.73	0.00
1000	198.126	180	20	9	209	0.05

In Figure 4-7, the relationship between the magnetising frequency and the hysteresis power loss and eddy current power loss at a magnetic field strength of 1.5 T is illustrated. The hysteresis power loss is calculated using the static hysteresis loops of the material, while the

eddy current power loss is determined by employing an equation that models it as a linear function of the magnetising frequency.

The static hysteresis loops of the material are utilised to calculate the hysteresis power loss. These loops represent the magnetic behaviour of the material and provide insights into the energy dissipated during each magnetisation cycle. The equation that is used to calculate the hysteresis power loss incorporates the material's magnetic properties and the characteristics of its hysteresis loop.

The eddy current power loss is caused by the induction of circulating currents within the material when it is subjected to a varying magnetic field. These circulating currents generate heat and contribute to power loss. The relationship between the eddy current power loss per cycle and the magnetising frequency is approximated as a linear function. This linear relationship accounts for the influence of frequency on the magnitude of the circulating currents, and consequently on the eddy current power loss.

Figure 4-7 visually represents the relationship between magnetising frequency and the hysteresis power loss and eddy current power loss at a magnetic field strength of 1.5 T. The hysteresis power loss is calculated using the static hysteresis loops, while the eddy current power loss is determined through a linear equation that is based on the magnetising frequency. This analysis provides valuable insights into the contributions of hysteresis and eddy current mechanisms to the overall power loss in the material, which enables informed decision-making in electrical system design and optimisation.

Eddy current losses can be described using the following equation:

$$P_e = \frac{\pi 2}{6\rho} d^2 f^2 {B_{pk}}^2 \quad (4.13)$$

Where B_{pk} is the peak flux density, [T]; f is frequency, [Hz]; ρ is resistivity [Ω. m]; D is density, [kg/m^3]; and d is the thickness of the lamination [m] [116].

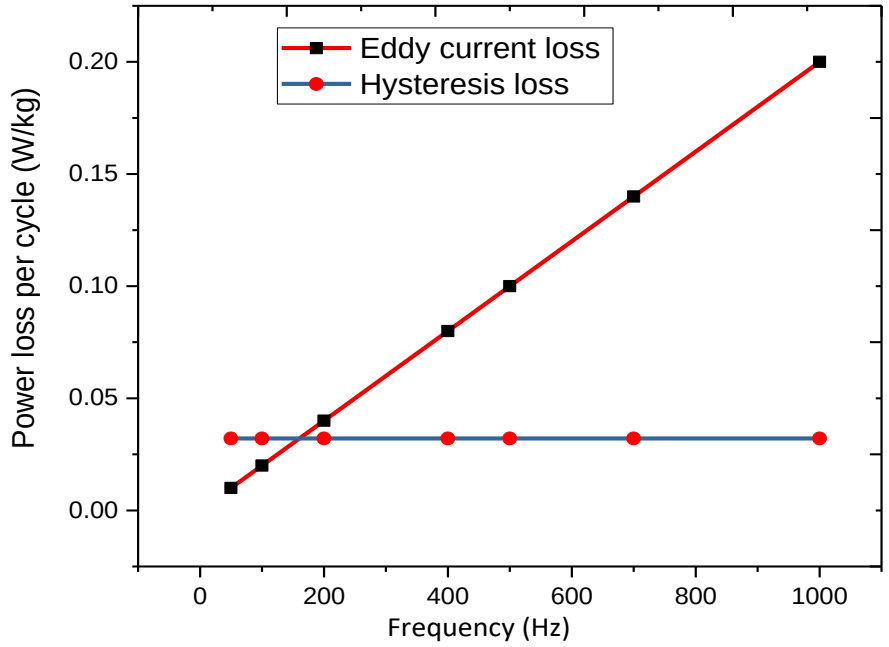

Figure 4-7 Eddy current and hysteresis loss per cycle versus frequency.

The power loss of non-oriented steel with a coating is a critical parameter because it helps us to assess its performance in various electrical applications. To determine the power loss characteristics, measurements were conducted at a peak flux density of 1.5 T, which represents the maximum magnetic field strength experienced by the material. The magnetising

frequencies used in the experiments were varied to investigate the impact of frequency on power loss.

Table 4-3 provides detailed information on the measured power loss per cycle at different frequencies. The total power loss per cycle takes into account the combined effects of various factors, including eddy currents, hysteresis, and any additional losses attributed anomalous loss.

The inclusion of a coating introduces an additional layer that may affect the magnetic properties and power loss behaviour of the steel. Therefore, it is crucial to evaluate the power loss with the coating to understand its impact on the material's performance. The data in Table 4-3 show how the power loss changes with varying magnetising frequencies. This information is valuable for designing efficient electrical components and optimising the selection of non-oriented steel with coatings for specific applications.

Table 4-3 Power loss of non-oriented steel is measured at a peak flux density of 1.5 T at different magnetizing frequencies with total power loss per cycle with coating.

Magnetising frequency (Hz)	**Measured power loss (W/kg)**	**Power loss per cycle (W/kg).sec**
50	1.91	0.04
100	4.40	0.05
200	12.00	0.06
400	35.71	0.09
500	52.68	0.11
700	99.30	0.14
1000	194.24	0.19

The power loss per cycle at different frequencies with coating is shown in Figure 4-8, plotted against the square root of the frequency. To accurately analyse the trend and characteristics of the power loss, a polynomial curve fitting technique is employed using Microsoft Excel. This curve fitting process allows us to determine the coefficients of the power loss components associated with the coating. By obtaining these coefficients, we can gain valuable insights into the individual contributions of factors such as eddy currents, hysteresis, and other losses influenced by the presence of the coating. This analysis aids in understanding the behaviour of power loss with coating across a range of frequencies and assists in optimising the design and performance of electrical systems utilising non-oriented steel with coatings.

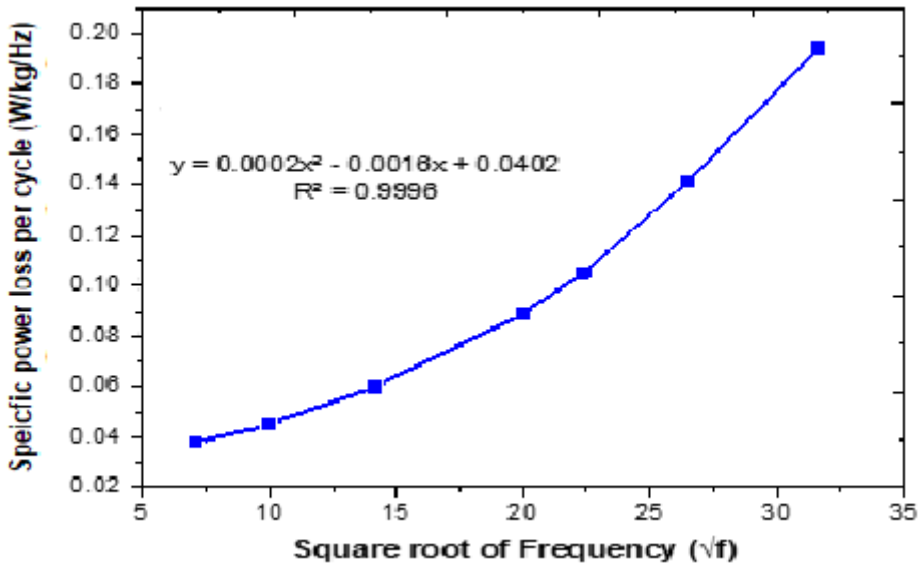

Figure 4-8 The total power loss per cycle of a magnetic sample made of NO steel at a 1.5 T flux density against the square root of Frequency.

The power loss separation results for the same material with a coating are presented in Table 4-4. This table provides the details of the individual components of power loss and their contributions when the material is coated. By analysing the data in Table 4-4, we can examine the power loss components, such as eddy current losses, hysteresis losses, any additional losses attributed anomalous loss. This table also allows us to quantify and compare the magnitudes of these different components. Understanding the power loss separation is crucial because it

enables the overall energy dissipation characteristics of the coated material to be evaluated. It also helps to identify the dominant factors contributing to power loss and assess the effectiveness of the coating in reducing losses.

Table 4-4 Power loss components of an SST of NO steel at various magnetising frequencies and a peak flux density of 1.5 [T] with coated samples.

Frequency (Hz)	**Measured power loss (W/kg)**	**P_e (W/kg)**	**P_h (W/kg)**	**P_a (W/kg)**	**$P_C = P_e + P_h + P_a$ (W/kg)**	**Error= $\frac{P\ calculated - P\ measured}{Pcalculated} \times 100\%$ (%)**
50	1.912	0.5	1.01	0.4	1.91	-0.00
100	4.400	2	2.02	0.8	4.82	0.09
200	12.00	6	5.04	0.9	11.94	-0.00
400	35.706	25	10.08	1.5	36.58	0.02
500	52.680	40	14	2	56	0.05
700	99.301	83	17	2.09	102.09	0.02
1000	194.237	170	20.21	4.5	194.71	-0.00

Table 4-5 compares the eddy current power loss obtained through the extrapolation method (experimental based) and the eddy current that is calculated using the conventional formula (theory-based). The purpose of this experiment was to assess the agreement between the calculated and observed eddy current losses in a sample under high induction and high frequency conditions. The findings of the experiment indicate that the eddy current loss calculated using the conventional formula closely matches the observed loss obtained through the extrapolation method. This suggests that at low induction and low frequency, the calculated

eddy current loss is nearly identical to the observed loss of around 90%. However, it is important to note that as the frequency and field strength change, the additional loss beyond the eddy current power loss varies. This implies that while the calculated eddy current loss remains consistent.

These results highlight the relationship between the calculated and observed eddy current losses and emphasise the influence of frequency and field strength on the additional losses. An understanding of this relationship will provide further insights into the behaviour of eddy currents and the factors that contribute to power loss in each system.

Table 4-5 Results obtained using by extrapolation method. A comparison of Equation (4.13) was used to find the eddy current power loss of an SST with a peak flux density of 1.5 T and different frequencies.

Magnetising frequency (Hz)	**Eddy current power loss (W/kg) by extrapolation method**	**Eddy current power loss (W/kg) by equation (4.13)**
50	0.5	0.39
100	2	1.48
200	6	7.44
400	25	30.78
500	40	47.16
700	83	91.83
1000	170	148.65

The study delved into the measurement of power loss for coated samples, as illustrated in Table 4.6. These measurements were meticulously conducted under peak flux densities of 1.3 T, 1.5 T, and 1.7 T, spanning magnetizing frequencies from 50 Hz to 1000 Hz for the coated samples. Consequently, power losses were meticulously recorded for each distinct flux density-

frequency combination. The paramount objective of this research endeavour was to shed light on the influence of employing manganese paste as a protective coating on cumulative power loss. The ensuing results, as presented herein, encapsulate the outcomes gleaned from three discrete sets of measurements.

The selection of 1.5 T as the peak flux density was deliberate, driven by the notable improvement observed in power loss at this specific level of induction.

Table 4-6 Specific power loss for a sample coated of three at different flux densities.

Total measured power loss (W/kg)							
B pk (T)	**50 Hz**	**100 Hz**	**200 Hz**	**400 Hz**	**500 Hz**	**700 Hz**	**1000 Hz**
1.3	1.373	3.347	8.95	26.49	38.27	70.79	143.77
1.5	1.912	4.400	12.00	35.706	52.680	99.301	194.237
1.7	2.215	5.502	14.725	44.481	65.892	127.129	249

Table 4-7 provides valuable information about the percentage reduction in power loss for both uncoated and coated samples at various frequencies. This table confirms that the peak reduction in power loss occurs at a flux density of 1.5 T. In addition, this table sheds light on the influence of manganese (IV) oxide diffusion on power loss reduction at specific frequencies.

The results reveal that the diffusion of manganese (IV) oxide within the samples leads to a noticeable reduction in power loss. Specifically, at a frequency of 400 Hz, the power loss is reduced by approximately 7% when compared to samples without manganese (IV) oxide diffusion. Similarly, at a frequency of 500 Hz, the power loss is reduced by approximately 6%.

These findings demonstrate that the presence of manganese (IV) oxide has a positive impact on reducing power losses in the samples, particularly at these frequencies.

Table 4-7 also highlights the significance of the internal effects of the flux distribution within the material, even when subjected to AC magnetism. It is observed that the uneven distribution of manganese within the samples creates a resistivity gradient. This resistivity gradient helps to lower the eddy current losses, which are a major source of power loss in magnetic materials. By minimising eddy current losses, the samples exhibit reduced power loss.

In summary, Table 4-7 provides quantitative evidence of the reduction in power loss for both uncoated and coated samples at different frequencies the peak reduction occurs at a flux density of 1.5 T, calculated using the percentage decrease formula for any percentage decrease calculation. Reduction in power loss = (P uncoated – P coated) / P_ uncoated × 100%. The diffusion of manganese (IV) oxide within the samples demonstrates its effectiveness in reducing power losses, particularly at frequencies of 500 Hz and 400 Hz. In addition, the uneven distribution of manganese within the samples creates a resistivity gradient, which minimises eddy current losses and further contributes to the reduction in power loss. These findings emphasise the importance of both external factors, such as frequency and flux density, as well as internal factors, such as material composition and magnetic properties, in achieving significant power loss reductions.

Table 4-7 The percent decrease in power loss on uncoated and coated samples at various frequencies at 1.5 T.

Magnetising frequency (Hz)	**Measured power loss with uncoating (W/kg)**	**Measured power loss with coating (W/kg)**	**Reduction in power loss (%)**
50	1.921	1.912	0.5
100	4.584	4.400	4
200	12.505	12.00	4
400	38.143	35.706	7
500	56.428	52.680	6
700	102.282	99.301	3
1000	198.126	194.237	2

Table 4-8 gives the percentage reduction in permeability for both coated and uncoated specimens at various frequencies. This allows us to examine the influence of frequency and the presence of manganese (IV) oxide on the magnetic permeability of the samples, with a peak flux density of 1.5 T.

When analysing the uncoated samples, it is evident that the permeability is visibly affected by increasing frequencies from 100 Hz to 700 Hz. As the frequency increases within this range, the permeability of the uncoated samples decreases. This suggests that higher frequencies have an adverse effect on the magnetic permeability of the uncoated samples. In contrast, the behaviour of the coated samples is different. With the presence of a coating, the coated specimens achieve higher magnetic permeability, specifically at 1 kHz, when compared to the uncoated samples. This indicates that the coating enhances the magnetic properties of the material, which results in improved permeability at this specific frequency. Furthermore, the coated samples show the highest percentage decrease in permeability at 50 Hz when the coating is applied. This implies that at this particular frequency, the presence of the coating has

a significant impact on reducing the magnetic permeability of the samples. The coating may introduce additional magnetic or structural effects that alter the permeability response at this frequency range. Moreover, the diffusion of manganese (IV) oxide into the Si-Fe strips leads to a reduction in magnetic permeability, even when considering the same flux density. The presence of manganese (IV) oxide affects the texture of the material, resulting in a higher anisotropic coefficient. This change in texture and anisotropy contributes to the decrease in the relative permeability of the coated material. The altered microstructure due to the diffusion of manganese (IV) oxide introduces new magnetic interactions, which can affect the overall permeability response.

In summary, Table 4-8 provides valuable insights into the percentage reduction in permeability for coated and uncoated specimens at different frequencies. The uncoated samples exhibit a decrease in permeability with increasing frequencies, while the coated samples show improved permeability at 1 kHz with the coating. The diffusion of manganese (IV) oxide leads to a reduction in magnetic permeability, and the presence of the coating introduces changes in the material's texture and anisotropic properties, which results in a decrease in relative permeability. These findings highlight the complex interplay between frequency, coating, and the presence of manganese (IV) oxide in determining the magnetic permeability characteristics of the examined samples.

Table 4-8 The percent decrease in permeability for coated and uncoated specimens at various frequencies at 1.5 T.

Magnetising frequency (Hz)	**Measured relative permeability (μ_r) with uncoating**	**Measured relative permeability (μ_r) with coating**	**Reduction in relative permeability (μ_r) (%)**
50	784.798	479.746	39
100	652.928	501.857	24
200	670.574	506.774	25
400	795.923	506.620	38
500	875.002	553.971	37
700	937.858	576.248	39
1000	852.695	620.494	27

4.5.5 Magnetic properties

Figure 4-9 provides a visualisation of the hysteresis loop for both coated and uncoated samples. The hysteresis loop represents the relationship between the magnetic field strength and the magnetic induction of the material. In this case, size of the loop determines the loss hysteresis reflects the diffusion and distribution of manganese within the samples, which is directly proportional to the amount of material energy. Comparing the hysteresis loops of the coated and uncoated samples, it is observed that the coated samples exhibit a larger loop area and higher saturation flux density when compared to the raw material. This indicates that the coating process has a significant impact on the magnetic properties of the samples. The presence of the coating, along with the diffusion and distribution of manganese, enhances the magnetic performance of the material.

To evaluate the AC core losses, calculations were performed at a frequency of 500 Hz, and the steel strips were magnetised to saturation. At saturation, the 500 Hz flux density

approaches 1.5 T, based on the magnetising current frequency. The core loss represents the energy dissipated in the material due to the magnetisation process, which is an important factor to consider in practical applications. At lower frequencies, it was observed that the lowest core loss is measured at an annealing temperature of 525 °C. As the annealing temperature increases beyond 525 °C, the core loss gradually increases. This suggests that the optimal annealing temperature for minimising core losses at lower frequencies lies around 525 °C. Meanwhile, at higher frequencies, the minimum core loss is observed at an annealing temperature of 800 °C. This indicates that the optimal annealing temperature for minimising core losses at higher frequencies lies around 800 °C. Consequently, to investigate the magnetic properties, specifically focusing on the hysteresis loop, a combination of 500 Hz frequency and 1.5 T flux density was chosen. This combination allows for a comprehensive analysis of the magnetic behaviour and performance of the samples under specific conditions.

In summary, Figure 4-9 illustrates the hysteresis loop for both coated and uncoated samples, highlighting the diffusion and distribution of manganese. The coated samples exhibit a larger loop area and higher saturation flux density, indicating improved magnetic performance. The AC core losses were evaluated at 500 Hz, with the optimal annealing temperature for minimising core losses differing at lower and higher frequencies. Finally, the 500 Hz frequency and 1.5 T flux density were selected to investigate the magnetic properties, providing a comprehensive understanding of the magnetic behaviour and performance of the studied samples.

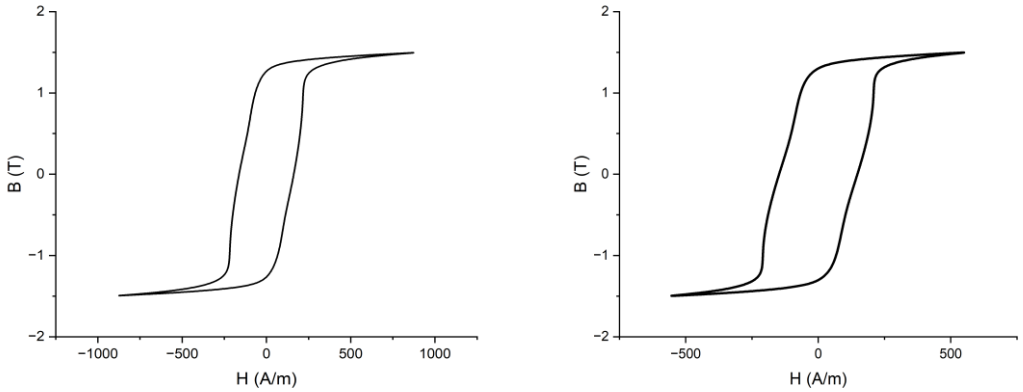

(a) (b)

Figure 4-9 The hysteresis loop at 500 Hz and 1.5 T. (a) uncoated sample, (b) coated sample.

4.6 Discussion of the use of manganese paste

The results of using manganese paste showed that it was possible to reduce the power losses of the material by up to 11% when magnetised to 1.5 T at 400 Hz. This contrasted with the results obtained using silicon paste [119] ,when such reductions were only possible when non-oriented steel. However, this led to an increase in the already large number of variables in the system. This problem was compounded when it was found to be necessary to add further components to the paste to make it usable. Many of the pastes employed failed to produce reductions in power loss and in some cases yielded considerable increases. The reasons for this failure were frequently obvious, such as poor adhesion, inhomogeneity or bubbling producing non-uniform manganese distributions. On these occasions, the reproducibility of the results was understandably poorer than when good pastes were used. Differences of 20% in power loss could be found between individual samples where the paste had flaked, and the samples had buckled compared with only a few percent when the conditions were correct. A selection of these results has been included but most have been excluded because samples with buckled

or bubbled surfaces make the samples virtually useless and impossible to analyse. A paste of manganese oxide and silicon oil to help maintain the manganese in suspension gave beneficial results. Firing at 525°C under nitrogen and annealing for 2 hours under argon led to reductions in power loss of 7% at 1.3 T and 8% at 1.5 T. The reduction in power loss varied with flux density. It was apparent that the firing conditions and paste compositions that gave good results were considerably changed when the powder size was increased. This may be seen by comparing, for example, the pastes shown in Figure 4-1. For constant firing conditions, the changes in power loss vary with the percentage of manganese powder in the paste. The improvements discovered in the stress sensitivity characteristics of the steel were not limited to cases where the zero-stress value had succeeded in being reduced. The improvement in reduction of stress sensitivity is reduced on further annealing, although the zero-stress values were improved. Increasing the frequency of magnetisation from 50 Hz to 400 Hz did not produce any significant increase in the percentage changes in power loss. As with the silicon experiments [65], the relationship between the 50 Hz and 400 Hz was unpredictable, though in certain cases an apparent minimum for power loss was seen at the higher frequency. This did not correspond to a minimum at 50 Hz.

4.6.1 The SEM observations

Showed that the level of manganese on the surface of the samples was only of the order of a few percent. This agrees with the observation that little increase in resistivity of the bulk material was seen. The concentration gradients may seem surprising considering the anneals undertaken and may be due to the incomplete removal of the paste or intermetallic layer subsequent to firing.

A sample of the completely coated material was pasted on one side with a mixture comprising 0.5 gm silicon oil solution per gram of manganese powder and was then fired for 1

hour at 800°C. This paste composition was used even though it had not yielded especially good results because it had been observed to be easily removable subsequent to firing. It was felt that it was important that the bending should be observed without the presence of a hard well adhered paste because this could influence the stress patterns considerably. If considerable forces were required to remove the paste, then annealing would be required to remove the stresses so formed, which would possibly modify the stresses generated by manganese. The residual paste was extremely flaky and was easily brushed off with no change in the curvature, showing that it had not caused the bending. Deducing the stress distribution inside the material is somewhat problematic. In the case of phosphate-coated material, the tensile stresses in the metal are balanced by compressive stresses in the coating. However, this is not the case in manganese-decorated steel.

This experiment was much more difficult to carry out satisfactorily than the equivalent one for manganese due to the increase in non-uniform heating along the length of the sample at the higher firing temperature. Therefore, localised radii of smaller dimensions could be produced by non-uniform silicon distribution [119].

This contrasts with the results obtained when silicon paste was employed, and the beneficial results were only successfully obtained where non-oriented steel was the starting material. In the case where non-oriented material was the starting material, the improvements in power loss could be attributed simply to the increase in resistivity that the addition of manganese brought about. As shown by the SEM micrographs, the amount of manganese added was up to several percent at the surface and penetrated well into the thickness of the material. The stresses that were shown to be set up by the firing of manganese paste would not be expected to have strong effects because the material only has a weak texture in the rolling direction. Not all experiments succeeded in producing large reductions in power loss, which

may be attributed to various reasons. A certain amount of porosity was found at the surface of some of the specimens, although this was small compared to that found in most siliconized samples. This could have been produced by the same mechanisms cited for the siliconized samples (i.e., the creation of vacancies by the forces that were set up or the formation and dissociation of intermetallic compounds). Another source of inclusion could be formed if oxygen, either from moisture in the paste which might become entrapped or left by incomplete purging of the furnace tube, caused some inter-oxidation of the manganese to form alumina. This could cause large increases in coercivity and power loss if present as a fine dispersion. An inhomogeneous introduction of aluminium over the surface areas both in terms of quantity and depth of penetration could also cause unfavourable flux distributions [67].

4.6.2 Power loss reductions

It would appear that the power loss reductions of up to 15% are too great to be explained purely by the small surface resistivity increase, which would be afforded by the small amounts of silicon added [65]. Therefore, it would seem that the effects of tensile stress at the surface are of at least equal importance. The fact that much greater amounts of manganese were required to achieve similar reductions in the power loss of non-oriented material emphasises this conclusion, as does the observation that the improvements are not increased at higher magnetisation frequencies. The decrease in the improvement in power loss with the increase of flux density may be explained by the fact that any improvement in the flux distribution that might appear at low flux densities would disappear as saturation was neared and uniformity approached. In addition, the small amount of surface disturbance observed coupled with the manganese addition might result in a lowering in the saturation magnetisation in the surface regions. The reduction in stress sensitivity of both power loss and magnetostriction under both

tensile and (more importantly) compressive stresses is again an indicator of the importance of the stresses produced.

The fact that improvements in power loss only seem to occur when small amounts of manganese are added with small penetrations depth suggests that the desired stress distribution is of a small layer containing moderately high tensile stress, which can then be balanced by fairly small stresses over a proportionately large area. The compressive stresses should be small enough to avoid the destruction of the longitudinal bar domain structure. If larger amounts of manganese are added, then larger stresses will be set up for the same penetration depth. Increasing the annealing time to reduce the concentration gradients will then have the effect of increasing the compressive stresses acting in the centre due to a reduction in the area over which they can act. The other effect of adding more manganese will be to decrease the saturation magnetisation at the surfaces. Improvement in the stress sensitivity of the material is not necessarily accompanied by improvements in power loss. The stress sensitivity under compression of a sample whose power loss was increased relative to that obtained prior to treating was considerably reduced. In this case, measurements of power loss and stress sensitivity were carried out prior to the phosphate coating being removed. Therefore, the values of power loss in the uncoated state may be estimated by increasing those of the coated state by 10%. Annealing the sample produced a reduction in power loss, but this was accompanied by a reduction in the improvement in stress sensitivity. The latter effect is unsurprising when it is considered that annealing will cause a reduction in the concentration gradients, and hence in the stresses present. It thus appears that improvements in both power loss at zero stress and under compression may be improved by the addition of suitable quantities of manganese, but that the optimum conditions for the two will not be the same. Most of the quoted results have given the changes in properties relative to the values obtained subsequent to phosphate coating

removal. However, it was not practical with the facilities available to replace the phosphate coating subsequent to manganese, and therefore the effects that this might have decorated been deduced from the stress sensitivity curves. In addition to reducing the stress sensitivity of power loss, manganese also reduces the stress sensitivity under tension. Therefore, the expected improvements in zero-stress power loss will be less than the 10% normally expected. A further reduction in the stress sensitivity of power loss under compression would also be anticipated. The critical nature of the quantity and distribution of the manganese that was added to the steel was reflected in the sensitivity of the paste composition in the results. If the paste was either inhomogeneous or did not adhere consistently to the steel surface, then this would result in the non-uniform diffusion of manganese over the sheet surface.

The relative diffusion characteristics of the paste and the steel are in part responsible for the manganese distributions obtainable through the thickness of the sheet. It appears that defining the proportion by weight of manganese in the paste is insufficient because the treatment temperatures required to obtain the same results when coarse and fine powders were considerably different. If it is accepted that the outer layer of the particles will become oxidised to a certain depth during the aqueous phase of the paste, then the amount of manganese that will be free to diffuse into the steel will depend on the volume of unoxidized metal remaining. In the case of fine powder, the oxidised material may constitute a considerable fraction of the material, while in the case of coarser material this would not be the case. Transferring the same amount of material from each paste (assuming that neither paste becomes exhausted) would take a higher temperature or longer firing. The size of powder employed is clearly important. Although the quantity of manganese transferred from the paste to the steel may be controlled up to a point by varying the firing conditions, the powder will settle out if it is too large it will settle out, while if it is too fine it will become completely oxidised.

Adhesion issues were commonly observed, often accompanied by bubbling, especially with specific paste compositions. The introduction of additional parameters, stemming from the inclusion of additives, significantly complicated the process of result evaluation. Notably, the presence of a small amount of manganese seemed to yield slightly more favourable outcomes, whereas pastes with a ratio closer to or greater than unity yielded limited results.

4.7 Summary

In this chapter a new material manganese (IV) oxide as a paste has been proposed to increase the resistivity of Si-Fe for the sake of reducing power losses. Having ascertained that manganese could be successfully used to reduce the power loss of non-oriented silicon-iron, manganese has been demonstrated to diffuse into steel from a paste consisting of the relevant element in powder form diluted silicone oil solution. With the addition of manganese, the power loss of non-oriented 2.4 wt % silicon-iron was reduced by up to 7% at 1.5 T. The reason for the reduction appears to be a straightforward resistivity increase. In the case of silicon diffusion, the degree of improvement was often silicon content at the surface [65]. This layer was probably in effect virtually nonmagnetic, and therefore brought about a reduction in saturation magnetisation of the whole steel. The thickness of this layer was believed to be related to the relative rates of diffusion of manganese through the paste and metal, and in consequence was dependent strongly on the composition of the paste. When applied to different temperature non-oriented steel materials, the results obtained from three pasted samples were considerably different and power loss reduction be achieved using manganese. The best results obtained were a reduction of up to 8% at 1.5T.

Chapter 5: Experiments using cobalt paste

5.1 Introduction

There are two fundamental ways of controlling the quantity of cobalt that diffuses into the steel sheet from the paste. The first method is to limit the amount of cobalt that is available for diffusion, which may be achieved by controlling the composition of the paste and the thickness of the coating that is applied to the sheet. The sample is then fired under suitable conditions of time and temperature so that all of the available cobalt is transferred from the paste to the steel. The other method is to provide sufficient paste, such that there is more cobalt than is required available, and to control the amount of cobalt that enters the steel by altering the time and temperature of firing. It would then be necessary to remove the residual coating, assuming that the diffusion constant for cobalt through the paste is the same as that for its diffusion through silicon-iron at any given temperature.

In the second method, the amount of cobalt present in the paste is vastly greater than the amount that is to be diffused into the sheet. If the amount of cobalt present is only slightly greater than that which is to be diffused in, then maybe will be applicable as before. However, there is no reason to believe that the diffusion constant for cobalt in the paste will be the same as that in the steel (as was assumed above). It would appear likely that if this were not to be the case, then the diffusion constant would be related to the composition of the paste. The relative speeds of diffusion in the paste and the steel could be important for several reasons[125]. In the finite source method, if the rate at which the cobalt diffuses through the steel is much greater than the rate at which it arrives at the steel surface, then the steepness of the concentration gradient that can be achieved will be limited. If the reverse is true, then high concentrations of cobalt could form on the surface of the sheet. This could be undesirable because of the

considerable stresses set up by concentration gradients, as evidenced by the buckling of samples in the preliminary experiments and because of the formation of intermetallic compounds, such as Fe, Si, $FeSi_3$, and Fe Si [126]. However, this would be unlikely in the case of a thin paste whose composition would change considerably. A further complication arises because if there is a contact resistance between the paste and the sheet, then there will be a concentration difference across the boundary that will diminish to zero as equilibrium is approached. Therefore, it would seem that even if the diffusion constant for cobalt in a paste of any given composition could be determined, it would be impossible to estimate with any confidence the diffusion characteristics that could be obtained from any given firing conditions[127]. The concentration profile may be modified once the requisite amount of cobalt has been introduced into the steel by further annealing of the sample. This may be done to reduce the concentration gradients and increase the penetration depth of the cobalt. If the finite source method is employed, then whether the residual paste is removed or not it is irrelevant from the point of view of the cobalt distribution because it will be exhausted [128]. In cases where an excess of cobalt has been applied, the removal of any residue becomes imperative to prevent the ongoing addition of cobalt to the steel during annealing. This implies that, while in the first method, annealing can seamlessly follow the firing treatment as a single integrated process, the second method necessitates the use of two distinct processes to achieve the desired outcome.

5.2 The properties of sodium silicate

To understand the characteristics of the pastes, it is necessary to consider the physical and chemical properties of sodium silicate. Sodium silicate is not just one specific chemical but is the name for a family of compounds whose composition may vary over a large range, such as orthosilicate (Na SiO_4), metasilicate (Na_2SiO_3) and disilicate ($NaSi_2O_5$). However, in

both the solid and aqueous states, the composition may be varied continuously. The chemical composition of sodium silicate is generally given as SiO_2/Na_2O, where x may take non-integral values.

Sodium silicate solutions consist of monomeric (SiO_4) ions, disilicate ($Si_2 O_3$) ions, and colloidal silica micelles [129]. The proportions of the ions and colloids will change with the composition of the solution. Where the ratio of SiO_2/ Na_2O is less than about two, no colloidal component is present, whereas above this value it is formed to an increasing degree. All of the solutions are alkaline, and the pH increases as the proportion of Na_2O present becomes greater.

In the solid form sodium silicate forms an anhydrous glass whose structure consists of SiO tetrahedra, with the sodium ions being randomly dispersed in the interstices. The softening point of the material varies considerably, although in common with other glasses no specific melting point can be given. If sodium silicate solutions of various compositions are allowed to air dry at room temperature, then they will have considerably differing characteristics [130] .

5.3 The desired characteristics of the paste.

The function of the paste is to provide a source of the element which is required to be diffused into the steel sheet. It is necessary that this element transfer should occur to a controllable extent and uniformly over the surfaces of the sheet. Therefore, the paste must be homogeneous and form a consistent interface with the metal. For the paste to be homogeneous, it is necessary for the powdered element to remain in suspension in the sodium silicate solution and not settle out. If this were to occur, then the concentration of the paste would be liable to vary on the sheet. The conditions under which a powder will remain in suspension are complex to define, but the most important are:

(a) The size and shape of the powder particles. In the case of a particle of any given shape and density the larger the particle, the greater will be its tendency to sink in a liquid. A large surface-to-volume ratio favours the suspension of a particle. The shape of a powder is generally related to the method of its manufacture and may be spherical, angular, acicular granular, irregular, or flake.

(b) The viscosity of the sodium silicate solution. The powder will have a lesser tendency to settle out in a more viscous sodium silicate solution. The viscosity of the solution will depend both on its surface and on the SiO_2/ NaO_2 ratio of the silicate. For solutions of constant weight percentage, the viscosity is a minimum for a SiO2/ Na_2O ratio of 1.9 and rises rapidly as it increases towards 4.0. At a constant solid weight percentage of 38%, increasing the ratio from 2.0 to 3.3 increases the viscosity from 100 to 350 centipoises. Strictly speaking, colloidal suspensions, which are found in any material with a ratio greater than 2.0, do not constitute true solutions; however, their presence has the effect of increasing the viscosity of the silicate. The solid-to-liquid ratio also has a profound effect on viscosity, especially with concentrated solutions. For solutions a ratio of 2.0, increasing the solid weight percentage from 42 to 45% causes the viscosity to change from 250 to 2000 centipoise.

(c) The surface chemistry of the particle liquid interfaces. Strong bonding between the liquid and the solid particles will hinder the movement of the particles, and thus promote their suspension. An important effect in sodium silicate solutions having a ratio of greater than 2 is the effect of colloids. Colloids comprise polyanions that may be chemisorbed onto the surface of the powder, thereby giving the particles a strongly negative surface charge. Therefore, the particles repel each other and settling is opposed. To maintain a constant interface between the paste and the sheet, it is essential for the paste to wet the surface and adhere to it upon drying. Therefore, the surface of the steel must be clean before the application of the paste to ensure

that this is so. In particular, it is necessary to ensure that no greasy layer is present on the surface that might impair this process.

5.3.1 Paste in the solid state

When the paste is dried subsequent to being applied to the sheet surface, it will consist of powder particles set in a glassy matrix. The relative volumes of the two will be dependent on the initial composition of the paste. Given that it appears that cobalt will react with sodium silicate in the aqueous state, the particles will presumably have a surface layer of high silicon silicate. The liquid will continue to be removed from the paste at a temperature of over 600°C when the silicate will be close to the anhydrous state, but it is not clear whether or not there is any reaction between the silicate and the cobalt at elevated temperatures.

The cobalt powder that was purchased was of 99% purity, granular, and of size, approximately 45 µm, while the sodium silicate solution of unspecified composition had a strength of 1.57 gm/L. A measurement of the pH value of the solution indicated that the design of the silicate was of SiO_2/ NaO_2. The preferable value of this ratio is not immediately apparent because the increased colloid content and reduced alkalinity of the higher ratio solutions are offset by the increasing brittleness and friability of the solid forms. Given that the solution had produced workable pastes in the preliminary experiments, it was decided to use to this composition.

5.4 Experimental procedure

It was decided to investigate the effect of altering the sodium silicate to cobalt powder ratio under constant firing conditions to determine the optimum paste composition. It was not anticipated that the quantity of liquid added to give the paste the desired consistency would

ultimately affect the properties of the paste because it was to be added merely to permit the coating application and would be removed prior to firing. Although the thickness of the coating was difficult to control using a brushing on technique, no ready alternative was apparent. This meant that control of the amount of cobalt entering the steel had to be achieved through alteration of the firing conditions rather than by making a finite amount of cobalt available. Pre-drying was to be carried out at ambient temperature until the paste was found to be touch dry, which was usually of the order of 30 minutes. The samples were frequently pasted further in advance of the firing time. It was decided to maintain a constant firing temperature of 800°C. Although the best results in terms of power loss had been achieved at 890°C, it was felt that the increased difficulty in magnetising the samples was too great. In addition, it was estimated that most of the available cobalt from the paste had been transferred to the steel, which was undesirable due to the possible effects in non-uniform coating thicknesses on the available cobalt. In addition, if all the paste has been removed from the sheet, then varying the composition of coats of constant thickness would be certain to result in very different amounts of manganese being transferred in each case. It was felt that one obstacle to achieving good power loss results was the buckling of the samples from the sodium silicate until relatively high temperatures.

Having selected the most suitable paste from the experiments carried out on non-oriented material, it was then tried on samples of non-oriented 2.4% silicon-iron. The characteristics that were sought included consistent adhesion of the paste and a reduction in the surface porosity of the steel caused by the processing.

5.5 Results of SEM observations

Figures 5-1a to 5-1c display micrographs illustrating the morphology of the samples and the variation in cobalt concentration across their thickness. It's worth noting that the depth of manganese diffusion remained consistent in all tested samples, it shows observations of material extending 300 µm deep into each of the side strips. In Figure 5, we delve into the SEM and EDS analysis of typical inclusions found in the final annealed samples. Prior to analysis, the samples underwent a coating and polishing process using Acetone. The primary focus of the SEM and EDS analysis was to examine the presence of cobalt inclusions. The EDS analysis uncovered a significant presence of cobalt within the samples. These inclusions, primarily with sizes less than 300 µm, are readily observable in Figures 5-1a to 5-1c. Interestingly, various inclusions with differing cobalt contents are discernible in these micrographs. Further details from the EDS analysis are presented in the accompanying tables, corresponding to each figure. Further SEM microstructural examination revealed that cobalt-rich precipitates were truant in the 5.4 wt % cobalt specimen (Figure 5-1a) but became apparent in the 73 wt % cobalt specimen (Figure 5-1c) and the cobalt concentration variation through their thickness. The photographs also show a spectrum from which the cobalt concentration may be determined. The main feature of the specimens is a porous layer of high cobalt content on their surface. The limit of the cobalt concentration which could be measured on the ratemeter peak possibly (1.731 keV), which used was 70%. This value was generally exceeded in the porous areas, where the trace levels were out at the maximum value. The extent of the porous layer was dependent on the composition of the paste being used and, to a lesser extent, on the firing temperature. The composition profile in the regions that were not affected by porosity varied less than the thickness of the porous layers but ran from place to place in any given sample. The maximum width of the porous layer was ~ 72% of the half-sheet thickness, while the minimum was found

to be < 5%. The paste composition for these two samples was 1 ml sodium silicate solution per gram of cobalt and 1/3 ml per gram respectively. The cobalt concentrations at the porous/nonporous interface varied considerably from place to place in any given sample but were generally of the order of 5–8%, with a penetration depth of 32.9% of the half-sheet thickness when the firing was carried out at 890°C. All of the quoted penetration depths are measured from the porous-nonporous interface rather than the steel surface because it is thought that the porous layer is probably relatively magnetically unimportant.

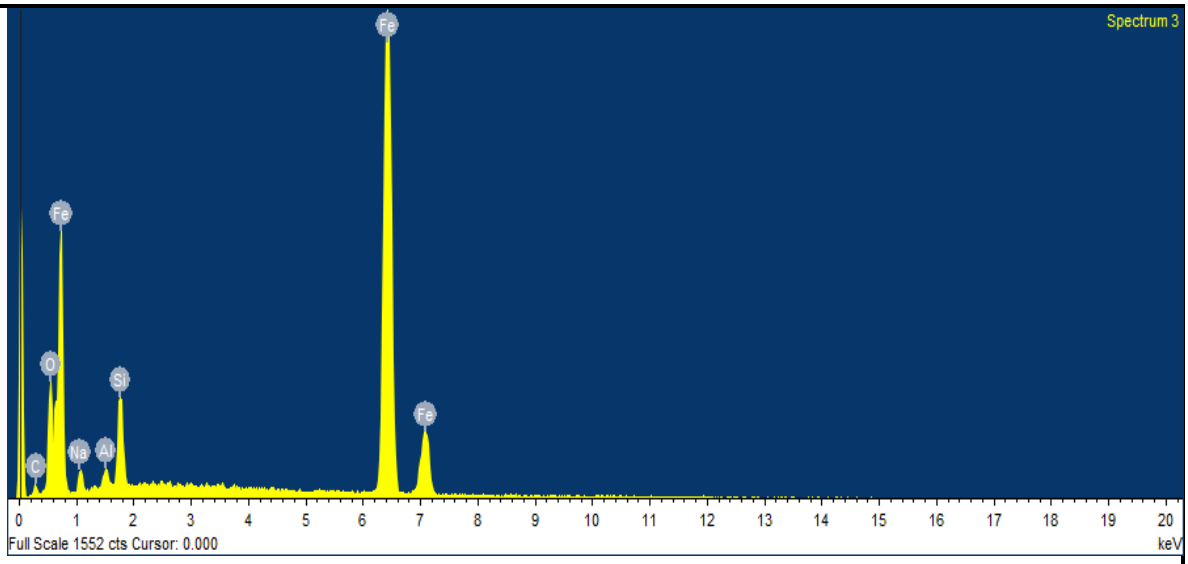

(i)

Element	Weight%	Atomic%	Oxide%	Formula
C	8.56	13.27	31.36	CO_2
Fe	63.59	34.25	81.81	FeO
O	54.04	62.92		
Al	2.74	1.89	5.18	Al_{2O3}
Na	6.66	5.40	8.98	Na_2O
Si	21.67	14.37	46.36	SiO_2
Co	5.40	1.71	6.86	CoO
Ca	0.73	0.34	1.02	CaO
K	0.20	0.10	0.24	K_2O
Totals	100.00			

(ii)

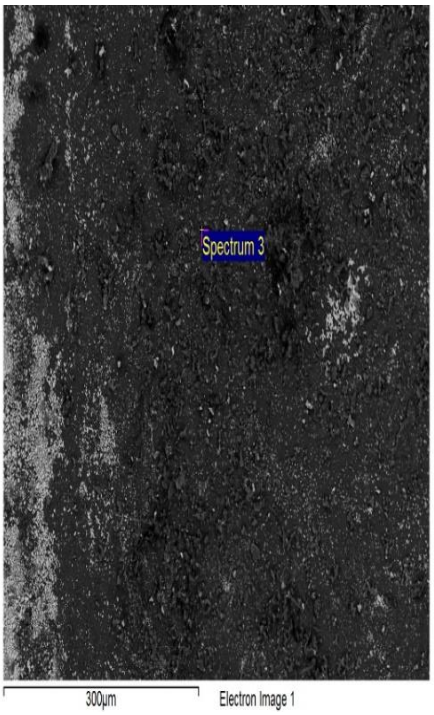

(iii)

(a) The containing Co 5.40 w%.

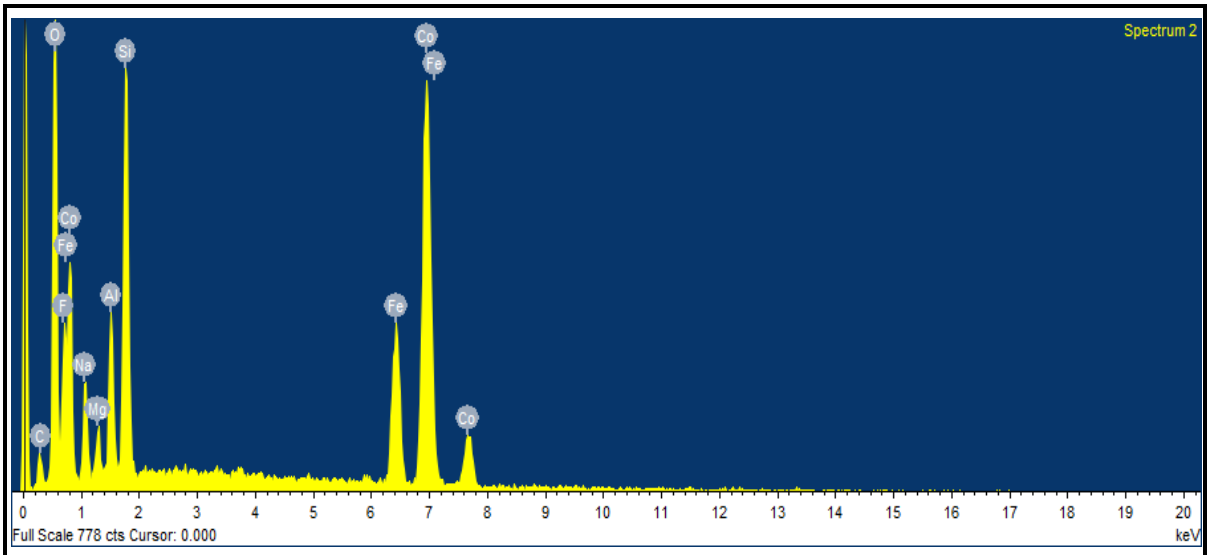

(i)

Element	Weight%	Atomic%	Oxide%	Formula
C	4.19	8.73	15.36	CO_2
Fe	10.53	4.72	13.55	FeO
O	35.11	54.92		
F	3.03	3.99	0.00	
Al	2.95	2.73	5.57	Al_{2O3}
Na	3.70	4.03	4.99	Na_2O
Si	6.43	5.73	13.76	SiO_2
Mg	1.13	1.17	1.88	MgO
Co	32.93	13.98	41.87	CoO
Totals	100.00			

(ii)

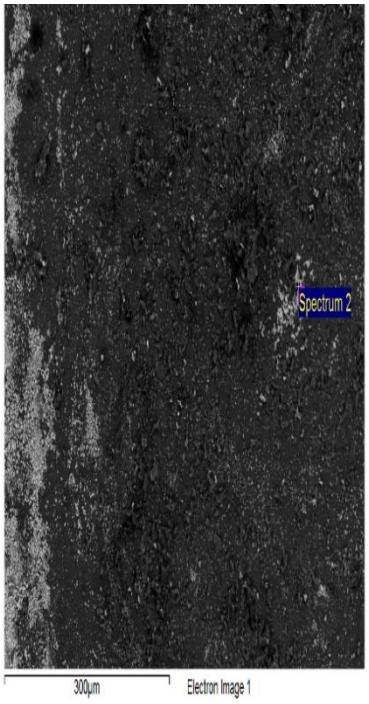

(iii)

(b) The containing Co 32.93 w%.

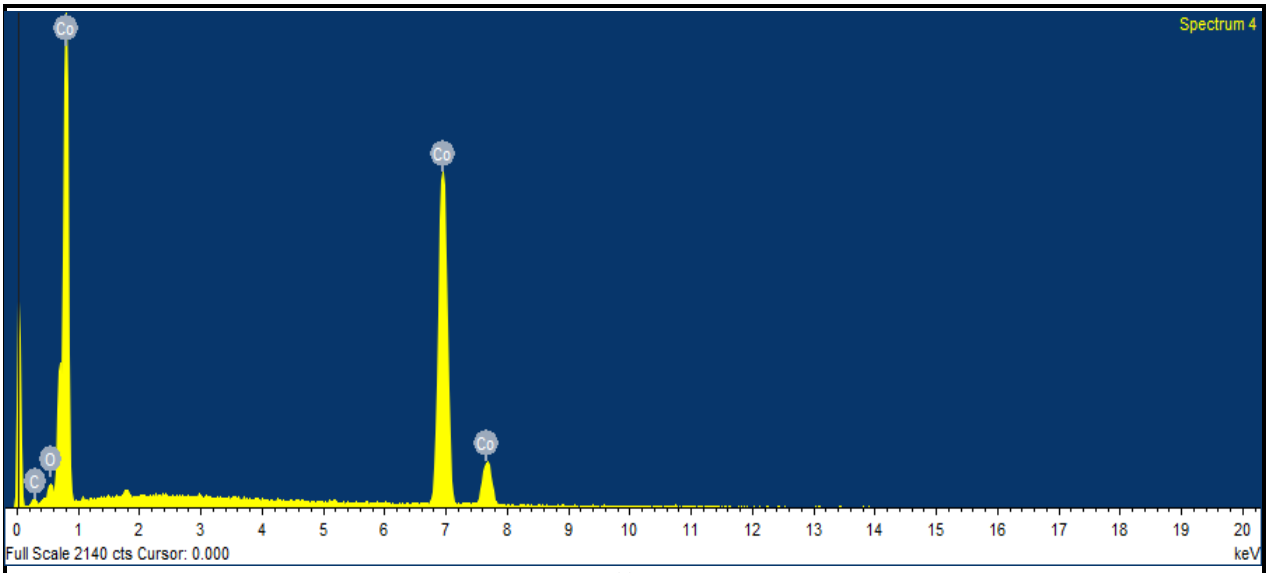

(i)

Element	Weight%	Atomic%	Oxide%	Formula
C	0.26	8.25	11.95	CO_2
O	25.11	54.92		
Na	2.30	4.62	4.71	Na_2O
Si	0.46	0.50	0.99	SiO_2
Co	72.33	40.88	91.97	CoO
Totals	100.00			

(ii)

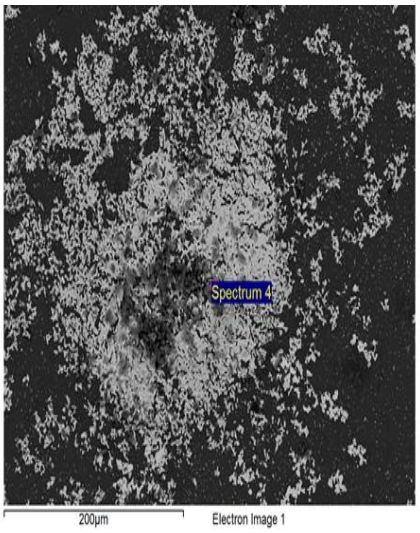

(iii)

(c) The containing Co 72.33 w%.

Figure 5-1 Distribution of elements after heat treatment with EDS analysis of X-rays using SEM. (i) EDX spectra of the sample. (ii) Table EDS analysis of inclusions from Figure (iii). (iii) Complex inclusions in the sample of NOES sheet.

5.6 Results of magnetic testing

5.6.1 Effects on power loss

The measurement was carried out at 1.5 T with different frequencies. The starting material in each case was 2.4% silicon non-oriented steel. All samples were fired at 890°C, being kept at the soak temperature for 1 hour under an atmosphere of hydrogen. From the results obtained by applying the following method to calculate power loss separation, the power loss of the NOES samples was measured using the SST in which all power loss measurements were made, as shown in Table 5-1.

Table 5-1 Power loss of NO steel measured at various magnetising frequencies, with a total power loss per cycle uncoating at a peak flux density of 1.5 T.

Magnetising frequency (Hz)	**Measured power loss (W/kg)**	**Power loss per cycle (W/kg).sec**
50	3	0.06
100	7.19	0.07
200	19.01	0.01
400	57.80	0.14
500	87	0.17
700	163	0.23
1000	327	0.33

Figure 5-2 shows the measured power loss per cycle versus the frequency's square root. We can find the coefficients of the power loss parts by fitting a polynomial curve to this curve in Microsoft Excel.

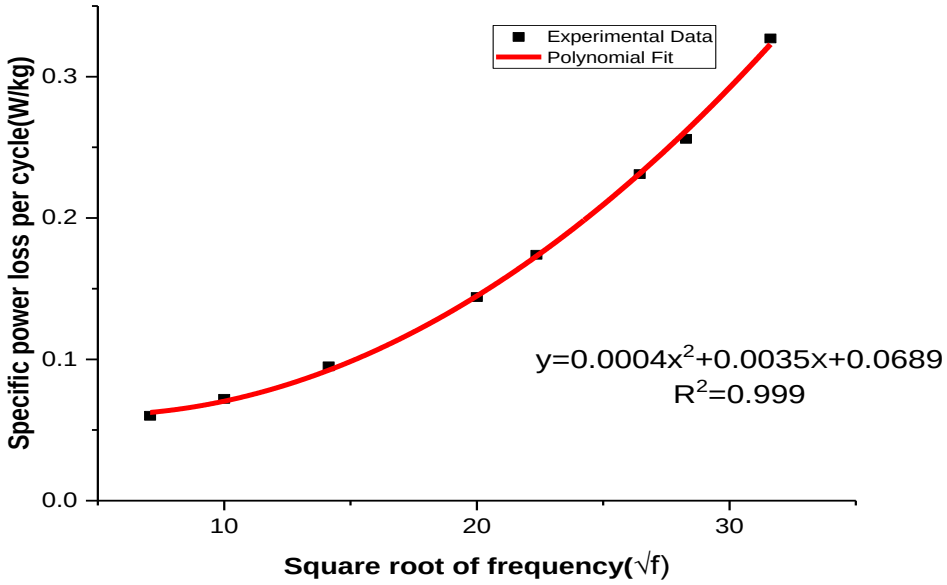

Figure 5-2 Total power loss per cycle of a magnetic uncoated sample made of non-oriented steel at a 1.5 T flux density against the square root of frequency.

The fitting equation's residual values are often very near to unity, or R^2= 0.999, which suggests that this is an accurate approximation. Table 5-2 shows the results of determining the power loss components at various frequencies using the equations from Figure 5-2.

$$A = C_h B_{pk}^n = 0.0689 \qquad (5\text{-}1)$$

$$B = C_e f {B_{pk}}^2 = 0.0004 \qquad (5\text{-}2)$$

$$C = C_a (f B_{pk})^{1.5} = 0.0035 \qquad (5\text{-}3)$$

The power loss components, as illustrated in Table 5-2, are calculated by applying these coefficients in Equation (4.6), as mentioned in the previous chapter. Figure 5-3 demonstrates the relationship between the magnetising frequency, and the hysteresis power loss and eddy current power loss at 1.5 T. The static hysteresis loops are used to calculate hysteresis loss. However, the following equation may be used to calculate eddy current power loss per cycle as a linear function of the magnetising frequency:

$$P_e = \frac{\pi^2}{6\rho} d^2 f^2 {B_{pk}}^2 \qquad (5\text{-}4)$$

Table 5-2 Power loss components of SST of NO steel at various magnetising frequencies and a peak flux density of 1.5 [T] with uncoated samples.

Frequency (Hz)	**Measured power loss (W/kg)**	**P_e (W/kg)**	**P_h (W/kg)**	**P_a (W/kg)**	**$P_c=P_e+P_h+P_a$ (W/kg)**	**Error= $\frac{P\ calculated - P\ measured}{Pcalculated} \times 100\%$ (%)**
50	3.00	0.1	3.44	0.637	4.17	0.28
100	7.19	0.4	6.89	1.75	9.04	0.20
200	19.01	1.6	13.78	4.95	20.33	0.06
400	57.80	6.4	27.80	14	48.2	-0.12
500	87	10	34.45	39.13	83.58	-0.04
700	163	19.6	48.23	64.82	132.56	-0.22
1000	327	40	68.9	110.77	219.67	-0.48

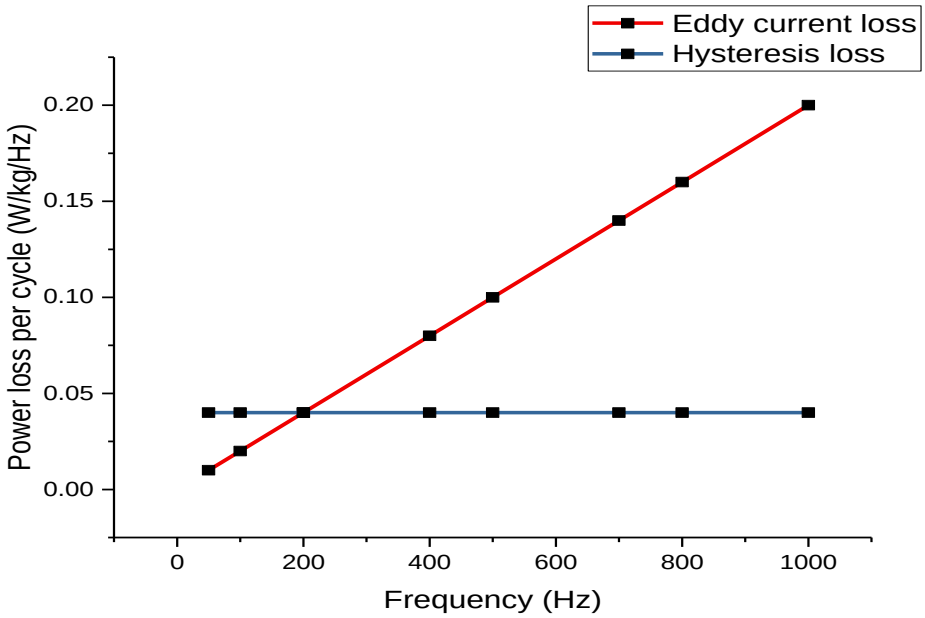

Figure 5-3 Eddy current and hysteresis loss per cycle versus frequency.

The power loss of non-oriented steel is measured at a peak flux density of 1.5 T at different magnetising frequencies with a total power loss per cycle with coating as shown in Table 5-3.

Table 5-3 Power loss of non-oriented steel measured at a peak flux density of 1.5 T at different magnetising frequencies with total power loss per cycle with coating.

Magnetising frequency (Hz)	**Measured power loss (W/kg)**	**Power loss per cycle (W/kg).sec**
50	2.88	0.058
100	6.78	0.068
200	17.50	0.088
400	49.41	0.123
500	71.99	0.144
700	130.35	0.186
1000	251.80	0.251

Figure 5-4 shows the measured power loss per cycle versus the frequency's square root. We can find the coefficients of the power loss parts with coating by fitting a polynomial curve to this curve in Microsoft Excel.

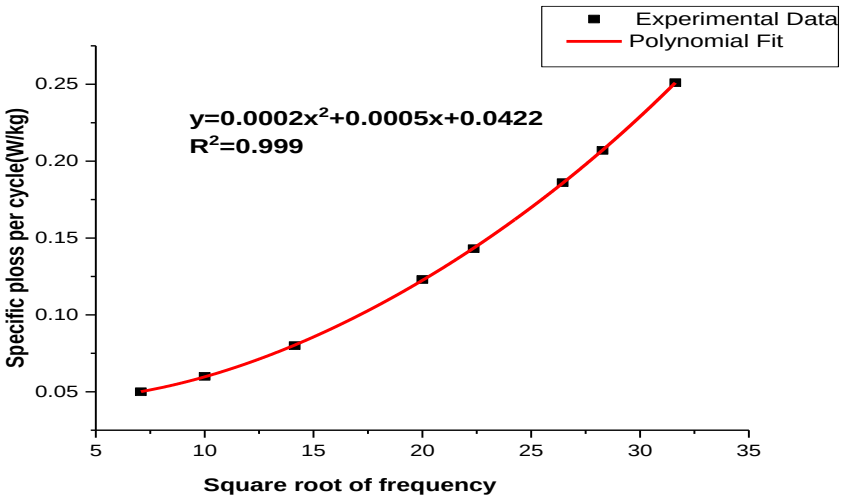

Figure 5-4 The total power loss per cycle of a magnetic sample made of NO steel at a 1.5 T flux density against the square root of frequency.

The power loss separation findings for the same material with a coating are shown in Table 5-4.

Table 5-4 Power loss components of an SST of NO steel at various magnetising frequencies and a peak flux density of 1.5 [T] with coated samples.

Frequency (Hz)	**Measured power loss (W/kg)**	**P_e (W/kg)**	**P_h (W/kg)**	**P_a (W/kg)**	**$P_C = P_e + P_h + P_a$ (W/kg)**	**Error= $\frac{P\ calculated - P\ measured}{Pcalculated} \times 100\%$ (%)**
50	2.88	0.5	2.11	0.177	2.78	-0.03
100	6.78	2	4.22	0.50	6.72	-0.008
200	17.50	8	8.44	1.41	17.85	0.02
400	49.41	32	16.88	4.00	52.88	0.06
500	71.99	50	21.1	5.60	76.70	0.06
700	130.35	98	29.55	9.26	136.80	0.04
1000	251.80	200	42.21	15.81	258.01	0.02

Table 5-5 illustrates a comparison of the eddy current power loss obtained by the extrapolation method (experimental based) and the eddy current calculated by the conventional formula (theory-based). This experiment indicates that the eddy current loss calculated in a sample at low induction and low frequency is virtually equal to that observed by the extrapolation method. Most of the extra loss changes with the frequency and strength of the field at the same eddy current power loss.

Table 5-5 Results obtained using the extrapolation method and a comparison of Equation (4-13) to find the eddy current power loss of an SST with a peak flux density of 1.5 T and different frequencies.

Magnetising frequency Hz	**Eddy current power loss (W/kg) by extrapolation method**	**Eddy current power loss (W/kg) Calculated by equation (5-4)**
50	0.5	0.37
100	2	1.55
200	8	6.88
400	32	24.12
500	50	37.30
700	98	72.25
1000	200	147.45

Table 5-6 displays the percentage reduction in power loss for uncoated and coated samples at various frequencies, and verifies that the reduction in power loss occurs at a peak flux density of 1.5 T. The diffusion of cobalt (II, III) oxide reduces losses by approximately 23% at 1000 Hz at the value flux density of 1.5T. Moreover, because the effects of the internal

flux distribution are greater, even when AC magnetism was used, the unequal amount of Co causes a resistivity gradient that lowers eddy current loss.

Table 5-6 The percent decrease in power loss on uncoated and coated samples at various frequencies at 1.5 T.

Magnetising frequency (Hz)	**Overall power loss with uncoating (W/kg)**	**Overall power loss with coating. (W/kg)**	**Reduction in power loss (%)**
50	3.00	2.88	4
100	7.19	6.78	6
200	19.01	17.50	8
400	57.80	49.41	15
500	87.00	71.99	18
700	163	130.35	21
1000	327	251.80	23

Figure 5-5 illustrates the reduction in permeability for both coated and uncoated specimens across various frequencies. In the case of uncoated samples, it's evident that the permeability is significantly impacted as frequencies increase from 100 Hz to 700 Hz. Conversely, the coated samples exhibit an increase in magnetic permeability, particularly notable at 1 kHz with coating, and the most substantial percentage decrease in permeability occurs at 50 Hz with a coating at a peak flux density of 0.9 T. This observed increase in magnetic permeability can be attributed to the diffusion of cobalt (II, III) oxide into the material, notably affecting the texture of the Si-Fe strips.

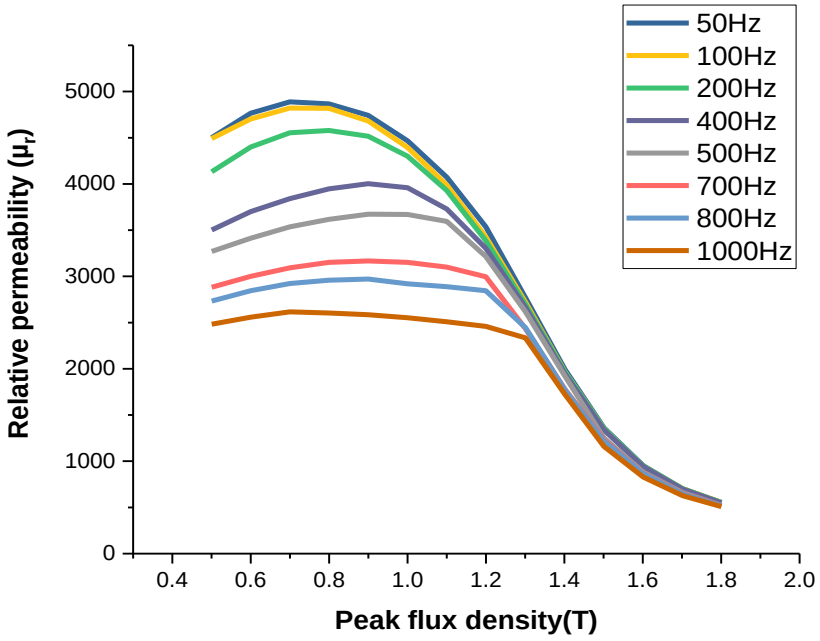

(a)

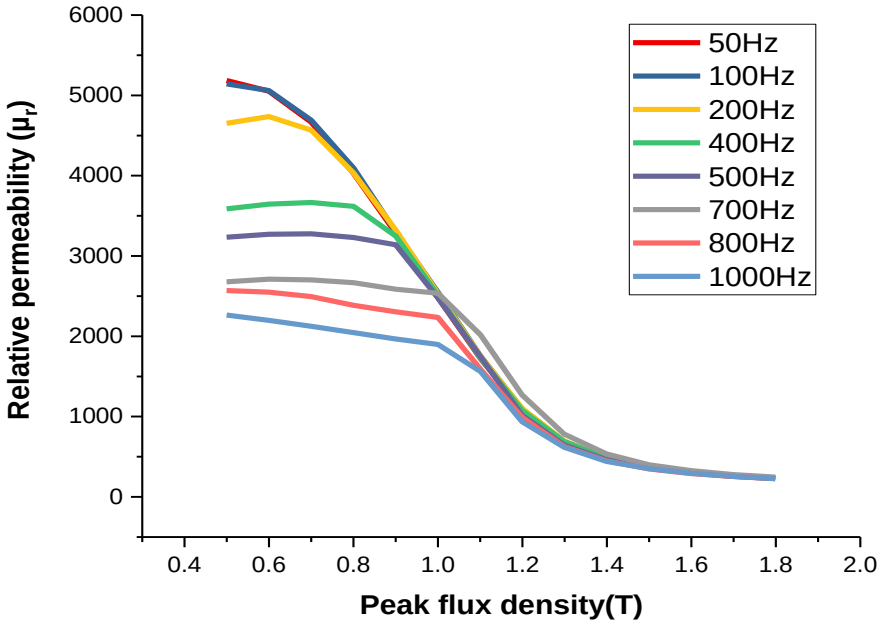

(b)

Figure 5-5 Relative permeability testing for coated and uncoated specimens at different frequencies: (a) uncoated sample, and (b) coated sample.

5.6.2 Magnetic properties

The hysteresis loop is a graphical representation that demonstrates the behaviour of a magnetic material when subjected to an alternating magnetic field. It shows the relationship between the magnetic field strength (H) and the resulting magnetic flux density (B) as the magnetic field is cycled through both positive and negative values. In this context, the hysteresis loop is being used to compare the magnetic properties of the coated and uncoated samples. The size of the hysteresis loop indicates the amount of magnetic energy stored within the samples, which reflects the diffusion and distribution of cobalt. A larger loop suggests a greater quantity of losses. Magnetic permeability is an important factor in determining the behaviour of a material in a magnetic field. In particular, it quantifies how easily a material can be magnetised and how it responds to changes in magnetic fields. In addition, it is influenced by the characteristics of the material itself and remains consistent, regardless of the material's shape or geometry. The coated samples exhibit a smaller hysteresis-loop area compared to the uncoated material, indicating that they energy less magnetic material. Additionally, the coated samples have a lower saturation flux density, which refers to the maximum amount of magnetic flux that a material can sustain before reaching saturation, which occurs when further increases in the magnetic field strength do not result in corresponding increases in the magnetic flux density. To investigate the magnetic properties further, AC core losses were calculated at a specific frequency of 500 Hz. Core losses refer to the energy dissipated in a magnetic core when subjected to alternating magnetic fields. In this case, the steel strips were magnetised to saturation, meaning they were exposed to a magnetic field that maximised their magnetisation. At the point of saturation, the 500 Hz flux density reached approximately 1.5T based on the frequency of the magnetising current. This specific combination of frequency and flux density was chosen to evaluate the magnetic properties of the samples in question. By using a

standardised set of conditions, it is possible to compare and analyse the magnetic characteristics of different materials or samples consistently.

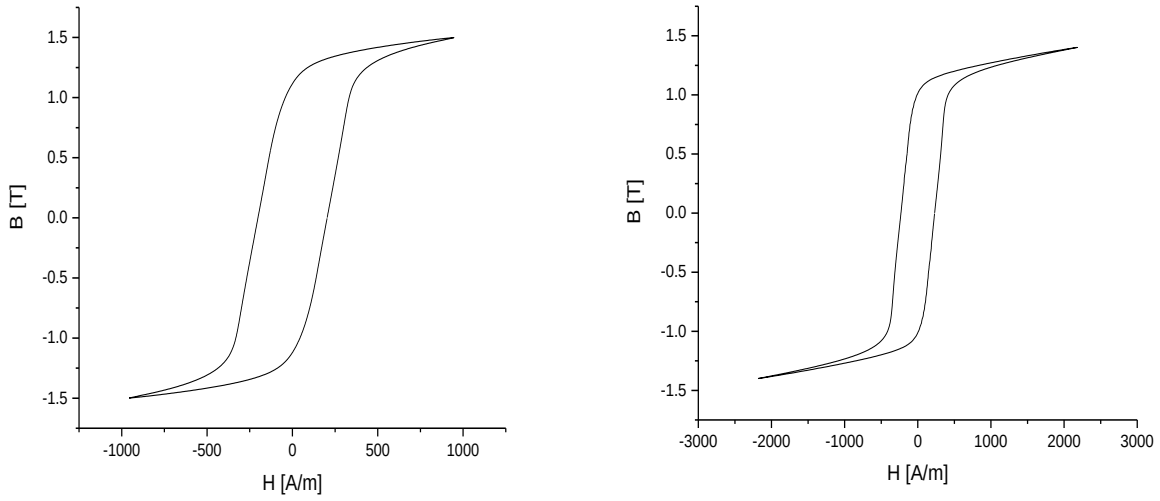

(a) (b)

Figure 5-6 The hysteresis loop at 500 Hz and 1.5 T: (a) uncoated sample, and (b) coated sample.

5.7 Discussion of the use of cobalt paste

It was shown that the power loss of the lower grades of non-oriented silicon-iron could be reduced under magnetising frequencies of both 50 Hz and 400 Hz. The reduction was smaller when fired at 890°C than when fired at higher temperatures during the preliminary experiments. This suggests that the transfer of the cobalt from the paste was incomplete, and that the penetration depth was reduced. Little difference was seen between the samples fired with pastes in the range of 1/3 to 1 ml sodium silicate solution per gram of cobalt. The relationship between the change in power loss at 50 Hz and that at 400 Hz was inconsistent, although in general the improvement in power loss at the higher frequency was not as

proportionately large as might have been anticipated. The largest improvement in power loss at 400 Hz was 15%, which was accompanied by an improvement at 50 Hz of 4%. The difference in power loss of the coated and uncoated samples from a magnetic flux density of 0.5 T to 1.7 T at a frequency of 50 Hz is shown in Figure 5-7. Meanwhile, the difference in power loss of the coated and uncoated samples from a magnetic flux density of 0.5 T to 1.7 T at a frequency of 400 Hz is shown in Figure5-8. The relationship between the behaviours at the two frequencies may be different from that of homogeneous materials because the flux distribution will be different in the two cases. In particular, the flux distribution will be more uniform through the thickness of the sheet at lower frequencies compared to higher frequencies when it will be concentrated more at the surface. The regions close to the surface of the steel will be most disturbed by the firing process in terms of concentration changes, stresses set up. This might account for the unpredictable behaviours of the samples when magnetised at higher flux densities.

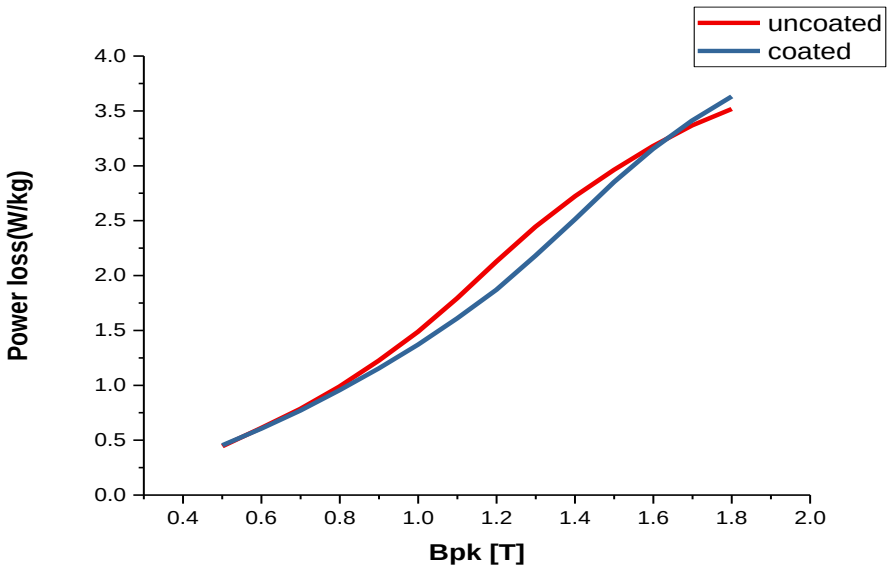

Figure 5-7 The difference in power loss of the coated and uncoated samples from a magnetic flux density of 0.5 T to 1.7 T at a frequency of 50 Hz.

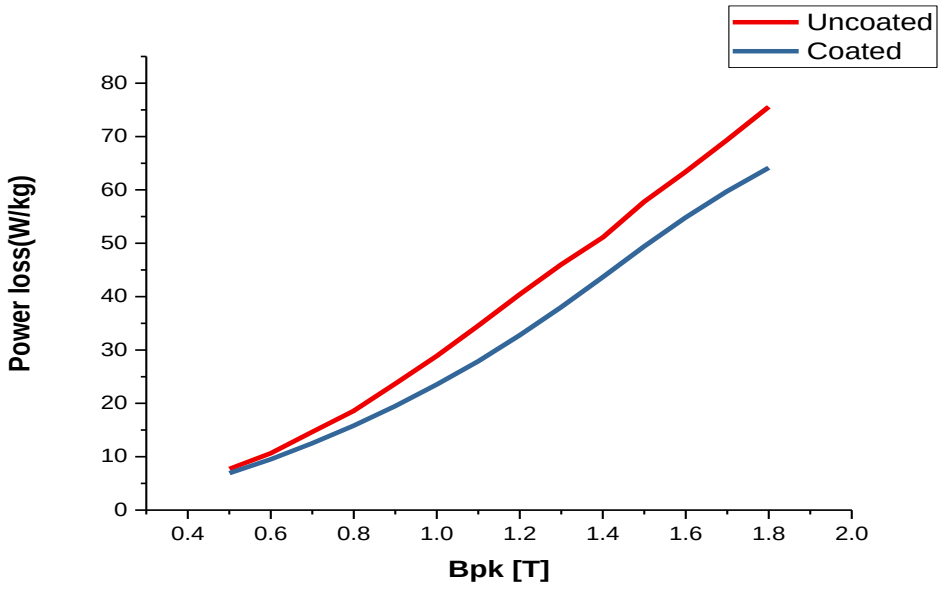

(b)

Figure 5-8 The difference in power loss of the coated and uncoated samples from a magnetic flux density of 0.5 T to 1.7 T at a frequency of 400 Hz.

Experiments on the higher grade of non-oriented steel produced improvements in a power loss of up to 8.6% but with an accompanying increase in the 50 Hz loss. The paste was predicted to contain a considerable amount of porosity. Upon studying the samples using the SEM, it became apparent that the deductions that had been made from the magnetic testing and observation of the pasting behaviours were basically correct. The SEM pictures showed that a considerable amount of porosity was generated in the region close to the sample surfaces. These areas had confused structures but well-defined boundaries, within which the cobalt content often exceeded the limit of the analytical scale being used. It is quite likely that intermetallic compounds could be found, but this was not investigated. which is dependent on the diffusion constants of cobalt in the paste and the metal. While it may be unsurprising that diluting the cobalt concentration by increasing the sodium silicate content should lower the activity, the effect of greatly the sodium silicate content is less obvious.

For the greatest rate of diffusion through the paste, it must form a coherent matrix. However, because it is not desirable to maximise the rate of diffusion through the paste but rather reduce it to a certain level, it is necessary to evaluate the methods by which this may be achieved. The method of increasing the sodium silicate content of the paste up to a level such that porosity is reduced has the disadvantage that the paste is prone to cracking, which results in the non-uniform distribution of the cobalt (as described earlier). Decreasing the silicate content will eventually lead to less coherent coatings. Reducing the silicate content also means that more moisture must be added to the paste to ensure that it is liquid enough to be brushed on. This will mean that the liquid phase of the paste will be thinner, and therefore less able to maintain the powder in suspension, while the paste becomes less tacky. Pastes with less silicate content will become progressively more difficult to brush evenly with good wetting of the surface. An alternative method is to use a ceramic powder. However, the viability of this depends on what happens to the residual paste after firing because a greater proportion of sodium silicate and dilutant to cobalt will leave a greater amount of residue. If the residue is to be removed, then this is unimportant. However, if the residue is to remain and perhaps be incorporated in an insulating coating, then this is a serious disadvantage.

Figure 5-9 shows the relative permeability testing of the uncoated and coated samples at 50Hz. The effect of the porous layer on the magnetic properties of the sheet would effectively reduce the thickness of the layer because the layer would have very low saturation magnetisation and very poor permeability**.** A comparison of relative permeability variation testing uncoated and coated for sample at 400Hz is shown Figure 5-10.

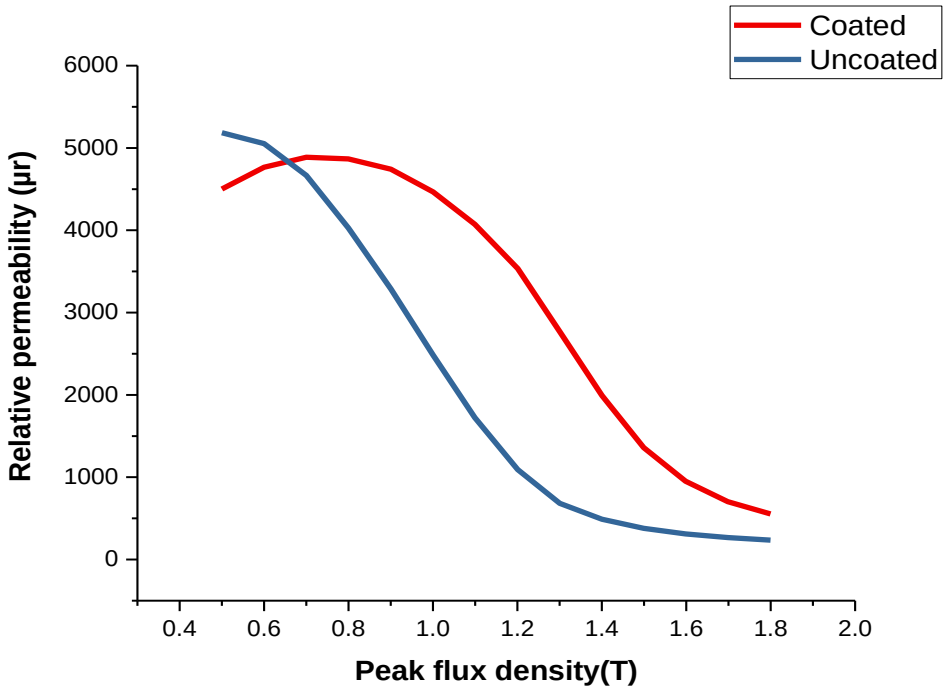

Figure 5-9 Relative permeability testing of uncoated and coated samples at 50Hz.

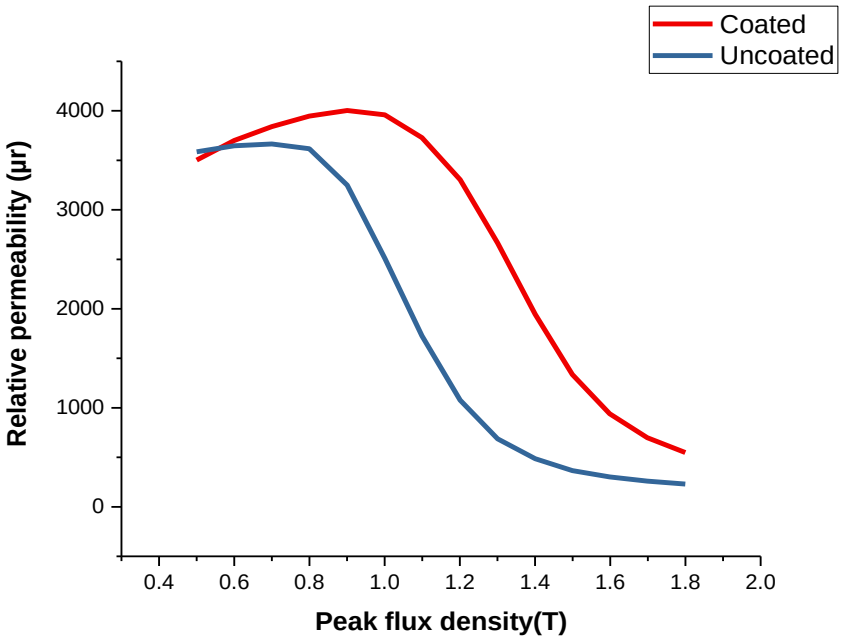

Figure 5-10 Comparison of relative permeability variation testing of uncoated and coated samples at 400Hz.

The presence of this sample made the removal of the residual layer even more difficult to accomplish because it was often not easy to be certain where the porous layer began, and the coating ended. Assuming that the porous layer is practically nonmagnetic, which considering its structure and probable composition would appear to be likely, the magnetic properties of the steel must depend on the thickness of the undamaged layer and the cobalt distribution within it. In cases in which the porous layer was broad, its thickness varied noticeably along the strip. This indicates either differences in contact resistance between the paste and the steel or inhomogeneity in the paste layer itself. This inconsistency also manifested itself in variations of the concentration gradients in the undamaged part of the sheet and less cobalt was transferred to the same regions. The factors affecting these profiles become increasingly complex because the variables that have already been quoted as governing them must be increased to include terms relating to the thickness and diffusion characteristics of the porous layer. It is evident from the SEM photographs that in many cases only a small proportion of the cobalt added to the steel reached the undamaged section of the steel. This would explain why relatively low reductions in the power loss of the materials were recorded because most of the cobalt added was ineffective. Given that the flux density was measured assuming that the thickness of the steel was unchanged from that of the untreated state, the reasons for the apparent increase in magnetisation field to achieve the higher values become clear (as shown in Figure 5-11).

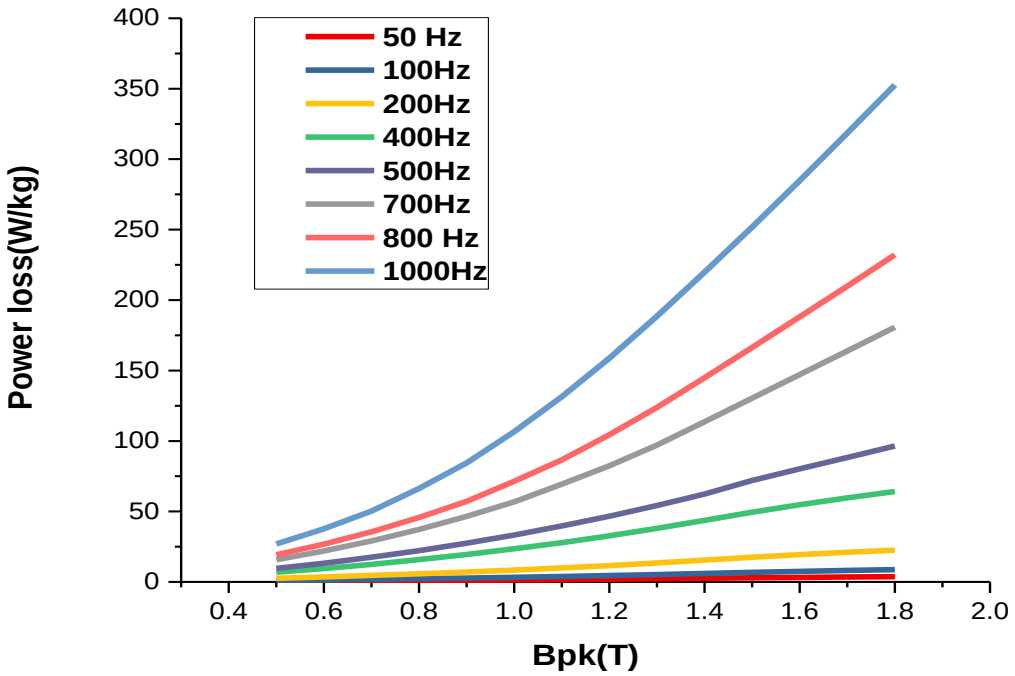

Figure 5-11 Power loss testing for the coated sample for different frequencies.

The generation of the porous layer reduces the thickness of these domains, while the roughness of the interfaces would provide pinning points for them, thus causing an increase in the hysteresis loss. In addition, it has been shown that the cobalt cognising process causes stress within the material, and it is probable that this would have deleterious effects on the magnetic properties. The massive increase in power loss that was observed after firing was largely reversed by subsequent annealing, which suggests that it was caused by stress effects. The effect of further heat treatment on the fired samples from which the residual coating had been removed would be to transfer some of the cobalt from the cobalt-rich porous regions into the interior of the steel. However, no mechanism is apparent whereby the porous layer could be reconverted to a solid phase having the same grain structure as the rest of the steel. The effects of producing resistivity gradients by increasing the cobalt concentration of a sheet near its surfaces are obscured by the production of porous regions and by the stresses that are thereby

set up. Compressive stress of only a few MP when applied to this material is more than sufficient to nullify the benefits obtained from the increase in resistivity brought about by increasing its cobalt content by one or two percent.

When compared to the methods used by Ames [131] for siliconization, the benefits of a paste method are that it does not require as much specialised equipment as that process and is certainly less hazardous. Although cobalt may be readily transferred from a paste, there are several problems to be overcome before it can be usefully exploited. Primarily, these are the production of a stable paste whose diffusive characteristics relative to those of the steel are such as to avoid the formation of porous layers. This could possibly be achieved by controlling the reduced values of the sodium silicate solution and its content proportional to that of the cobalt powder. However, problems could remain. For example, producing such a change on the fired samples from which the residual coating had been removed would transfer some of the cobalt from the cobalt-rich porous regions into the interior of the steel. However, no mechanism is apparent whereby the porous layer could be reconverted to a solid phase having the same grain structure as the paste having the required adhesive properties together with homogeneity. The other main difficulty with the residual layer is that it must either be made more difficult to remove, removable after firing, or else more tenacious for it could be incorporated in the insulating layer.

5.8 Comparisons of coated specimens for different materials

Previous studies have utilised the same diffusion technique to investigate the characteristics of aluminium [132]. The research study covered in this thesis has instead compared the properties of two alternative materials, manganese and cobalt, after applying a coating and measuring flux density at low frequencies (specifically, 50 Hz). The findings

indicate notable variations in the power loss rates among these materials at different flux densities.

At a magnetic induction level of 1 T, aluminium demonstrates a significant increase in power loss (-14.3%). This means that at this induction level, aluminium is not very efficient, and it incurs substantial power losses. For a magnetic induction of 1 T, manganese shows only a minimal change in power loss (-2%), indicating that its power loss remains nearly constant at this induction level. At a magnetic induction level of 1 T, cobalt demonstrates a reduction in power loss (2%), indicating that it becomes more efficient at this induction level. Therefore, at 1 T magnetic induction, aluminium shows increased power loss, manganese exhibits a stable power loss, and cobalt demonstrates decreased power loss. Therefore, the choice of material depends on the specific induction level and the desired behaviour in response to that level. If minimizing power loss at 1 T induction is crucial, cobalt would be preferred.

At a magnetic induction level of 1.5 T, aluminium exhibits a reduction in a power loss of -11%. This means that aluminium becomes more efficient at this induction level compared to lower levels, resulting in a decrease in power loss. For a magnetic induction of 1.5 T, manganese shows a very slight reduction in power loss of 0.5 %. This indicates that its power loss remains relatively stable at this induction level but doesn't significantly decrease. At a magnetic induction level of 1.5 T, cobalt exhibits a remarkable reduction in a power loss of 4 %. This suggests that it maintains its efficiency at this induction level. Thus, at a magnetic induction level of 1.5 T, aluminium shows a notable decrease in power loss, manganese maintains stable power loss, and cobalt continues to exhibit efficient behaviour. Therefore, the choice of material depends on the specific induction level and the desired behaviour in response to that level. If minimizing power loss at 1.5 T induction is crucial, aluminium and cobalt may be preferred choices, with cobalt having a slight advantage.

At a magnetic induction level of 1.7 T, aluminium shows a very slight reduction in a power loss of -0.8%. This suggests that aluminium's power loss remains relatively stable at this induction level, with a minimal decrease. For a magnetic induction of 1.7 T, manganese shows a minor increase in power loss of 0.3%. This indicates that its power loss slightly rises at this induction level. At a magnetic induction level of 1.7 T, cobalt exhibits a minor increase in power loss of 0.4%. This suggests that it becomes slightly less efficient at this induction level. Furthermore, at a magnetic induction level of 1.7 T, aluminium shows stable power loss, manganese exhibits a minor increase in power loss, and cobalt starts to become slightly less efficient. Therefore, the choice of material depends on the specific induction level and the desired behaviour in response to that level. If maintaining consistent power loss at 1.7 T induction is crucial, aluminium may be considered a stable choice, while cobalt and manganese show slight increases in power loss. These observations are visually represented in Tabel 5–7.

This study also highlights the potential of diffusing manganese and cobalt into steel using a paste formulated from powdered forms of these elements. The addition of manganese and cobalt resulted in a reduction of power loss in NOES. These improvements appear to stem from a straightforward increase in resistivity. However, when using cobalt, the extent of improvement was often constrained by the formation of a highly porous layer on the surface, which was characterised by a high cobalt content. This layer likely exhibited virtual nonmagnetic properties, subsequently causing a reduction in the saturation magnetisation of the entire sheet. The thickness of this layer was believed to be influenced by the relative rates of cobalt diffusion through the paste and the metal, thereby being heavily dependent on the paste composition.

Table 5-7 The percent decrease in power loss after coating with different materials measured at 1.0 T, 1.5 T and 1.7 T, at 50 Hz.

Flux density (T)	**Reduction in power loss (%)**		
	AL	Mn	Co
1	-14.3	-2	2
1.5	-11	0.5	4
1.7	-0.8	0.3	0.4

5.9 Summary

It has been demonstrated that the power loss of non-oriented 2.4% Silicon-Iron may be reduced by the cobalt paste method. The major problem to be overcome is to formulate a paste whose characteristics are such that the formation of porous layers during the firing process is avoided. The paste must also have good adhesion during the firing process to ensure that the cobalt distribution over the surface areas is homogeneous. The magnetic properties of samples fired with silicon paste are governed by the extent of the porous layer by the cobalt distribution in the nonporous regions and the stresses set up within the steel. The power loss relationships between those measured at 50 and 400 Hz are unpredictable, presumably due to the variations of flux distributions in non-homogeneous samples. Problems are also encountered with the residual layers, which must either be more easily removable subsequent to firing or thinner, more even, and more tenacious if they are to be used as part of the insulating coating. If the latter course is to be taken, then the thickness of the coating must be strictly controlled to limit the amount of silicon that enters the steel.

If the formation of porous layers can be avoided and anneals can be used to remove any undesirable stresses, then there is no obvious reason why this method should not be able to produce improvements in non-oriented material. In this case, the method would have considerable advantages in terms of convenience and hazardousness over actions that are dependent on the reactions of cobalt tetrachloride vapour.

By investigating the effects of a cobalt oxide coating and diffusion process on the magnetic and energetic properties of the laminations, this research provides valuable insights into the potential benefits of utilising cobalt oxide as a surface treatment to improve the performance of silicon-iron materials.

Chapter 6: Conclusions and future work

6.1 Conclusions

The results of this research showed that there was a decrease eddy current percentage in the core losses of electrical steels. It has been shown that manganese and cobalt may be diffused into steel from a paste made from the appropriate element in paste -form solutions. Reductions in the power loss of non-oriented 2.4% silicon-iron by the addition of manganese and cobalt have been achieved, which are up to 9% at 1.5 T using manganese and 15% at 1.5 T using cobalt at 400 Hz. The reason for the reductions appears to be a straightforward resistivity increase.

In the case of cobalt, the degree of improvement was often severely limited by the formation of a highly porous layer of high cobalt content at the surface. This layer was probably in effect virtually nonmagnetic, and therefore brought about a reduction in the saturation magnetisation of the whole sheet. The thickness of this layer was believed to be related to the relative rates of diffusion of cobalt through the paste and the metal, and in consequence was strongly dependent on the composition of the paste, with power loss reductions being achieved using cobalt but not with manganese. The best results obtained were reductions of up to 23% at 1.5 T with 1kHz, but the conditions required to achieve this were found to be extremely critical. In the samples in which beneficial results were obtained, only small (less than 1%) amounts of cobalt were found to have been added. It had been noted that when inhomogeneous manganese addition had taken place over the surface of the sheet, that buckling of the sample resulted. Experiments conducted with uncoated samples have unveiled the potential for significant stresses to develop during the measurement process, with these stresses playing a notable role in shaping the steel's properties. It is postulated that the annealing process,

designed to alleviate surface stress, could contribute to reducing stress sensitivity. To optimize the overall performance of the material, it becomes evident that achieving a consistent distribution of manganese across the sheet's surface is of paramount importance. Such uniformity serves as a pivotal factor in averting detrimental stresses and, intriguingly, holds the potential to enhance power loss characteristics. Therefore, while annealing serves as a stress-mitigating technique, addressing surface stress and ensuring a homogeneous manganese distribution emerge as indispensable prerequisites for the effective management of material properties. Paste composition was found to be extremely critical, not only in terms of the relative proportions of the ingredients but also of their physical characteristics. The size and shape of the manganese powder and the viscosity of the silicon oil solution were both seen to be important. Manganese particles size governs the ease with which it may be made into a homogeneous paste and on the amount of that element that remains to diffuse after oxidation by the liquid. If stress is believed to be the most important factor in the improvement of the non-oriented material, then other elements that do not have such a drastic effect on resistivity might prove to give beneficial results. Which elements would be likely to produce the best effects is not easy to predict because the stresses that are setup do not appear to follow simply from size factor or lattice parameter considerations This process would appear to have applications to the improvement of non-oriented steel by incorporation in the production line, or locally to increase the resistivity of non-oriented steel. Careful evaluation of the cost-effectiveness of the process would be necessary, together with further research to optimise the possible benefits and to evaluate the effects of the various parameters on the system. Higher frequency will lead to higher power losses, smaller size, less raw materials, and thus lower cost.

6.2 Future work

The selection of elements for enhancing resistivity requires further investigation. The results obtained with manganese and cobalt pastes did not align with predictions based on atomic size factors. Exploring alternative elements, such as chromium, which is known for its effectiveness in increasing iron resistivity, could be considered. However, initial attempts to diffuse chromium into silicon-iron have been unsuccessful and the reasons for this problem remain unclear. It is possible that the unpredictable nature of the paste rather than the steel's characteristics played a role. Notably, chromium is prone to oxidation, which may have occurred on a significant scale in some pastes. Additional experiments on pure iron have failed to replicate earlier findings, which suggests the need for further investigations in this area.

Copper is often recommended for various applications due to its excellent suitability for high-frequency and electrical resistance requirements. Its properties, including high electrical conductivity and low resistivity, make it an ideal choice for applications where electrical performance and minimal power loss are crucial. Additionally, copper's ability to efficiently conduct electricity at high frequencies makes it valuable in a range of electronic and electrical applications, including wiring, electrical connectors, antennas, and more. Its combination of electrical properties and versatility makes copper a preferred material for many electrical and high-frequency applications. Instead of the paste method, an alternative approach could involve depositing copper onto the metal surface by precipitation from an acidified copper sulphate solution. However, care should be taken to prevent phase transformation, which requires the firing temperatures to be kept below 820°C. Observing little change in power loss after firing at 800°C and minimal alteration in stress sensitivity, which cannot be solely attributed to experimental errors, suggests the need for a more comprehensive

investigation of this problem. Understanding the underlying factors contributing to the lack of change in the characteristics would be valuable in refining this deposition method.

6.3 Limitations

This study has observed the following limitations:

1. Controlling the diffusion characteristics by reducing the silicate content faced challenges due to a lack of coherency.
2. The formation of a porous layer on the steel surface, whose depth was influenced by the paste composition, posed a problem.
3. Sodium silicate application resulted in the formation of a solid layer, which further complicated the diffusion process.
4. Significant variations in resistivity were observed along the length of the strip, which indicate uneven transfer of cobalt from the paste to the steel.
5. Rough interfaces and surface porosity were observed between the paste and the metal, with instances of unequal diffusion of manganese from opposite faces of the sample, particularly in the buckled samples.
6. Several pastes used in the study failed to reduce power loss, and in some cases even resulted in considerable increases. This failure could be attributed to poor adhesion, inhomogeneity, or bubbling, leading to non-uniform material distributions.
7. Removal of the paste residue was also much more difficult for cobalt than for manganese.

References

[1] Y. Hayakawa, “Electrical Steels,” *Encycl. Mater. Met. Alloy.*, vol. 2, pp. 208–213, 2021, doi: 10.1016/B978-0-12-819726-4.00004-1.

[2] Y. Du, R. J. O’Malley, M. F. Buchely, and P. Kelly, “Effect of rolling process on magnetic properties of Fe-3.3 wt% Si non-oriented electrical steel,” *Appl. Phys. A Mater. Sci. Process.*, vol. 128, no. 9, pp. 1–9, 2022, doi: 10.1007/s00339-022-05902-5.

[3] I. V. Gervasyeva, V. A. Milyutin, F. V. Mineyev, and Y. Y. Babushko, “Assessment of the Textured State of the Nonoriented Electrical Steel for Electromobiles and the Effect of the Texture on the Basic Magnetic Characteristics,” *Phys. Met. Metallogr.*, vol. 121, no. 7, pp. 618–623, 2020, doi: 10.1134/S0031918X20070030.

[4] H. Herrmann and H. Bucksch, “Saturation Magnetization,” *Dict. Geotech. Eng. Geotech.*, pp. 1170–1170, 2014, doi: 10.1007/978-3-642-41714-6_190698.

[5] K. Verbeken, I. Infante-Danzo, J. Barros-Lorenzo, J. Schneider, and Y. Houbaert, “Innovative processing for improved electrical steel properties,” *Rev. Metal.*, vol. 46, no. 5, pp. 458–468, 2010, doi: 10.3989/revmetalm.1010.

[6] A. Coombs, M. Lindenmo, D. Snell, and D. Power, “Review of the types, properties, advantages, and latest developments in insulating coatings on nonoriented electrical steels,” *IEEE Trans. Magn.*, vol. 37, no. 1, pp. 544–557, 2001, doi: 10.1109/20.914376.

[7] Y. Du, R. O’Malley, and M. F. Buchely, “Review of Magnetic Properties and Texture Evolution in Non-Oriented Electrical Steels,” *Appl. Sci.*, vol. 13, no. 10, 2023, doi: 10.3390/app13106097.

[8] T. Ros-Yanez, M. De Wulf, and Y. Houbaert, “Influence of the Si and Al gradient on the magnetic properties of high-Si electrical steel produced by hot dipping and diffusion annealing,” *J. Magn. Magn. Mater.*, vol. 272–276, no. SUPPL. 1, pp. 2003–2004, 2004, doi: 10.1016/j.jmmm.2003.11.295.

[9] J. Kartigeyan and M. Ramaswamy, “Effect of material properties on core loss in switched reluctance motor using non-oriented electrical steels,” *J. Magn.*, vol. 22, no. 1, pp. 93–99, 2017, doi: 10.4283/JMAG.2017.22.1.093.

[10] G. Ouyang, X. Chen, Y. Liang, C. Macziewski, and J. Cui, “Review of Fe-6.5 wt%Si high silicon steel—A promising soft magnetic material for sub-kHz application,” *J. Magn. Magn. Mater.*, vol. 481, no. February, pp. 234–250, 2019, doi: 10.1016/j.jmmm.2019.02.089.

[11] J. S. Shin , J.S. Baeb, H.J. Kimb, H.M. Leeb, T.D. Leeb, E.J. Lavernia c and Z.H. Lee “Ordering-disordering phenomena and micro-hardness characteristics of B2 phase in Fe-(5-6.5%)Si alloys,” *Mater. Sci. Eng. A*, vol. 407, no. 1–2, pp. 282–290, 2005, doi:

10.1016/j.msea.2005.07.012.

[12] T. Moses, "Opportunities for exploitation of magnetic materials in an energy conscious world," *Interdiscip. Sci. Rev.*, vol. 27, no. 2, pp. 100–113, 2002, doi: 10.1179/030801802225003187.

[13] Q. Ren, Z. Hu, L. Cheng, and L. Zhang, "Effect of rare earth elements on magnetic properties of non-oriented electrical steels," *J. Magn. Magn. Mater.*, vol. 560, no. June, p. 169624, 2022, doi: 10.1016/j.jmmm.2022.169624.

[14] H. H. Lee, J. Jung, J. I. Yoon, J. K. Kim, and H. S. Kim, "Modelling the evolution of recrystallization texture for a non-grain oriented electrical steel," *Comput. Mater. Sci.*, vol. 149, no. March, pp. 57–64, 2018, doi: 10.1016/j.commatsci.2018.03.013.

[15] N. Leuning, S. Steentjes, and K. Hameyer, "Effect of grain size and magnetic texture on iron-loss components in NO electrical steel at different frequencies," *J. Magn. Magn. Mater.*, vol. 469, no. March 2018, pp. 373–382, 2019, doi: 10.1016/j.jmmm.2018.07.073.

[16] N. P. Goss, "New Development in Electrical Strip Steels Characterized by Fine Grain Structure Approaching the Properties of a Single Crystal," *Trans. A.S.M.*, vol. 23, pp. 511–531, 1935.

[17] T. Ye, Z. Lu, and C. Ma, "Evolution of Microstructure and Texture with the Low-Silicon in Non-Oriented Silicon Steel," *IOP Conf. Ser. Earth Environ. Sci.*, vol. 170, no. 4, 2018, doi: 10.1088/1755-1315/170/4/042086.

[18] L. Yue-Lin, Z. Ying, H. Rong-Jie, and L. Guang-Hong, "Study of the theoretical tensile strength of Fe by a first-principles computational tensile test," *Chinese Phys. B*, vol. 18, no. 5, pp. 1923–1930, 2009, doi: 10.1088/1674-1056/18/5/033.

[19] IEC 60404-2, "Magnetic materials - Part 2: Methods of measurement of the magnetic properties of electrical steel strip and sheet by means of an Epstein frame," vol. 1996, 2008.

[20] J. D. Siovert, "Determination of AC magnetic power loss of electrical steel sheet: Present status and trends," *IEEE Trans. Magn.*, vol. 20, no. 5, pp. 1702–1707, 1984, doi: 10.1109/TMAG.1984.1063278.

[21] P. Marketos, S. Zurek, and A. J. Moses, "Calculation of the mean path length of the Epstein frame under non-sinusoidal excitations using the double Epstein method," *J. Magn. Magn. Mater.*, vol. 320, no. 20, pp. 2542–2545, 2008, doi: 10.1016/j.jmmm.2008.04.085.

[22] N. Leuning *et al.*, "Impact of the interaction of material production and mechanical processing on the magnetic properties of non-oriented electrical steel," *AIP Adv.*, vol. 8, no. 4, 2018, doi: 10.1063/1.4994143.

[23] A. J. Moses, "Effects of stress on the magnetic properties of grain-oriented silicon-iron

magnetized in various directions," *IEEE Trans. Magn.*, vol. 17, no. 6, pp. 2872–2874, 1981, doi: 10.1109/TMAG.1981.1061559.

[24] T. Ros-Yañez, Y. Houbaert, and V. Gómez Rodríguez, "High-silicon steel produced by hot dipping and diffusion annealing," *J. Appl. Phys.*, vol. 91, no. 10 I, pp. 7857–7859, 2002, doi: 10.1063/1.1449445.

[25] G. Lyudkovsky, P. K. Rastogi, and M. Bala, "Nonoriented Electrical Steels," *Jom*, vol. 38, no. 1, pp. 18–26, 1986, doi: 10.1007/BF03257950.

[26] Y. Zhang, M. C. Cheng, and P. Pillay, "A novel hysteresis core loss model for magnetic laminations," *IEEE Trans. Energy Convers.*, vol. 26, no. 4, pp. 993–999, 2011, doi: 10.1109/TEC.2011.2160866.

[27] Y. Chen and P. Pillay, "An improved formula for lamination core loss calculations in machines operating with high frequency and high flux density excitation," *Conf. Rec. - IAS Annu. Meet. (IEEE Ind. Appl. Soc.*, vol. 2, pp. 759–766, 2002, doi: 10.1109/IAS.2002.1042645.

[28] B. S. G. H. R. Hiziroglu, *Electric Machinery and Transformers*, Third edit. Oxford University press, 2001.

[29] Z. B. Popović and B. D. Popović, "Introductory electromagnetics: practice, problems and labs." p. 305, 2000. [Online]. Available: All Papers/Miscelaneous/Introductory Electromagnetics (Herber... - Introductory Electromagnetics (Herbert P. Neff).pdf%0AAll Papers/Other Books/Introductory Electromagnetics - Z. Po... - Introductory Electromagnetics - Z. Popovic, B. Popovic.pdf

[30] M. Ibrahim and P. Pillay, "Advanced testing and modeling of magnetic materials including a new method of core loss separation for electrical machines," *IEEE Trans. Ind. Appl.*, vol. 48, no. 5, pp. 1507–1515, 2012, doi: 10.1109/TIA.2012.2210012.

[31] W. Loss and G. Oriented, "Method for producing a super low watt loss grain oriented electrical steel sheet," *Pat. (19)*, no. 19, pp. 1–6, 1976.

[32] T. Yamamoto and T. Nozawa, "Effects of tensile stress on total loss of single crystals of 3% silicon-iron," *J. Appl. Phys.*, vol. 41, no. 7, pp. 2981–2984, 1970, doi: 10.1063/1.1659348.

[33] V. Goel, P. Anderson, J. Hall, F. Robinson, and S. Bohm, "Electroless Plating: A Versatile Technique to Deposit Coatings on Electrical Steel," *IEEE Trans. Magn.*, vol. 52, no. 5, pp. 8–11, 2016, doi: 10.1109/TMAG.2016.2514745.

[34] J. W. Shilling and G. L. Houze, "A.J. Moses, D.C. Jiles, in: S. Takahashi, H. Kikuchi (Eds.), Electromagnetic Nondestructive Evaluation, IOS Press, 2007, p. 4.," *IEEE Trans. Magn.*, vol. 10, no. 2, pp. 195–223, 1974, doi: 10.1109/TMAG.1974.1058317.

[35] D. C. J. A.J. Moses, "Origin, Measurement and Application of the Barkhausen Effect in Magnetic Steeltle,", Measurement and Application of the Barkhausen Effect in

Magnetic Steeltle, IOS Press, 2007, pp. pp4-8. [Online]. Available: https://orca.cardiff.ac.uk/id/eprint/13660

[36] A. J. Moses, "Energy efficient electrical steels: Magnetic performance prediction and optimization," *Scr. Mater.*, vol. 67, no. 6, pp. 560–565, 2012, doi: 10.1016/j.scriptamat.2012.02.027.

[37] P. R. Calvillo, *Deformation analysis of high-Si-steel during torsion and compression testing*. PhD Thesis, 2007. [Online]. Available: http://hdl.handle.net/1854/LU-8598031%0A

[38] I. Transactions, "Magnetic properties and dynamic domain behavior in grain-oriented 3 % Si-Fe(Article)," vol. 32, no. 2, 1996.

[39] E. Lewis, A. Initiating, S. Vii, T. Halide, Z. Halide, and I. Systems, "High Electrical Resistivity and Permeability of Soft Magnetic Granular Alloys," *Polymer (Guildf).*, vol. 2, no. 6, pp. 10403–10411, 1991, doi: 10.1016/j.ifacol.2015.08.036.

[40] A. J. Moses, "Electrical steels. Past, present and future developments," *IEE Proc. A Phys. Sci. Meas. Instrumentation. Manag. Educ. Rev.*, vol. 137, no. 5, pp. 233–245, 1990, doi: 10.1049/ip-a-2.1990.0039.

[41] O. Honda, S. Kaya, and Y. Masuyama, "On the magnetic properties of single crystals of iron," *Nature*, vol. 117, no. 2952, pp. 753–754, 1926, doi: 10.1038/117753a0.

[42] E. P. Wohlfarth and A. S. Arrott, " Ferromagnetic Materials: A Handbook on the Properties of Magnetically Ordered Substances, Vols. 1 and 2 ," *Phys. Today*, vol. 35, no. 3, pp. 63–64, 1982, doi: 10.1063/1.2914974.

[43] B. E. Publishing, *The Britannica guide to electricity and magnetism*, Firest. New York, 2011. [Online].Available:https://books.google.co.uk/books.

[44] M. G. S. M A Laughton, *Electrical Engineer's Reference Book*, Fourteenth. Elsevier, 2013. doi: https://doi.org/10.1016/C2009-0-30456-0.

[45] Y. Oda, T. Okubo, and M. Takata, "Recent development of non-oriented electrical steel in JFE steel," *JFE Tech. Rep.*, vol. 21, no. 21, pp. 7–13, 2016.

[46] D. Binesti and J. P. Ducreux, "Core losses and efficiency of electrical motors using new magnetic materials," *IEEE Trans. Magn.*, vol. 32, no. 5 PART 2, pp. 4887–4889, 1996, doi: 10.1109/20.539278.

[47] F. E. Werner and R. I. Jaffee, "Energy-efficient steels for motor laminations," *J. Mater. Eng. Perform.*, vol. 1, no. 2, pp. 227–234, 1992, doi: 10.1007/BF02648621.

[48] T. Nakayama, N. Honjou, A. Nagai, and H. Yashiki, "Non-oriented electrical steel sheets," *Sumitomo Met.*, vol. 48, no. 3, pp. 39–44, 1996.

[49] D. Hawezy, "The influence of silicon content on physical properties of non-oriented silicon steel," *Mater. Sci. Technol. (United Kingdom)*, vol. 33, no. 14, pp. 1560–1569,

2017, doi: 10.1080/02670836.2017.1295519.

[50] M. Testing *et al.*, "Standard Classification of Insulating Coatings for Electrical Steels by Composition , Relative Insulating Ability and Application 1," vol. i, pp. 1–5, 2013, doi: 10.1520/A0976-13.2.

[51] K. N. Shrivastava, *Flux Quantization*. Publisher Name Springer, Dordrecht, 2000. doi: 10.1142/9789812792143_0002.

[52] Q. Tang, "Investigation of Magnetic Properties of Electrical Steel and Transformer Core at High Flux Densities," p. 92, 2015.

[53] L. Gao, L. Zeng, J. Yang, and R. Pei, "Application of grain-oriented electrical steel used in super-high speed electric machines," *AIP Adv.*, vol. 10, no. 1, 2020, doi: 10.1063/1.5130151.

[54] M. Heathcote, *J & P Transformer Book*, Thirteenth. Amsterdam; London; Oxford: Elsevier,2011.[Online].Available:https://books.google.co.uk/books?op=lookup&id=paPKsOXn5FMC&continue=https://books.google.co.uk/books%3Fhl%3Den%26lr%3D%26id%3DpaPKsOXn5FMC%26oi%3Dfnd%26pg%3DPP1%26dq%3DM.%2BJ.%2BHeathcote,%2BThe%2BJ%2B%2526%2BP%2Btransformer%2Bbook%2B:%2Ba%2Bpractical%2Bt

[55] B.D. Cullity and C. D. Graham, "Introduction to Magnetic Magnetic Materials, Second Edition," *IEEE Pres&Wiley, New Jersey, USA*, p. 322, 2009.

[56] F. Brailsford and J. M. Burgess, "Internal waveform distortion in silicon-iron laminations for magnetization at 50 c/s," *Proc. IEE Part C Monogr.*, vol. 108, no. 14, p. 458, 1961, doi: 10.1049/pi-c.1961.0062.

[57] P. D. Agarwal and L. Rabins, "Rigorous Solution of Eddy Current Losses in Rectangular Bar for Single Plane Domain Wall Model," vol. 248, no. 1960, 2009.

[58] S. TAGUCHI, "Review of the Recent Development of Electrical Sheet Steel," *Tetsu-to-Hagane*, vol. 62, no. 7, pp. 905–915, 1976, doi: 10.2355/tetsutohagane1955.62.7_905.

[59] J. B. Goodenough, "A theory of domain creation and coercive force in polycrystalline ferromagnetics," *Phys. Rev.*, vol. 95, no. 4, pp. 917–932, 1954, doi: 10.1103/PhysRev.95.917.

[60] R.- Eisen, *Fe—Si Iron—Silicon*. 1982.

[61] K. Baumann and H. Vogel, "Positronium," *Fortschritte der Phys.*, vol. 3, no. 9–10, pp. 429–438, 1955, doi: 10.1002/prop.19550030902.

[62] T. Ros-Yáñez, D. Ruiz, J. Barros, and Y. Houbaert, "Advances in the production of high-silicon electrical steel by thermomechanical processing and by immersion and diffusion annealing," *J. Alloys Compd.*, vol. 369, no. 1–2, pp. 125–130, 2004, doi: 10.1016/j.jallcom.2003.09.070.

References

[63] P. R. Calvillo, P. Bernárdez, and Y. Houbaert, "Production of electrical steel by hot dipping in aluminium," *Defect Diffus. Forum*, vol. 273–276, no. January 2015, pp. 63–68, 2008, doi: 10.4028/www.scientific.net/ddf.273-276.63.

[64] S. Taguchi and A. Sakakura, "Characteristics of magnetic properties of grain-oriented silicon iron with high permeability," *J. Appl. Phys.*, vol. 40, no. 3, pp. 1539–1541, 1969, doi: 10.1063/1.1657752.

[65] A. J. Moses and G. J. Thursby, "Assessment of a novel method of improving the characteristics of electrical steels by a surface diffusion technique," *J. Mater. Sci.*, vol. 18, no. 6, pp. 1650–1656, 1983, doi: 10.1007/BF00542059.

[66] S. Tumanski, *Magnetic measurements*, vol. 121, no. 3050. 1928. doi: 10.1142/9789812831750_0007.

[67] F. Anayi, A. J. Moses, and K. Jenkins, "Effect of aluminium diffusion into electrical steel on power loss under flux distortion conditions," *J. Magn. Magn. Mater.*, vol. 254–255, pp. 36–38, 2003, doi: 10.1016/S0304-8853(02)00744-8.

[68] K. Marques Marra, L. Carneiro Marra, and V. Tadeu Lopes Buono, "Effect of Aluminium Addition on the Magnetic Properties of a Semi-Processed Electrical Steel," *Mater. Res.*, vol. 19, no. 5, pp. 1162–1166, 2016.

[69] J. Hong, H. Choi, S. Lee, J. K. Kim, and Y. mo Koo, "Effect of Al content on magnetic properties of Fe-Al Non-oriented electrical steel," *J. Magn. Magn. Mater.*, vol. 439, pp. 343–348, 2017, doi: 10.1016/j.jmmm.2017.03.082.

[70] G. Couderchon and P. Brissonneau, "Magnetic Properties of Goss-Textured Si-Fe Sheets with the Addition of Al," *IEEE Trans. Magn.*, vol. 10, no. 2, pp. 170–172, 1974, doi: 10.1109/TMAG.1974.1058320.

[71] Jennifer Anne Haley, "Characterization Of Phase Equilibria And Oxidation Behavior O F Aluminum-Uthium Alloys By Electron, Ion And Neutron Beams," *Dissertation*, p. 274, 2001.

[72] K. Chwastek, A. Wodzyński, A. P. S. Baghel, and S. V. Kulkarni, "Anisotropic properties of electrical steels," *Proc. - 2015 16th Int. Conf. Comput. Probl. Electr. Eng. CPEE 2015*, no. 3, pp. 21–23, 2015, doi: 10.1109/CPEE.2015.7333328.

[73] K. Senda, M. Uesaka, S. Yoshizaki, and Y. Oda, "Electrical steels and their evaluation for automobile motors," *World Electr. Veh. J.*, vol. 10, no. 2, 2019, doi: 10.3390/wevj10020031.

[74] R. Felix *et al.*, "Influence of Grain Size and Additions of Al And Mn on The Magnetic Properties of Non-Oriented Electrical Steels With 3 wt . (%) Si 3 . Results and Discussions," vol. 11, no. 1, pp. 51–55, 2008.

[75] L. A. Johnson, E. P. Cornell, D. J. Bailey, and S. M. Hegyi, "Application of Low Loss Amorphous Metals in Motors and Transformers," *IEEE Power Eng. Rev.*, vol. PER-2,

no. 7, pp. 49–50, 1982, doi: 10.1109/MPER.1982.5521089.

[76] Z. Valkovic, “Recent problems of transformer core design,” *Phys. Scr.*, vol. 1988, no. T24, pp. 71–74, 1988, doi: 10.1088/0031-8949/1988/T24/010.

[77] N. Rajmohan, J. A. Szpunar, and Y. Hayakawa, “Goss Texture Development in Fe–Si Steels,” *Textures Microstruct.*, vol. 32, no. 1–4, pp. 153–174, 1999, doi: 10.1155/tsm.32.153.

[78] Anon, “Electrical Steel Sheets.,” *Nippon Steel Tech. Rep.*, no. 21, pp. 127–134, 1983.

[79] J. R. Birchak and G. W. Smith, “Magnetomechanical damping and magnetic properties of iron alloys,” *J. Appl. Phys.*, vol. 43, no. 3, pp. 1238–1246, 1972, doi: 10.1063/1.1661245.

[80] T. R. Yanez, Y. Houbaert, O. Fischer, and J. Schneider, “Experimental thermomechanical processing of high Si-steels (up to 6.5%Si),” *Mater. Sci. Forum*, vol. 373–376, pp. 773–776, 2001, doi: 10.4028/www.scientific.net/msf.373-376.773.

[81] A. F. Feb, “Diffusing metals into low carbon steel sheet,” 1922.

[82] R. Hessen, “The Transformation of Bethlehem Steel,” *Steel Titan*, pp. 163–188, 1975, doi: 10.2307/j.ctt6wrdvd.12.

[83] R. H. W. Rodewald, *Magnetic materials : fundamentals, products, properties, applications*. Erlangen : Publicis ; Hanau, Germany: VAC, VACUUMSCHMELZE, 2013. [Online]. Available: http://www.worldcat.org/oclc/824490498%3E

[84] R. V. M. and C. M. Orrock, “HIGH SATURATION TERNARY COBALT-IRON BASED ALLOYS,” *IEEE Trans. Games*, vol. 11, no. 3, pp. C2–C2, 1988, doi: 10.1109/tg.2019.2939692.

[85] R. H. Yu *et al.*, “High temperature soft magnetic materials: FeCO alloys and composites,” *IEEE Trans. Magn.*, vol. 36, no. 5 I, pp. 3388–3393, 2000, doi: 10.1109/20.908809.

[86] M. Cossale, A. Krings, J. Soulard, A. Boglietti, and A. Cavagnino, “Practical Investigations on Cobalt-Iron Laminations for Electrical Machines,” *IEEE Trans. Ind. Appl.*, vol. 51, no. 4, pp. 2933–2939, 2015, doi: 10.1109/TIA.2015.2394404.

[87] H. VACUUMSCHMELZE GmbH & Co. KG, “Soft Magnetic Materials and Semi-finished Products Soft Magnetic Materials and Semi-finished Products Contents Main Headings :,” 2002.

[88] R. Brand and J. Nunn, “» Material developments,” *Magn. Technol. Int.*, pp. 16–19.

[89] V. Gmbh, R. U. S. A. Data, F. Application, and P. Data, “ELECTRIC MOTOR FOR USE INA STERILIZABLE DENTAL HANDPIECE,” vol. 2, no. 12, 2013.

[90] A. Krings, A. Boglietti, A. Cavagnino, and S. Sprague, “Soft Magnetic Material Status

and Trends in Electric Machines," *IEEE Trans. Ind. Electron.*, vol. 64, no. 3, pp. 2405–2414, 2017, doi: 10.1109/TIE.2016.2613844.

[91] P. K. Rastogi, "Effect of manganese and sulfur on the texture and magnetic properties of non-oriented steel," *IEEE Trans. Magn.*, vol. 13, no. 5, pp. 1448–1450, 1977, doi: 10.1109/TMAG.1977.1059560.

[92] K. C. Liao, "The effect of manganese and sulfur contents on the magnetic properties of cold rolled lamination steels," *Metall. Trans. A*, vol. 17, no. 8, pp. 1259–1266, 1986, doi: 10.1007/BF02650106.

[93] H. Yashiki and T. Kaneko, "Effects of Mn and S on the Grain Growth and Texture in Cold Rolled 0.5 % Si Steel," *Isij Int.*, vol. 30, no. 4, pp. 325–330, 1990, doi: 10.2355/isijinternational.30.325.

[94] T. Kubota, "Recent Progress on Non-oriented Silicon Steel," *J. Chem. Inf. Model.*, vol. 76, no. 9, pp. 1689–1699, doi: 10.1017/CBO9781107415324.004.

[95] T. Nakayama, N. Honjou, T. Minaga, and H. Yashiki, "Effects of manganese and sulfur contents and slab reheating temperatures on the magnetic properties of non-oriented semi-processed electrical steel sheet," *J. Magn. Magn. Mater.*, vol. 234, no. 1, pp. 55–61, 2001, doi: 10.1016/S0304-8853(01)00208-6.

[96] P. Ghosh, R. R. Chromik, A. M. Knight, and S. G. Wakade, "Effect of metallurgical factors on the bulk magnetic properties of non-oriented electrical steels," *J. Magn. Magn. Mater.*, vol. 356, pp. 42–51, 2014, doi: 10.1016/j.jmmm.2013.12.052.

[97] Q. Ren, W. Yang, L. Cheng, Z. Hu, and L. Zhang, "Effect of calcium treatment on magnetic properties of non-oriented electrical steels," *Journal of Magnetism and Magnetic Materials*, vol. 494. 2020. doi: 10.1016/j.jmmm.2019.165803.

[98] M. Schulte, S. Steentjes, N. Leuning, W. Bleck, and K. Hameyer, "Effect of manganese in high silicon alloyed non-oriented electrical steel sheets," *J. Magn. Magn. Mater.*, vol. 477, no. July 2018, pp. 372–381, 2019, doi: 10.1016/j.jmmm.2018.07.025.

[99] P. K. Rastogi, "Effect of manganese and sulfur on the texture and magnetic properties of non-oriented steel," *IEEE Trans. Magn.*, vol. 13, no. 5, pp. 1448–1450, 1977, doi: 10.1109/TMAG.1977.1059560.

[100] I. Tanaka and H. Yashiki, "Magnetic properties and recrystallization texture evolutions of phosphorus-bearing non-oriented electrical steel sheets," *ISIJ Int.*, vol. 47, no. 11, pp. 1666–1671, 2007, doi: 10.2355/isijinternational.47.1666.

[101] W. Chen, J. Liu, Z. Cheng, X. Lin, and J. Zhu, "Effect of Chromium on Microstructure, Ordered Phase and Magnetic Properties of Fe-6.5 wt%Si Alloy," *Mater. Today Proc.*, vol. 2, pp. S314–S318, 2015, doi: 10.1016/j.matpr.2015.05.044.

[102] M. Komatsubara, K. Sadahiro, O. Kondo, T. Takamiya, and A. Honda, "Newly developed electrical steel for high-frequency use," *J. Magn. Magn. Mater.*, vol. 242–

245, pp. 212–215, 2002, doi: 10.1016/S0304-8853(01)01164-7.

[103] H. DONG, Y. ZHAO, X. jun YU, and F. zeng LIAN, "Effects of Sn Addition on Core Loss and Texture of Non-Oriented Electrical Steels," *J. Iron Steel Res. Int.*, vol. 16, no. 6, pp. 86–89, 2009, doi: 10.1016/S1006-706X(10)60033-7.

[104] A. Mathematics, "Recent ProgressonNon-oriented Silicon Steel," vol. 76, no. 6, pp. 1–23, 2016.

[105] M. O. Hideki Matsuoka, Koichi Osawa, Moriaki Ono, "Influence of Cu and Sn on Hot Ductility of Steels with Various C Content," */ISIJ Int.*, vol. 37, no. 1 997, pp. 255–262, 1997.

[106] C. Nagasaki and J. Kihara, "Effect of copper and tin on hot ductility of ultra-low and 0.2% carbon steels," *ISIJ Int.*, vol. 37, no. 5, pp. 523–530, 1997, doi: 10.2355/isijinternational.37.523.

[107] S. Cui *et al.*, "Thermodynamic and kinetic analysis of the melt spinning process of Fe-6.5 wt.% Si alloy," *J. Alloys Compd.*, vol. 771, pp. 643–648, 2019, doi: 10.1016/j.jallcom.2018.08.293.

[108] K. Honma, T. Nozawa, H. Kobayashi, Y. Shimoyama, I. Tachino, and K. Miyoshi, "Development of non-oriented and grain-oriented silicon steel (invited)," *IEEE Trans. Magn.*, vol. 21, no. 5, pp. 1903–1908, 1985, doi: 10.1109/TMAG.1985.1064102.

[109] X. Liu, Y. Gao, Z. Li, Z. Xu, W. Tian, and B. Tang, "Cr-Ni-Mo-Co surface alloying layer formed by plasma surface alloying in pure iron," *Appl. Surf. Sci.*, vol. 252, no. 10, pp. 3894–3902, 2006, doi: 10.1016/j.apsusc.2005.06.001.

[110] R. F. De Araujo Cardoso, M. A. Da Cunha, and L. P. M. Brandão, "Optimization of the magnetic losses of electrical steels through addition of Al and Si using a hot dipping process," *J. Mater. Res. Technol.*, vol. 2, no. 3, pp. 276–281, 2013, doi: 10.1016/j.jmrt.2013.02.014.

[111] R. T. S. and J. E. REED, "Iron a Materials Survey," *Biol. Cent.*, vol. 2, pp. v–413, 1972.

[112] Cogent Power, "Typical data for SURA ® M250-35A," no. June, p. 2008, 2008.

[113] Cogent Power, "Typical data for SURA ® M330-35A," p. 1, 2009.

[114] S. Standard, "Magnetic materials - Part 2: Methods of measurement of the magnetic properties of electrical steel sheet and strip by means of an Epstain frame," vol. 1, no. IEC 60404-2. pp. 2–5, 1996.

[115] S. Standard, "Magnetic materials Methods of measurement of the magnetic properties of," vol. 1, no. IEC Standard 60404-3. pp. 2–5, 1992.

[116] G. Bertotti, "General Properties of Power Losses in Soft Ferromagnetic Materials.," *IEEE Trans. Magn.*, vol. 24, no. 1, pp. 621–630, 1987, doi: 10.1109/20.43994.

References

[117] S. Somkun, “Magnetostriction and Magnetic Anisotropy in Non-oriented Electrical Steels and Stator Core Laminations,” *thesis*, no. Cardiff University.

[118] National Instruments, “DAQ NI 6115/6120 User Manual Multifunction I/O Devices for PCI/PXI/CompactPCI Bus Computers,” no. 322812. 2002.

[119] A. J. Moses and G. J. Thursby, “Improvement of magnetic properties of electrical steels using a surface diffusion technique,” *J. Mater. Sci.*, vol. 18, no. 6, pp. 1657–1665, 1983, doi: 10.1007/BF00542060.

[120] T. L. Mthombeni and P. Pillay, “Physical basis for the variation of lamination core loss coefficients as a function of frequency and flux density,” *IECON Proc. (Industrial Electron. Conf.*, no. 4, pp. 1381–1387, 2006, doi: 10.1109/IECON.2006.347545.

[121] D. M. Ionel, M. Popescu, S. J. Dellinger, T. J. E. Miller, R. J. Heideman, and M. I. McGilp, “On the variation with flux and frequency of the core loss coefficients in electrical machines,” *IEEE Trans. Ind. Appl.*, vol. 42, no. 3, pp. 658–667, 2006, doi: 10.1109/TIA.2006.872941.

[122] C. R. Boon and J. A. Robey, “Eddy-current losses in thin ferromagnetic sheets,” *Proc. Inst. Electr. Eng.*, vol. 105, no. 8, pp. 337–342, 1958, doi: 10.1049/piee.1968.0271.

[123] I. Mayergoyz and C. Serpico, “Nonlinear diffusion of electromagnetic fields and excess eddy current losses,” *J. Appl. Phys.*, vol. 85, no. 8 II A, pp. 4910–4912, 1999, doi: 10.1063/1.369139.

[124] H. J. Williams, W. Shockley, and C. Kittel, “Studies of the propagation velocity of a ferromagnetic domain boundary,” *Phys. Rev.*, vol. 80, no. 6, pp. 1090–1094, 1950, doi: 10.1103/PhysRev.80.1090.

[125] B. Frédéric, W. Thierry, and F. Hervé, “The use of iron-nickel and iron-cobalt alloys in electrical engineering, and especially for electrical motors,” *2007 Electr. Insul. Conf. Electr. Manuf. Expo, EEIC 2007*, pp. 394–401, 2007, doi: 10.1109/EEIC.2007.4562649.

[126] P. Jantaratana and C. Sirisathitkul, “Giant Magnetoimpedance in Electrodeposited Cobalt on Silver Wires,” *Walailak J Sci Tech*, vol. 3, no. 2, pp. 261–271, 2006.

[127] W. J. Sci, “Magnetic Properties of Cobalt-coated Silicon Steels Prepared by Electrodeposition,” vol. 4, no. 1, pp. 123–138, 2007.

[128] R. Plfurzluhv, “High-frequency magnetoimpedance effect in glass-coated amorphous Co 83.2B3.3Si5.9 Mn7.6 microwires,” vol. 6.

[129] M. Rece, “The Colloid Chemistry Of Silica And Silicates,” p. 7, 1955.

[130] E. Katoueizadeh, M. Rasouli, and S. M. Zebarjad, “The rheological behavior of the non-Newtonian thixotropic colloidal silica gels from sodium silicate,” *Mater. Chem. Phys.*, vol. 272, no. June, p. 124994, 2021, doi: 10.1016/j.matchemphys.2021.124994.

[131] M. Jeffrey and P. E. P. Sheehan, “Method of Refining Magnetic Domains of Barrier-

Coated Electrical Steels Useng Metallic Contaminants," no. 19, 1990.

[132] S. M. Park, J. S. Lee, J. S. Kim, K. S. Han, and Y. M. Koo, "Diffusion behavior of 3.2% Si-grain-oriented steel coated with Al by plasma vapor deposition," *Met. Mater. Int.*, vol. 21, no. 3, pp. 593–599, 2015, doi: 10.1007/s12540-015-4467-x.

Appendix 1:- The recording of the furnace cycle

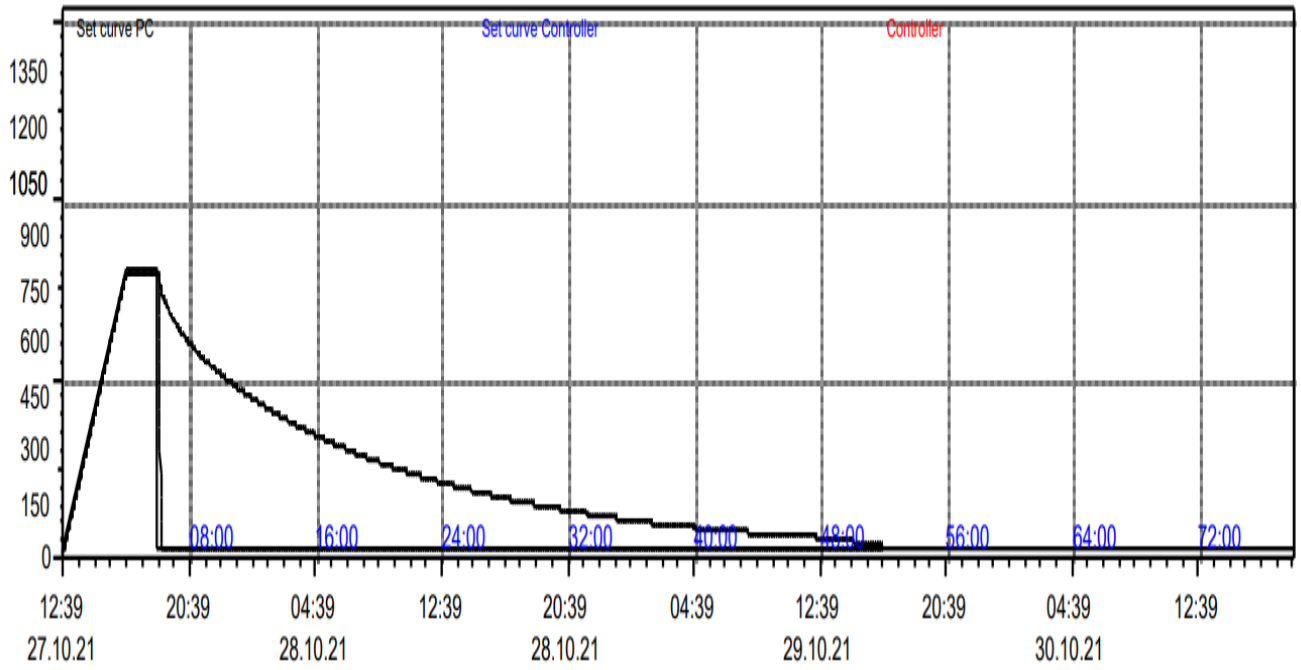

Figure A1: The recording of the furnace cycle temperature and times for the diffusion annealing process at 800°C.

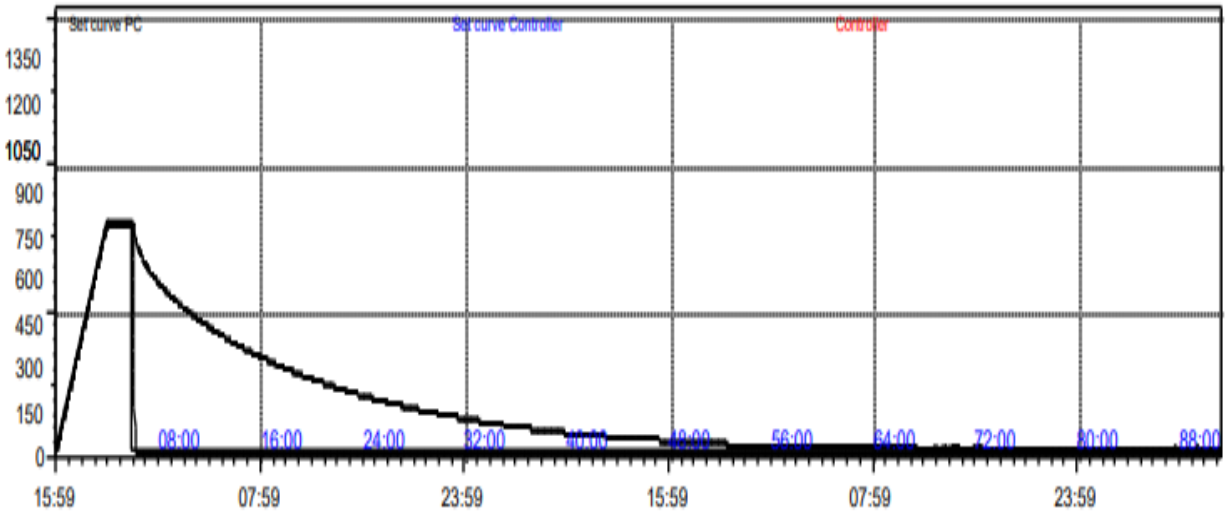

Figure A2: The recording of the furnace cycle temperature and times for the diffusion annealing process at 700°C.

Appendix

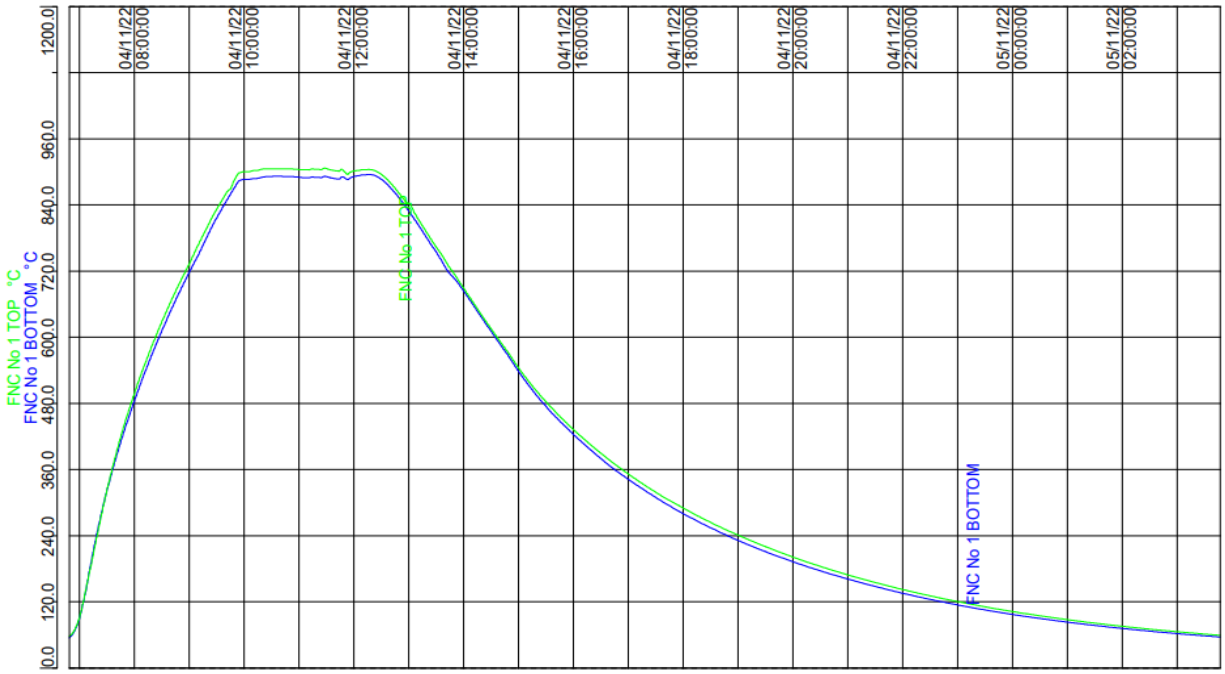

Figure A3: The recording of the furnace cycle temperature and times for the diffusion annealing process at 890°C.

Appendix 2:- Specific power loss for a sample

Table A1: Specific power loss for a sample uncoated at different flux densities for Mn.

Total measured power loss (W/kg)							
B pk (T)	50 Hz	100 Hz	200 Hz	400 Hz	500 Hz	700 Hz	1000 Hz
0.5	0.239	0.587	1.460	4.310	5.938	10.240	16.143
0.7	0.421	1.067	2.709	8.059	11.127	19.554	31.126
0.9	0.660	1.664	4.335	13.051	18.281	32.498	55.849
1.1	0.953	2.404	6.370	19.689	27.819	50.691	92.641
1.3	1.359	3.410	8.942	27.924	40.075	73.177	141.506
1.5	1.921	4.584	12.505	38.143	56.428	102.282	198.216
1.7	2.267	5.950	15.535	48.945	68.659	136.080	255.847

Table A2: Specific power loss for a sample coated at different flux densities for Mn.

Total measured power loss (W/kg)							
B pk (T)	50 Hz	100 Hz	200 Hz	400 Hz	500 Hz	700 Hz	1000 Hz
0.5	0.249	0.588	1.51	4.05	5.85	9.65	17.65
0.7	0.434	1.06	2.78	7.59	10.51	17.58	33.70
0.9	0.673	1.65	4.39	12.29	17.26	29.39	57.12
1.1	0.977	2.39	6.4	18.52	26.49	46.67	94.37
1.3	1.373	3.347	8.95	26.49	38.27	70.79	143.77
1.5	1.912	4.400	12.00	35.706	52.680	99.301	194.237
1.7	2.215	5.502	14.725	44.481	65.892	127.129	249

Appendix

Table A3: Specific power loss for a sample uncoated at different flux densities for Co.

Total measured power loss (W/kg)							
B pk (T)	50 Hz	100 Hz	200 Hz	400 Hz	500 Hz	700 Hz	1000 Hz
0.5	0.440	1.05	2.77	7.72	10.85	18.24	32.07
0.7	0.807	1.93	5.11	14.61	20.34	35.58	66.07
0.9	1.28	3.08	8.11	23.66	34.00	60.51	117.58
1.1	1.87	4.470	11.79	34.54	49.66	92.22	180.13
1.3	2.50	5.96	15.72	45.97	68.20	127.32	250.30
1.5	3.00	7.18	19.01	57.76	86.98	163.75	326.68
1.7	3.40	8.21	21.79	69.30	106.72	204.31	412.09

Table A4: Specific power loss for a sample coated at different flux densities for Co.

Total measured power loss (W/kg)							
B pk (T)	50 Hz	100 Hz	200 Hz	400 Hz	500 Hz	700 Hz	1000 Hz
0.5	0.453	1.049	2.61	6.92	9.60	15.76	26.97
0.7	0.769	1.814	4.58	12.50	17.48	29.10	50.27
0.9	1.149	2.72	7.02	19.49	27.45	46.50	84.40
1.1	1.627	3.83	9.91	27.88	39.68	69.40	131.43
1.3	2.210	5.19	13.44	37.99	54.22	97.06	188.51
1.5	2.88	6.78	17.50	49.40	71.99	130.35	251.80
1.7	3.45	8.13	21.05	59.68	88.23	163.87	318.53